A global compilation of diatom silica oxygen isotope records from lake sediment – trends, and implications for climate reconstruction

Philip Meister[1], Anne Alexandre[2], Hannah Bailey[3], Philip Barker[4], Boris K. Biskaborn[1], Ellie Broadman[5], Rosine Cartier[2,6], Bernhard Chapligin[1], Martine Couapel[2], Jonathan R. Dean[7], Bernhard Diekmann[1,8], Poppy Harding[9], Andrew C. G. Henderson[10], Armand Hernandez[11], Ulrike Herzschuh[1,12,13], Svetlana S. Kostrova[1], Jack Lacey[14], Melanie J. Leng[14, 15], Andreas Lücke[16], Anson W. Mackay[17], Eniko Katalin Magyari[18], Biljana Narancic[19,1], Cécile Porchier[20], Gunhild Rosqvist[21], Aldo Shemesh[22], Corinne Sonzogni[2], George E. A. Swann[23], Florence Sylvestre[2] and Hanno Meyer[1]

1 Alfred Wegener Institute Helmholtz Centre for Polar and Marine Research, Polar Terrestrial Environmental Systems, Potsdam, 14473, Germany
2 Aix Marseille University, CNRS, IRD, INRAE, Coll France, CEREGE, Aix-en-Provence, 13545, France
3 Water, Energy and Environmental Engineering Research Unit, University of Oulu, Oulu, P.O.Box 8000, Finland
4 Lancaster Environment Centre, Lancaster University, Lancaster, LA1 4YQ, United Kingdom
5 Laboratory of Tree-Ring Research, University of Arizona, Tucson, Arizona, AZ 85721-0045, United States
6 Lund University, Department of Geology, Lund, 223 62, Sweden
7 Department of Geography, Geology & Environment, University of Hull, HU6 7RX, United Kingdom
8 Institut für Geowissenschaften, Universität Potsdam, Potsdam, 14476, Germany
9 Geography, Environment & Planning, University of Hertfordshire, Hatfield AL10 9AB, UK
10 School of Geography, Politics and Sociology, Newcastle University, Newcastle upon Tyne, NE1 7RU, UK, UK.
11 GRICA Group, Centro Interdisciplinar de Química e Bioloxía (CICA), Faculty of Sciences, Universidade da Coruña, A Coruña, 15008, Spain.
12 Institute of Environmental Science and Geography, University of Potsdam, 14476, Germany
13 Institute of Biochemistry and Biology, University of Potsdam, 14476, Germany
14 National Environmental Isotope Facility, Isotope Geosciences Facility, British Geological Survey, Keyworth, Nottingham, NG12 5GG, UK.
15 Centre for Environmental Geochemistry, School of Biosciences, University of Nottingham, Sutton Bonington, LE12 5RD, UK.
16 Institute of Bio- and Geosciences, Agrosphere Institute IBG-3, Forschungszentrum Jülich GmbH, Jülich, 52428, Germany
17 Environmental Change Research Centre, Department of Geography, University College London, London, WC1E 6BT UK.
18 Department of Environmental and Landscape Geography, MTA-MTM-ELTE Research Group for Paleontology, Eötvös Loránd University, Budapest, 1117, Hungary
19 Laboratoire de Paléoécologie Aquatique, Centre d'Études nordiques & Département de géographie, Université Laval, Laval, G1V 0A6, Canada.
20 Department of Geography, University College London, London, WC1E 6BT, UK.
21 Department of Physical Geography, Stockholm University, Stockholm, 106 91, Sweden.
22 Department of Earth and Planetary Sciences, the Weizmann Institute of Science, Rehovot, 76100, Israel.
23 School of Geography, University of Nottingham, University Park, Nottingham, NG7 2RD, UK

Correspondence to: Hanno Meyer (hanno.meyer@awi.de)

Abstract. Oxygen isotopes in biogenic silica ($\delta^{18}O_{BSi}$) from lake sediments allow for quantitative reconstruction of past hydroclimate and proxy–model comparison in terrestrial environments. The signals of individual records have been attributed to different factors, such as air temperature (T_{air}), atmospheric circulation patterns, hydrological changes, and lake evaporation. While every lake has its own local set of drivers of $\delta^{18}O$ variability, here we explore the extent to which regional or even global signals emerge from a series of paleoenvironmental records. This study provides a comprehensive compilation and combined statistical evaluation of the existing lake sediment $\delta^{18}O_{BSi}$ records, largely missing in other summary publications (i.e. PAGES network). For this purpose, we have identified and compiled 71 down–core records published to date and complemented these datasets with additional lake basin parameters (e.g. lake water residence time and catchment size) to best characterize the signal properties. Records feature widely different temporal coverage and resolution ranging from decadal–scale records covering the past 150 years to records with multi–millennial scale resolution spanning glacial–interglacial cycles. Best coverage in number of records (N=37) and datapoints (N=2112) is available for northern hemispheric (NH) extra–tropic regions throughout the Holocene (roughly corresponding to Marine Isotope Stage 1; MIS 1). To address the different variabilities and temporal offsets, records were brought to a common temporal resolution by binning and subsequently filtered for hydrologically open lakes with lake water residence times <100 yrs. For mid– to high–latitude (>45° N) lakes, we find common $\delta^{18}O_{BSi}$ patterns among the lake records during both Holocene and Common Era (CE). These include maxima and minima corresponding to known climate episodes such as the Holocene Thermal Maximum (HTM), Neoglacial Cooling, Medieval Climate Anomaly (MCA) and the Little Ice Age (LIA). These patterns are in line with long–term air temperature changes supported by previously published climate reconstructions from other archives as well as Holocene summer insolation changes. In conclusion, oxygen isotope records from NH extratropic lake sediments feature a common climate signal at centennial (for CE) and millennial (for Holocene) time scales despite stemming from different lakes in different geographic locations and, hence, constitute a valuable proxy for past climate reconstructions.

1 Introduction

1.1 Scientific background

Oxygen isotopes are ubiquitous within the global water cycle and are among the best (hydro)climate proxies worldwide as a result of their potential quantitative interpretability. The most abundant isotope ^{16}O and the rarer isotope ^{18}O are subject to fractionation during water phase transformation and transport processes (Fig. 1). As a result, the relative abundance of these isotopes varies across space, time, and reservoirs. The IAEA's standard Vienna Standard Mean Ocean Water (VSMOW) serves as a baseline, closely resembling the isotopic composition of modern seawater. Relative abundance of ^{18}O with regard to ^{16}O is expressed relative to the VSMOW standard as $\delta^{18}O$ and given in units of permil.

Measuring $\delta^{18}O$ in water, vapor, snow and ice allows for quantifying hydroclimatic processes in the global water cycle and has been used to this end for many decades (Dansgaard, 1964; Konecky et al., 2020). In addition to its use in present–day hydrology, $\delta^{18}O$ in environmental archives also serves as a powerful proxy for past hydrology and, in turn, climate. As such, $\delta^{18}O$ is a crucial and quantitative tool for both reconstructions of past climate and for comparison of proxy data to climate–model outputs.

Oxygen isotope records are available from different paleoenvironmental archives e.g. in glaciers and ice sheets (Andersen et al., 2004), permafrost (Meyer et al., 2015b), marine (Spielhagen and Mackensen, 2021) and lacustrine (Leng, 2006) environments as well as different materials, such as carbonates (Kwiecien et al., 2014), silicates (Leng, 2006), biomarkers (Lasher et al., 2017), cellulose (Wolfe et al., 2007), glacier ice (Andersen et al., 2004) and ground ice (Opel et al., 2017). Therefore, oxygen isotopes offer the possibility for directly comparing data from different paleoenvironmental archives.

The predictability of isotope fractionation processes in the water cycle due to clear physical constraints allows for using $\delta^{18}O$ not only as a quantitative tool for past (hydro)climate reconstructions, but also for implementing $\delta^{18}O$ in global climate models (e.g. Danek et al. 2021). However, challenges persist in understanding and comparing data and model outputs, partly due to complex signal formation in environmental archives (Danek et al., 2021).

Lake sediments are prominent and widespread archives in terrestrial environments (Leng, 2006; Biskaborn et al., 2016; Subetto et al., 2017). Like glaciers and ice caps, lakes may record the isotopic signature of past precipitation (Shemesh et al., 2001a). The signal formation in lakes, however, is fundamentally different from that in glaciers and ice caps, with the lake water body acting as a buffer of the enclosed (hydro)climate signal, influenced by factors such as catchment hydrology, lake ontogeny, and sediment accumulation rates (Bittner et al., 2021). While biogenic silica is also found in phytoliths, sponge spicules and chrysophytes, this study focuses exclusively on diatoms. Diatoms are microscopic algae that synthesize their frustules from lake water and the silica dissolved therein, thereby preserving the isotope signal of past lake water. The oxygen isotope composition of the biogenic silica of diatom frustules ($\delta^{18}O_{BSi}$) buried in lake sediment therefore provides valuable insight on past lake water and, in turn, precipitation.

Naturally, the interplay of hydrological and sedimentological processes limits the time span and resolution over which environmental information can be obtained from a lake system, and this varies from lake to lake. Most commonly, $\delta^{18}O_{BSi}$ has

been applied to lake sediments devoid of carbonates. These lakes are especially common in high altitude and high latitude regions (Leng and Barker, 2006).
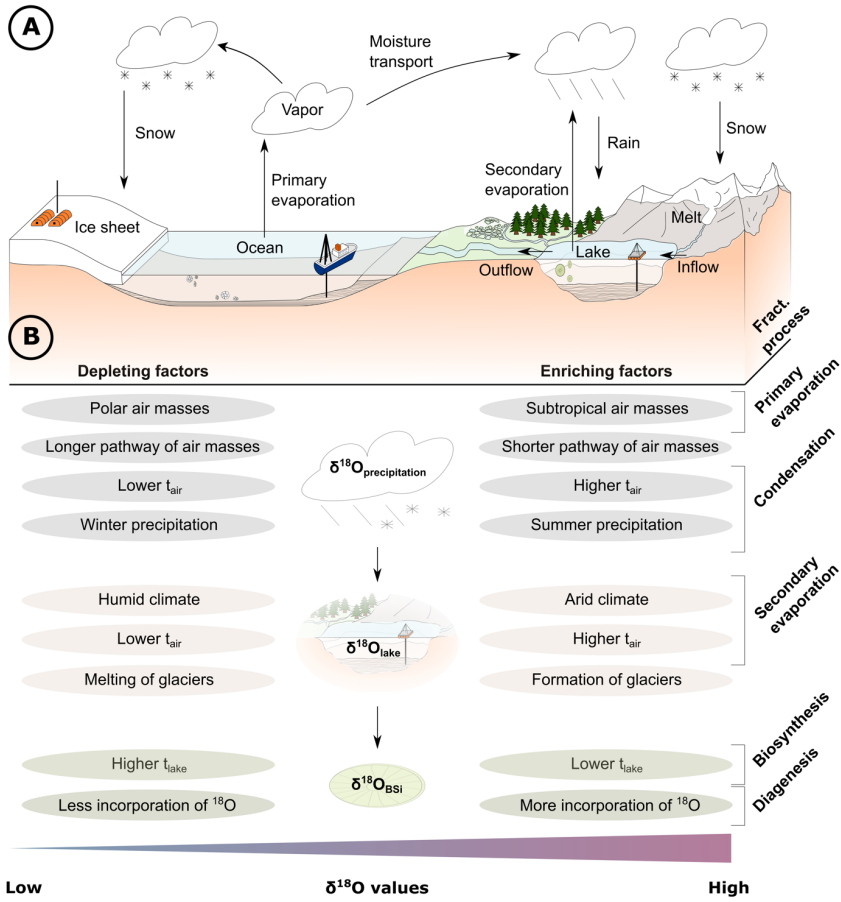
130 **Figure 1. Schematic overview of select reservoirs and processes within the global water cycle influencing the $\delta^{18}O_{BSi}$ signal of records. (a) Overview of the global water cycle with reservoirs and processes. (b) Depleting and enriching factors influencing $\delta^{18}O$ values in precipitation, lake water, and biogenic silica. Corresponding fractionation processes are indicated on the right-hand side.**
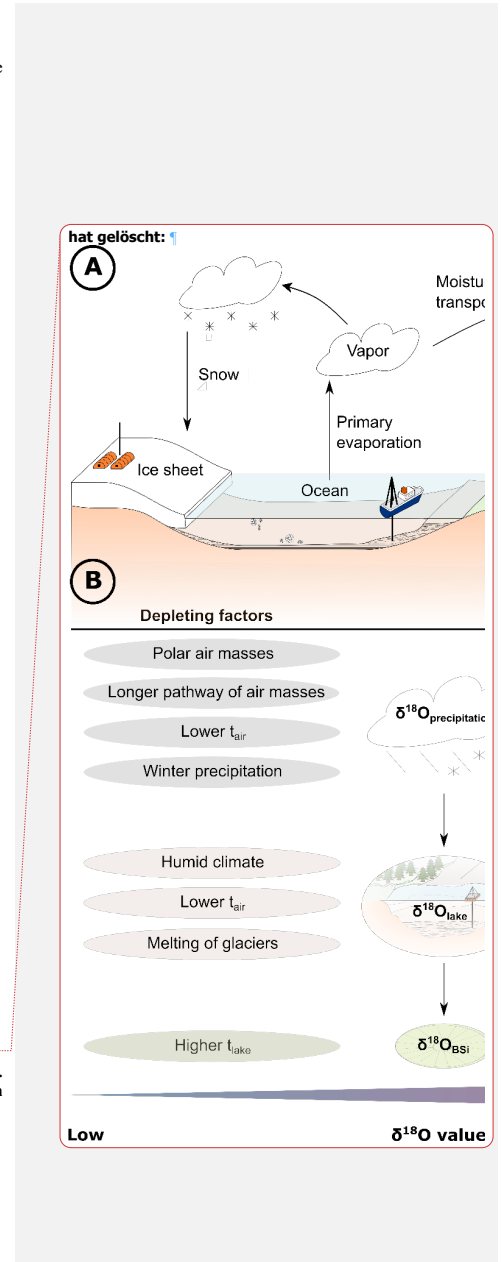
1.2 Controls on $\delta^{18}O_{BSi}$

Due to the complex signal formation in $\delta^{18}O_{BSi}$ records, most authors refer to a combination of factors for interpreting any given individual record. A schematic overview of some of the main processes is provided in Fig. 1 and by Leng and Barker (2006). Lake water temperature (T_{lake}) imparts a direct effect on $\delta^{18}O_{BSi}$ due to temperature–dependent fractionation during biosynthesis of biogenic silica. Temperature–dependent fractionation coefficients were initially determined for marine environments (Leclerc and Labeyrie, 1987; Matheney and Knauth, 1989) and later estimated for lacustrine sediments as ca. – 0.2‰/°C during biosynthesis (Dodd and Sharp, 2010; Moschen et al., 2005). However, the applicability of these calibrations to sedimentary records is debated due to possible disequilibrium between diatom frustules and lake water, as well as taphonomic and diagenetic processes (Leng and Barker, 2006; Ryves et al., 2020; Smith et al., 2016; Tyler et al., 2017).

More commonly, changes in $\delta^{18}O_{BSi}$ are attributed to $\delta^{18}O$ changes of lake water ($\delta^{18}O_{lake}$) and thereby, with the lake as a buffer, to the isotopic composition of precipitation ($\delta^{18}O_{precipitation}$). Locally, $\delta^{18}O_{precipitation}$ is primarily influenced by air temperature (T_{air}) with a fractionation of 0.7‰/°C on global average (Dansgaard, 1964). On a broader scale, parameters such as precipitation, moisture source and air-mass trayectory patterns are important, and changes in $\delta^{18}O_{BSi}$ records may be indicative of shifting atmospheric circulation patterns (Bailey et al., 2015), that affect the local ratio of precipitation to evaporation (P/E). The parameter P/E refers to the balance between the amount of precipitation and evaporation within a lake's catchment. Typically, water loss through evaporation leads to higher $\delta^{18}O_{lake}$ values due to evaporative enrichment, and therefore higher $\delta^{18}O_{BSi}$. Precipitation amount and seasonality (e.g., rain vs. snow) will also strongly impact the isotope signal of the lake water (Meyer et al., 2022). Disentangling the effects of precipitation and evaporation in $\delta^{18}O_{BSi}$ records is thus a major challenge and therefore some authors commonly refer to P/E–changes in conjunction with other factors (Hernandez et al., 2013; Rosqvist et al., 2013; Broadman et al., 2020a).

Shemesh et al. (2001a) have attributed the $\delta^{18}O_{BSi}$ signal changes of Lake 850 in Swedish Lapland to different contributions of main source regions of precipitation, namely the Atlantic and Arctic Oceans. Indeed, for this location, changes in atmospheric circulation patterns imply changes in both, T_{air} and humidity.

Additionally, $\delta^{18}O_{precipitation}$ may also be linked to shifts in the seasonality of precipitation (Swann et al., 2010; Kostrova et al., 2016; Harding et al., 2020), which is linked to T_{air} change, but also atmospheric circulation patterns (Shemesh et al., 2001a; Jones et al., 2004; Leng et al., 2005; Rosqvist et al., 2013) and, on longer timescales, insolation (Swann et al., 2010; Kostrova et al., 2019; Kostrova et al., 2021). T_{air} as often inferred from $\delta^{18}O_{BSi}$ can, therefore, be a parameter with local, regional and global significance.

Insolation is not an environmental parameter that can be inferred from $\delta^{18}O_{BSi}$ records. It is, however, commonly used as an explanatory variable and underlying driver of Holocene climate change. Insolation can be calculated for any given place throughout time (Laskar et al. 2004), which allows for direct comparison with $\delta^{18}O_{BSi}$ time series. Insolation primarily influences T_{air} and, indirectly, the P/E balance and atmospheric circulation patterns.

Moreover, hydrological processes within a lake's catchment may substantially impact $\delta^{18}O_{lake}$ and hence, $\delta^{18}O_{BSi}$. Some of these processes are closely linked to climate and precipitation patterns described above. Most notable are variations in the amount of snow melt (Mackay et al., 2013; Rosqvist et al., 2013; Meyer et al., 2022) and glacial influx (Meyer et al., 2015a) to a lake. Glaciers or snow fields in the hinterland, may provide more melt (with lower/depleted $\delta^{18}O$) in warm phases – and may counter the influence of warming on $\delta^{18}O_{precipitation}$ (Meyer et al., 2015a).

Other hydrological processes, however, are only indirectly linked to climate. These include the formation and closure of outflows to the lake which change the lake's hydrological setting (Hernandez et al., 2008; Vyse et al., 2020; Bittner et al., 2021). Associated changes in the mass–balance of a lake, and, thus P/E–balance, may lead to a different $\delta^{18}O_{BSi}$ signal. Within the lake itself, long-term diagenetic effects on diatoms include recrystallisation and incorporation of heavier ^{18}O from silanol bonds into the Si-O-Si crystal lattice – a process that may increase the original $\delta^{18}O_{BSi}$ signal (cf. Akse et al., 2022; Fig. 1). However, despite notable recrystallisation, Chapligin et al. (2012b) found no significant diagenetic effect in records spanning the past 250 kyr.

To interpret a given $\delta^{18}O_{BSi}$ record, information about the present hydrology is thus important as it provides insight on which processes influence $\delta^{18}O_{lake}$ and, in turn, $\delta^{18}O_{BSi}$. Naturally, as the hydrology of a given lake can only offer snapshots of present–day constraints, caution has to be applied when extrapolating these into the past. The isotopic composition of three components is of interest for assessing the signal properties of $\delta^{18}O_{BSi}$ records: (1) $\delta^{18}O_{lake}$, (2) $\delta^{18}O$ of inflows to the lake, and (3) $\delta^{18}O_{precipitation}$. The lake water composition can provide insight on whether lake water is isotopically homogenous, both spatially and at different depths of the lake basin. Offsets of $\delta^{18}O_{lake}$ from the Local Meteoric Water Line (LMWL) give hints as to whether or not lake evaporation may have had a significant effect on lake water isotopic composition. $\delta^{18}O_{lake}$ can also be used in conjunction with T_{lake} and the most recent $\delta^{18}O_{BSi}$ value for testing the temperature–dependent fractionation and, in turn, the applicability of the proxy for paleoclimate reconstructions (cf. Meyer et al. 2015a). Complementary isotope measurements of lake inflows (i.e. rivers, streams) provide further information on specific hydrological constraints. For larger lakes and catchments, the different inflows and their effect on the lake's isotopic mass balance have been used for inferring changing hydrology or precipitation regimes in different parts of the catchment (e.g. Mackay et al. 2011). Additionally, while $\delta^{18}O_{precipitation}$ data are critical for constraining modern climate-isotope relationships, they are often not available and only few monitoring studies of $\delta^{18}O_{precipitation}$ and $\delta^{18}O_{lake}$ in combination with $\delta^{18}O_{BSi}$ exist (Kostrova et al., 2019; Hernandez et al., 2010). A possible alternative can be derived from the GNIP database (IAEA/WMO, 2022) and spatial interpolations thereof, e.g. The Online Isotopes in Precipitation Calculator (Bowen, 2017).

1.3 Sample preparation and measurement

Extracting pure diatom valves (frustules) from lake sediments is a complex process and depends on a sufficiently high diatom concentration in the sediment. Various cleaning procedures for diatom extraction exist, which are mainly based on the use of H_2O_2 for removing organic matter from the sediment and HCl for the removal of carbonate (Chapligin et al., 2012a). Detrital

components are often separated through centrifugation in heavy liquid solution (i.e. sodium polytungstate) at variable specific densities (Morley et al., 2004; Chaplygin et al., 2012a). Different procedures in sample preparation, i.e. different temperatures, may result in offsets of measured $\delta^{18}O_{BSi}$ (Swann et al., 2010; Chaplygin et al., 2012b; Tyler et al., 2017). Impurities due to incomplete removal of detrital components may also affect the measured $\delta^{18}O_{BSi}$ (Lamb et al., 2005; Chaplygin et al., 2012b). To account for this, the purity of samples is usually assessed prior to measurement by visual inspection or direct measurement of the amount of contaminants of a given sample (Bailey et al., 2018; Broadman et al., 2020a). Fewer studies determine the isotopic composition of detrital contaminants to apply a correction to the measured $\delta^{18}O_{BSi}$ values (Brewer et al., 2008; Mackay et al., 2011; Wilson et al., 2014a; Bittner et al., 2021; Kostrova et al., 2021). Consequently, caution has to be applied when comparing absolute values of different individual $\delta^{18}O_{BSi}$ records, as offsets between individual records may result from both different preparation and measurement techniques, as well as regional differences in $\delta^{18}O_{lake}$. The potential and challenges associated with data stemming from different preparation and measurement techniques have already been addressed (Chaplygin et al., 2011; Mackay et al., 2011).

1.4 Aim of this work

A comprehensive compilation and assessment of the lacustrine $\delta^{18}O_{BSi}$ records published to date is missing. Due to the crucial role of lake and catchment hydrology in signal formation, such a compilation needs to include individual lake basin parameters, such as lake volume and water residence time (t_{res}), to provide reliable constraints for interpreting and comparing the individual records. Proxy data compilations have already addressed a lack of standardized metadata, data availability and data uniformity of paleo–data (Pfalz et al., 2021). However, such compilations generally do not include $\delta^{18}O_{BSi}$ records and their associated lake basin parameters (Kaufman et al., 2020), or instead they have a limited temporal focus (Konecky et al., 2020). Consequently, no study has yet empirically linked the signal properties of $\delta^{18}O_{BSi}$ records and lake basin parameters in a harmonized dataset.

To overcome these gaps, this paper aims at providing a comprehensive compilation and combined statistical evaluation of all lake sediment $\delta^{18}O_{BSi}$–records published to date (between 1998 and 2022). We accomplish these objectives by means of the following working steps: 1) collecting available lake sediment $\delta^{18}O_{BSi}$–records published to date, 2) complementing these records with the individual lake basin parameters and, 3) assessing the signal properties of $\delta^{18}O_{BSi}$ records with regard to lake basin parameters, and 4) identify spatio–temporal patterns and trends in the $\delta^{18}O_{BSi}$ signals. This effort leads to a better understanding of the general constraints for interpreting lake sediment $\delta^{18}O_{BSi}$ records, whilst making these records more readily usable for future studies including proxy–model comparisons. It is, hence, a contribution to bridge the gap between modelling and isotope geochemistry approaches in paleoclimate science.

2. Methods

This study follows a three–stage approach: the first stage (data acquisition) comprises identifying lacustrine $\delta^{18}O_{BSi}$ datasets and publications published to date. A second stage includes acquiring the actual $\delta^{18}O_{BSi}$ datasets and archiving them in a standardized format. Where appropriate, the identified published datasets were arranged into longer continuous records. This includes records from the same sediment core published in different manuscripts, and records from different sediment cores from the same lake but similar locations. The third and final stage (record analysis) interprets the lacustrine $\delta^{18}O_{BSi}$ isotope records with respect to their hydrological and geographical constraints in order to identify possible common global or hemispheric trends and signal properties of all isotope records, as well as smaller spatially or temporally constrained datasets. Identification and acquisition of the datasets and publications in this work followed an additive approach, i.e. thorough literature survey. We have chosen this approach due to the limited number of laboratories and working groups worldwide measuring $\delta^{18}O_{BSi}$. In this study, we focused exclusively on down–core records from lacustrine sediments. Identified publications and datasets were entered into a uniform metadata table giving one entry to each publication and each dataset. If more than one publication was written about the same sediment core, each of these publications were given a separate entry. Likewise, if one publication presents data from more than one sediment core, each of the sediment cores were given a separate entry to the database.

For each of these entries, metadata on coring procedure, hydrological setting and chronology were supplemented. Data were extracted from the corresponding publication(s), from public repositories or directly from the authors. Hydrological parameters such as catchment area, average depth and t_{res} were additionally obtained from the HydroLAKES database (Messager et al., 2016) and stored as separate variables. For a detailed description on how the values in the HydroLAKES database were created, we refer to Messager et al. (2016). This procedure was necessary because original publications do not always specify all of these parameters and because parameters supplied in original publications may not be consistent. For further analysis and for linking the individual isotope records with lake basin parameters, the HydroLAKES database entries were given preference. Original publications were only used for lakes where no data were available from the HydroLAKES database. The parameter "maximum water depth" was always taken from the original publications since this parameter is not provided by the HydroLAKES database. While the geo–statistical approach of the HydroLAKES database may not provide the most precise values for individual lake basin characteristics, it ensures comparability among the different lake basins analyzed in this study. Therefore, and because some parameters (i.e. catchment size) are not essential to the discussion in this manuscript, we have chosen this approach favouring consistency over more data points. It also prevents potential issues arising from different authors providing conflicting values for the same lake basin (i.e. Lake Baikal, Lake El'gygytgyn).

Isotope datasets for each of the entries were archived in separate tables that specify depth, age and measured isotope values. Datasets were taken directly from the respective publication, where possible. If datasets were not available, within the original publications or their supplements, public repositories (e.g., www.pangaea.de; ncei.noaa.gov) were searched. In instances where datasets were unavailable from repositories, the lead authors were contacted directly. In case of published data unavailable

from repositories or authors, plots of the original publications were digitized, if possible (Rietti-Shati et al., 1998; Hu and Shemesh, 2003). Where digitizing plots was not feasible, records were excluded from further consideration; this was the case for Chondrogianni et al. (2004) and Hu et al. (2003).

Chronologies were adapted from the original publications, where available and stored in cal yrs BP format (relative to 1950 CE). Sample ages given in different formats (e.g. b2K or CE) were converted to cal yrs BP. This procedure also applies to radiocarbon–based chronologies. Chronologies were not recalculated because the effect of different ^{14}C–calibrations and different age model approaches is presumably minor with regard to the aim of this study. This is especially true when considering the fact that high–resolution datasets (annual to decadal resolution) are the exception among all datasets identified. The error introduced by the different age models is, thus, considered minor when compared to the resolution of the datasets. For applications requiring more precise chronologies and better comparability of datasets, we provide the radiocarbon measurements of respective datasets as well. This enables future users to create tailor–made chronologies if needed. Datasets without chronologies were stored using depth notation only.

For further analysis, datasets were partly regrouped and combined to generate longer continuous $\delta^{18}O_{BSi}$ datasets, herein referred to as «records». This comprised treating datasets with data from several coring sites or outcrops from the same lake as one single record, in agreement with the author's original interpretation (Quesada et al., 2015; Swann et al., 2018). Data stemming from the same sediment core but published in different manuscripts were combined into single continuous records. This applies to records from Lake Kotokel (Kostrova et al., 2013a; Kostrova et al., 2013b; Kostrova et al., 2014; Kostrova et al., 2016) and Lago Chungará (Hernandez et al., 2008; Hernandez et al., 2010; Hernandez et al., 2011; Hernandez et al., 2013). Likewise, data from different cores presented in different publications but stemming from identical or reasonably similar coring sites were combined to single records. This applies to data from Lake Nar (Dean et al., 2018) and Vuolep Allakasjaure (Rosqvist et al., 2004; Jonsson et al., 2010). Lakes consisting of several basins were generally treated as one, such as Lake Baikal and several smaller lakes.

For trend analysis and inter-comparison, we focused primarily on the Holocene and Common Era climate using records from northern hemisphere (NH) extratropic lakes (45–90° N) due to there being the highest spatial-temporal coverage of data, with a significant number of records which makes an interpretation departing from case studies feasible.

In a first step, records were binned to 1-kyr intervals (for the Holocene) and 200-year intervals (for the CE), respectively. These intervals were chosen based on the temporal resolutions of the original records in order to ensure continuous binned records with no empty bins. Choosing higher resolutions would have resulted in many records having empty bins with no datapoints, thus leading to different temporal resolutions even after binning. The binning was done by calculating the mean value of all samples within the respective age interval for each individual record. Datapoints with ages <150 yrs BP were excluded from the Holocene analyses to eliminate any possible effects of recent warming, though these data were retained for analysing the Common Era. To assess the timing of Holocene maxima and minima, records covering less than 10 bins were discarded. To evaluate Holocene and Common Era trends in $\delta^{18}O_{BSi}$, records covering less than seven bins were excluded from

the analysis (i.e., <7.0 and 1.4 kyrs, respectively). Obviously, the missing bins in both Holocene and Common Era compilations might have an effect on the mean value of the individual records, but not on the overall trend.

In order to eliminate offsets between individual binned records, the remaining records were standardized by subtracting their respective means. After this mean removal, two subsequent filtering steps were performed in order to exclude records most prone to secondary lake evaporation. First, a subset consisting only of records from open lakes was created, discarding records from semi–closed lakes, closed lakes and paleo–lakes. In a second step, this open–lakes–subset was filtered by discarding all records with t_{res}>100 years. This threshold was chosen in accordance with previous works classifying lakes and their isotopic signals with respect to hydrologic setting and t_{res} (Leng and Marshall, 2004).

After applying these filters, combined trends for geographical regions (NH, Eurasia, North America) were evaluated by calculating the mean of all records for each bin, in each respective region.

3. Results

3.1 Published datasets

Following a thorough literature survey, a total number of 71 published down–core datasets of $\delta^{18}O_{BSi}$ from 64 sites have been identified. Since the first published lacustrine $\delta^{18}O_{BSi}$ studies in 1998 (Rietti-Shati et al., 1998; Shemesh and Peteet, 1998), there has been a growing research interest and number of publications (Fig. A1). Only recently has there been a stagnation of the number of records published. A detailed overview of the identified publications and the records presented therein is provided in Tab. A1.

Most publications present the $\delta^{18}O_{BSi}$ data as time series, as is usual in paleoenvironmental studies. The chronologies rely on a wide variety of dating methods (Fig. A2), with ^{14}C (used on 46 records) being by far the most frequent. For subrecent time periods and shorter time scales, ^{210}Pb and ^{137}Cs are also used extensively (on 21 and 12 records, respectively). Globally or regionally correlated time markers such as tephra layers (Heyng et al., 2015) or high–resolution methods such as varve counts (Rozanski et al., 2010) are used relatively sparsely as they are not available for all time periods and/or lake basins.

3.2 Combined records

We combined separate records from the same lake sites to longer, continuous composite records, giving a total of 53 combined $\delta^{18}O_{BSi}$ records. Six of these are from paleolakes (three with/without chronology), while 47 records stem from extant lakes (42 with and five without chronology). An overview of these combined records is provided in Tab. A2, complemented by metadata of the records and the corresponding lake basins. Each individual record received a number (#X; Tab. A2, column 1; Tab. A1, last column) which is used consistently throughout the text.

The temporal coverage of these combined records (Fig. 2) varies from centennial–scale at Laguna Zacapu (#50, Leng et al., 2005) and a specific study at Lake Baikal (#51, Swann et al., 2018), to glacial–interglacial cycles e.g. 250 kyr at Lake

El'gygytgyn (#3, Chapligin et al., 2012b). Most records (N=32) cover the last several thousand years up to about 10 kyr BP, while only a few records cover several tens of thousands of years (e.g., #8 to #10). Likewise, the time periods covered do vary either due to the availability of lake sediments, diatom abundances in a lake and/or scientific foci of the research groups. By far the highest number of records is available for the Holocene (0-11.7 kyr BP; N=37) and especially for the last 2 kyr BP (N=48). Further back in time, Marine Isotope Stages (MIS) were used for assessing data coverage throughout time. Boundaries between MIS are according to Lisiecki and Raymo (2005). MIS 2 is still covered by 19 records, whereas towards MIS 3 (N=5) and beyond fewer records have been generated. However, single records cover even older time periods in MIS 11 (at Lake Baikal; #2) and beyond (MIS G1/104, #1), outlining the applicability of this proxy across a wide range of time scales. A paleo lake from the Baringo–Bogoria Basin (#1), is the oldest lacustrine $\delta^{18}O_{BSi}$ record and has been dated to the onset of MIS 104 in the late Pliocene (Wilson et al., 2014b).

Regarding the number of published records by continent (Fig. 3), there is a clear concentration on Asia and Europe with 21 and 15 records published, respectively. In Asia, there is a strong regional focus on Siberia, whereas most other parts of the continent are yet to be investigated using lake sediment $\delta^{18}O_{BSi}$. A regional focus also occurs in Africa and South America. While a sizeable number of records stemming from these continents have been published (N=10 and N=11, respectively), there are pronounced regional foci in the East African Rift and the Andes, respectively. Another focus region is Alaska, where most (N=6) of the published North American records (N=7) are located. $\delta^{18}O_{BSi}$ work has also been carried out in lakes from New Zealand (#42) and South Georgia (#19).

In summary, the distribution of available $\delta^{18}O_{BSi}$ data displays a bias towards the mid– to high latitudes of the northern hemisphere. Additionally, this distribution is also indicative of the site accessibility and (regional) research foci of the working groups. This has a rather pronounced effect on the spatial distribution of available $\delta^{18}O_{BSi}$ records. The geographical distribution is also indicative of cold regions devoid of carbonates where biogenic silica is the most promising archive to obtain oxygen isotope records from lake sediments. Moreover, high northern latitudes have by far the highest abundance of total area of water bodies (Downing and Duarte, 2009). Yet, it also accounts for the relatively lower number of northern records extending beyond MIS 1, as vast ice sheets covered much of the NH high-latitudes (e.g., Patton et al., 2016).

This pattern also affects the latitudinal distribution of the records (see also Tab. A2) with records ranging from 54.17 °S (#19) to 69° N (#39). Records stemming from low–latitude lakes (particularly in Africa and South America) are often located at high altitudes above 3000 m asl (above sea level; e.g., #11, 17, 18, 21). Lake Simba Tarn (record #34) features the maximum altitude for an individual $\delta^{18}O_{BSi}$ record of 4959 m asl. Altitudes below 1000 m asl, however, are most common (N=36), especially for high–latitude lakes. In total, 12 lakes are located below 100 m asl (e.g., #29, 35). Many of these low–altitude lakes are located in maritime locations in immediate proximity to the coast (e.g., #19, 30), or have even had marine intrusion stages in the past (a postglacial transgression at Nettilling Lake; #41). Extremely continental environments are tackled in central and eastern Siberia and the Lake Baikal region (e.g., #4, 8, 9, 10, 25).
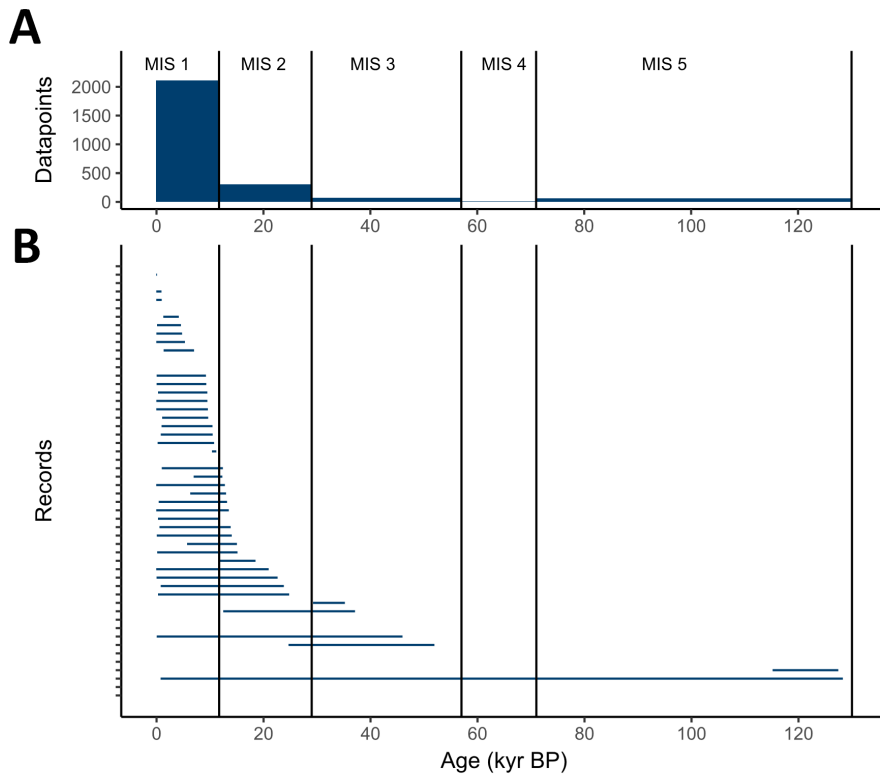
Figure 2. Temporal coverage by records and datapoints during MIS 1 – MIS 5. **Boundaries between MIS according to Lisiecki and Raymo (2005): MIS 1-2: 14kyr; MIS 2-3: 29kyr, MIS 3-4: 57 kyr, MIS4-5: 71 kyr, MIS 5-6: 130 kyr.** **a)**

Total number of datapoints available during each Marine Isotope Stage. b) Temporal coverage of records from young to old .
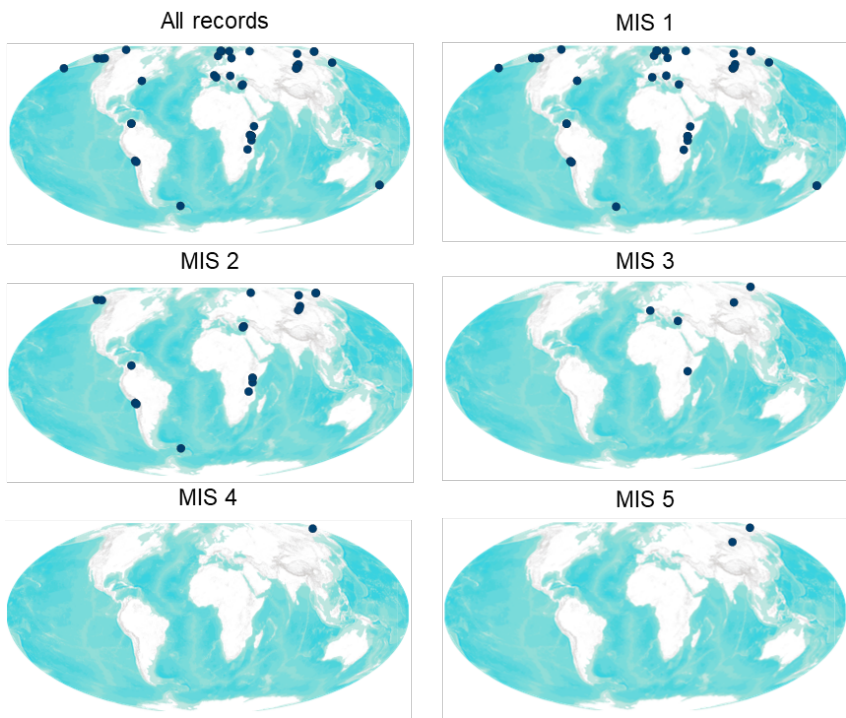
Figure 3. World map depicting the locations of $\delta^{18}O_{BSi}$ records with chronology. Note that one location may correspond to more than one records. ©ESRI 2022

3.3 Spatial coverage and resolution of combined records

Varying spatial resolution among the compiled isotope records is linked to the fact that lakes and their corresponding catchments are not points in space but areas. Consequently, lake water and the related $\delta^{18}O_{BSi}$–signal represent a spatial average, integrated over the catchment size of each respective lake. Lake surface areas range from small ponds of <1 km² (e.g., #19, 11, 23, 33, 34) to some of the largest lakes in the world, including Lake Malawi and Lake Baikal covering 29,544 km² and 31,968 km², respectively (Fig. 4A). Large and voluminous lakes are the exception, however, and most of the lakes represented here are <10 km² in size (N=25). Note that such parameters are not applicable to paleo lakes. While some authors provide estimates on paleo lake extent, these figures are not consistent with the values determined for present lakes and are therefore not included in the evaluation of the dataset. Catchment sizes vary by several orders of magnitude as well. For small lakes, catchments are often <10 km² (N=13; e.g., #22, 33, 37), whereas the largest lakes, Lake Malawi and Lake Baikal feature catchments of 128,727 km² and 569,176 km², respectively (Fig. 4A). Therefore, these lakes integrate the environmental signal over a large and potentially diverse hydrological region. While most of the lakes compiled in this study are primarily fed by surface runoff and/or precipitation (according to the original publications of records), groundwater influx may also play a pivotal role by introducing a large memory effect of past precipitation due to the generally long residence times of aquifers. This may have an impact on records especially when looking at short timescales. Groundwater input, however, is usually not accounted for and is thus beyond the scope of our study. In summary, both lake and catchment sizes vary by several orders of magnitude (Fig. 4A) among the sites with existing $\delta^{18}O_{BSi}$ records, and span from local signals to regional averages. However, most of the records (N=18) stem from lakes with catchments <100 km², suggesting rather local signals. While single local signals represent small areas, different local signals may well correlate on continental and hemispheric scales.

Figure 4. A) Depiction of corresponding lake and catchment sizes of the records compiled within this study. One lake may correspond to more than one record. Note that records from paleo-lakes and lakes with incomplete information on lake and catchment size were not considered for this figure (N=33). B) Depiction of corresponding sampling intervals and t_{res}. Note that records from lakes without information on t_{res} were not considered for this figure (N=37).

3.4 Temporal resolution of combined records

Temporal resolution of the records and the resulting signal properties are determined by both the lake basin itself (i.e. accumulation rates and preservation of diatom silica) and the sampling routine applied to the sediment core (i.e. the sampled intervals as well as the thickness of individual samples). Data on the thickness of single sediment samples taken from the cores are, however, scarce in the original publications. The same applies for information on the time interval or number of years represented by a single sediment sample. Consequently this parameter and its potential effect on the records' signal properties could not be investigated in detail in this manuscript. We therefore focus on t_{res} and sampling frequency of a core as a means of characterizing the records and their temporal resolution.

The t_{res} is closely linked to the size of lake basins and varies accordingly. It ranges from several weeks for small lakes (e.g., #49, 50) to centuries (219 and 375 years for Lake Malawi and Lake Baikal, respectively). On the whole, t_{res} of sub–annual to annual scale are most common (N=17) among the lakes considered in this study (Fig. 4B). It should be noted that longer t_{res} leads to averaging of the signal over a longer time period. Likewise, different t_{res} may also have an effect on absolute $\delta^{18}O_{BSi}$ values and variabilities. Lakes with very long t_{res} (t_{res}>100 years) are more susceptible to lake evaporation, and may effectively behave like closed–system lakes with regard to the $\delta^{18}O_{BSi}$ signal even if they are hydrologically open (i.e. have outflows). These are still referred to as hydrologically open in this work and hydrological settings and t_{res} are addressed separately in the discussion.

560

565

570

575

hat gelöscht: s

hat gelöscht: Paleo

hat gelöscht: coverage and

hat gelöscht: tendentially

Also the sampling frequency varies by several orders of magnitude (Fig. 4B). It stretches from annual to multi–millenial
timescales. Consequently, the signal properties and the recorded climatic and/or hydrological forcings of the identified records
can be expected to vary accordingly. Most records, however, plot in the top left half of graph of Fig. 4B, which indicates that
the temporal offset between two sediment samples exceeds t_{res}. This suggests that the sampling routine is the limiting factor of
the temporal resolution of these records. Only three records from Lake Baikal plot in the lower right half of Fig. 4B, suggesting
in these cases (#4, #20, #51) t_{res} to be the dominant factor in determining the record's resolution, at least with respect to inflow–
related changes.

We thus conclude that the sampling resolution is the main factor determining the temporal resolution of most records, with t_{res}
acting as an additional smoothing mechanism. A lake with a centennial–scale t_{res} can, therefore, display centennial–scale
changes of climate and hydrology to their full amplitude. Decadal–scale changes, on the other hand, can be expected to be
attenuated by an order of magnitude in a lake with centennial–scale t_{res}. When t_{res} is lower than the sampling frequency, the
hydroclimatic amplitude is also not fully captured (Richter and Turekian, 1993). It should be noted that temporal resolution is
non-uniform across the records, with generally higher resolution for more recent time intervals (Figs. 2 and 5A) that – in
addition to a sampling bias – may, in part, reflect increasing lake sediment compaction with depth and time. Based on t_{res} and
sampling resolutions of the records, comparing records on a centennial or millennial scale is the most promising approach for
assessing common patterns.

4 Discussion

4.1 Common Era Climate

For analysis of Common Era climate, only datapoints from 0 CE until today (corresponding to 1950 to -73 yrs BP) were
selected. The Common Era subset of records includes only records stemming from sites north of 45° N (Fig. 5A, N=19) and
comprises 460 datapoints. The records display considerable offsets with $\delta^{18}O_{BSi}$ values ranging from +19‰ (#34) to +33‰
(#35) VSMOW. These offsets can be linked to their individual environmental setting, e.g. latitudinal and continentality effects,
as well as to their potential to be prone for lake evaporation. Amplitudes in $\delta^{18}O_{BSi}$ of CE records vary from 0.4‰ (#24) to ca.
9‰ VSMOW (#35). This variability might correspond to their different hydrological settings. Closed lakes (such as Sunken
Island Lake; #26) have a tendency towards higher $\delta^{18}O_{BSi}$ amplitude due to evaporative enrichment of the lake water (Broadman
et al., 2020b).

Binned records (Fig. 5B, N=14) do not display any common pattern and feature $\delta^{18}O_{BSi}$ values ranging from +20‰ to +31‰
VSMOW. However, binning of datapoints and exclusion of shorter records reduces the $\delta^{18}O_{BSi}$ amplitudes of individual records
to less than 5‰. Offsets between individual records may be linked to site–specific characteristics of individual lakes and
catchments, as well as latitudinal and continentality effects.

After mean removal (i.e., standardization; Fig. 5C), the CE data suggest a common trend with higher $\delta^{18}O_{BSi}$ values at 1900 yrs BP and a general decrease until the present with the lowest values occurring in the last 400 years (two bins). Some records also show maxima between 500 and 1100 yrs BP and minima at ca. 1300 yrs BP. The subsets for hydrologically open lakes (N=13, Fig. 5D) and hydrologically open lakes with t_{res}<100yrs (N=9, Fig. 5E) show a similar pattern.

The combined CE records (Fig. 5F) comprise 8 records and show a general $\delta^{18}O_{BSi}$ decrease over the last 2 kyr amounting to ca. 2‰ VSMOW (slope: ~1‰/kyr). The $\delta^{18}O_{BSi}$ amplitude within individual bins, however, might exceed this number, most notably at 100, 1300 and 1900 yrs BP, which show the highest amplitudes of up to 5‰ for the CE. This is in line with differences between the timing of $\delta^{18}O_{BSi}$ maxima and minima between North American and Eurasian records. At centennial scale, these differences might also be linked to dating uncertainties. Moreover, the record of Lake Bolshoye Shchuchye (#16) features a much larger amplitude. Its exceptional $\delta^{18}O_{BSi}$ variability has been attributed to variations in snow and snow melt in the lake's catchment and therefore does represents a different kind of precipitation-based signal compared to most other records. The combined trend features its highest $\delta^{18}O_{BSi}$ values at 1900 yrs BP, followed by a decrease leading to a relative minimum at 1100 and 1300 yrs BP. This phase is followed by a second $\delta^{18}O_{BSi}$ peak at 700 and 900 yrs BP, after which a decrease can be observed. The decrease at 300 and 500 yrs BP features the least deviation between individual records. The most recent bin shows again a much larger $\delta^{18}O_{BSi}$ variability. While most records display the lowest values at this time, Lake Kotokel (#8) for instance shows an increase compared to the previous bins. This increase may or may not be related to recent warming; and due to the complex hydrology of the lake even lake evaporation cannot be ruled out. Most of the records however does not indicate a recent $\delta^{18}O_{BSi}$ maximum that might be indicative of recent warming.

660   **Figure 5. Common Era Northern hemispheric records (45-90 N) compiled in this study. A) Original records, B) data binned to 200-year intervals, only showing records covering at least 7 bins, C) binned records with mean of individual records removed, D) filtered for records from open lakes only, E) filtered for records from lakes with t_{res}<100 yrs, F) NH trend, calculated as mean of all records in each bin. Shadings show 1 and 2 standard deviations, respectively. G) North American and H) Eurasian trend.**

It should be noted that there is bias of data points towards the older end of the most recent bin. An absence of recent warming in the data therefore might be linked to this bias, and hence a reaction of lake systems to recent warming can not be ruled out. As Eurasian records constitute the majority of records (N=7), it is similar to the NH trend (Fig. 5H).

670 The trends calculated for the last 2 kyr (2K) for the NH (Eurasian) $\delta^{18}O_{BSi}$ stacks are high with -0.64‰/kyr (-0.85‰/kyr) for 10 bins, with even higher slopes of -1.6‰/kyr (-1.7‰/kyr) for bins 6-10 (1 to 2 kyr), and -1.4‰/kyr (-1.8‰/kyr) for bins 1-5 (corresponding to the last millennium). The negative slope is interrupted by three consecutive bins (4-6; 0.6-1.2 kyr BP) plus bin 8 (1.4-1.6 kyr BP) with higher $\delta^{18}O_{BSi}$ than the previous bin. For the last 2K, the other 5 bins (1-3, 7 and 9) show a negative sign for the NH and Eurasian $\delta^{18}O_{BSi}$ 2K reconstructions.

675 North American records (N=2) do not show a consistently decreasing trend (Fig. 5G), but slightly higher values at 1.7 and 1.9 kyr BP compared to the most recent bins (0.1 and 0.3 kyr BP, respectively). They do, however, show lower $\delta^{18}O_{BSi}$ values between 0.9 and 1.3 kyr BP, followed by a $\delta^{18}O_{BSi}$ maximum at 500 yrs BP. As there are only two records available after filtering, caution has to be applied in interpreting this pattern.

For the North American $\delta^{18}O_{BSi}$ 2K reconstruction, a lower overall gradient is observed (-0.12‰/kyr), which shows also a 680 steep slope for bins 6-10 with -1.5‰/kyr. In contrast to the NH and Eurasian $\delta^{18}O_{BSi}$ stack, bins 1-5 show a slight decrease of -0.4‰/kyr, only. This leads to slightly shifted minima and maxima between $\delta^{18}O_{BSi}$ reconstructions for the last two millennia: NH and Eurasian reconstructions have their absolute maxima in bin 10 or at 1.8-2.0 kyr (absolute minima: bin 1; 0-0.2 kyr) with intermediate minima at 1.2-1.4 kyr BP (bin 7) and maxima between 0.6-1.0 kyr BP (bins 4 and 5). In contrast, for the North American reconstruction, the absolute $\delta^{18}O_{BSi}$ minimum (maximum) is at 1.2-1.4 kyr BP or bin 7 (0.4-0.8 kyr BP (bins 685 3 and 4), whereas the early maximum (bin 10) and late minimum (bin 1) are less pronounced. In summary, we observe an overall decreasing trend in $\delta^{18}O_{BSi}$ for the last two millennia, for NH, Eurasian and North American stacks, which is accelerated in the first millennium.

Similar patterns among Eurasian, and possibly NH, $\delta^{18}O_{BSi}$ records do suggest a common NH signal throughout the CE. The observed maxima and minima correspond to previously described climatic events, notably the Roman Warm Period from 2.0 690 kyr BP to about 1.6 kyr BP (Ljungqvist, 2010), the Dark Ages Cold Period from 1.6 to 1.2 kyr BP (Büntgen et al., 2016; Helama et al., 2017) the Medieval Climatic Anomaly (MCA) from 1.2 to 0.8 kyr BP (Bradley et al., 2003; Mann et al., 2009) and the Little Ice Age from 0.7 to 0.1 kyr BP (Matthews and Briffa, 2005, Wanner et al., 2022). In Fig. 5F, the two main cold phases (Dark Ages Cold Period and Little Ice Age) are clearly represented. The good accordance of our data with these previously described warm and cold phases suggests that $\delta^{18}O_{BSi}$ records presented are influenced by T_{air} change, either directly 695 or via other parameters linked to T_{air}. Recent research has rejected the global nature of these climatic events and suggested that they are regionally constrained (Neukom et al., 2019). However, the accordance of our data – when assessed at centennial scale – with these climatic events is expected, because they were initially described for North America and Europe.

hat verschoben (Einfügung) [1]

hat gelöscht: has to

hat gelöscht: ¶

hat gelöscht: and

hat gelöscht: does not rule out

hat gelöscht: the Eurasian trend

hat gelöscht: picture

hat verschoben (Einfügung) [2]

hat gelöscht: 00

hat gelöscht: 00

hat gelöscht: yrs

hat gelöscht: 100

hat gelöscht: 300

hat gelöscht: yrs

hat gelöscht: 900

hat gelöscht: 1300

hat gelöscht: yrs

hat nach oben verschoben [2]: North American records (N=2) do not show a consistently decreasing trend (Fig. 5G), but slightly higher values at 1700 and 1900 yrs BP compared to the most recent bins (100 and 300 yrs BP, respectively). They do, however, show lower $\delta^{18}O_{BSi}$ values between 900 and 1300 yrs BP, followed by a $\delta^{18}O_{BSi}$ maximum at 500 yrs BP.

hat gelöscht: North American records (N=2) do not show a (N=2) do not show a consistently decreasing trend (Fig. 5G), but slightly higher values at 1700 and 1900 yrs BP compared to the most recent bins (100 and 300 yrs BP, respectively). They do, however, show lower $\delta^{18}O_{BSi}$ values between 900 and 1300 yrs BP, followed by a $\delta^{18}O_{BSi}$ maximum at 500 yrs BP. As there are only two records available after filtering, caution has to be applied in interpreting this pattern. ¶ ... [1]

hat gelöscht: Common Era

hat gelöscht: 2000

hat gelöscht: yrs

hat gelöscht: 1600

hat gelöscht: yrs

hat gelöscht: 1600

hat gelöscht: to 1200 yrs

hat gelöscht: 1200 yrs BP to 800 yrs

hat gelöscht: 700

hat gelöscht: yrs BP

hat gelöscht: 100 yrs

hat gelöscht: which are

hat gelöscht: makes sense

4.2 Holocene (corresponding to MIS 1) Climate

To facilitate comparison with other Holocene reconstructions, for deriving Holocene trends only 12 kyr (in 1 kyr-bins) are considered and the boundary between MIS 1 and MIS 2 is set to 12 kyr. Thus, the Holocene NH subset of records (covering the past ca. 12 kyr) consists of 21 records that display a considerable range in mean $\delta^{18}O_{BSi}$ values from +20‰ (#3) to +35‰ (#31) VSMOW (Fig. 6A) that reflect local site-specific difference. For example, Lake El'gygytgyn (#3) is located in a continental, high–latitude environment with little secondary evaporation (Chapligin et al., 2012b) whereas Lake Ladoga (#31) is situated in a less continental, lower latitude setting with a complex hydrological history of changing inflows and outflows (Kostrova et al., 2019).

Amplitudes of the individual Holocene records vary from less than 5‰ (#3) to 10‰ VSMOW (#20, #35). Lake El'gygytgyn (#3) is a voluminous, deep hydrologically open lake with little lake evaporation, whereas Heart Lake (#35) is a much smaller, less voluminous lake with a short t_{res} (2 weeks). Lake Baikal (#20) is a deep voluminous lake like Lake El'gygytgyn, however with a centennial–scale t_{res} making it effectively closed and thus potentially subject to secondary evaporation. Consequently, differences in their isotopic variability might correspond to their different hydrological settings. Closed lakes (such as Sunken Island Lake; #26) have a tendency towards higher $\delta^{18}O_{BSi}$ values that are likely due lake evaporation leading to a more enriched isotope signature of lake water (Broadman et al., 2020b; Hernandez et al. 2008).
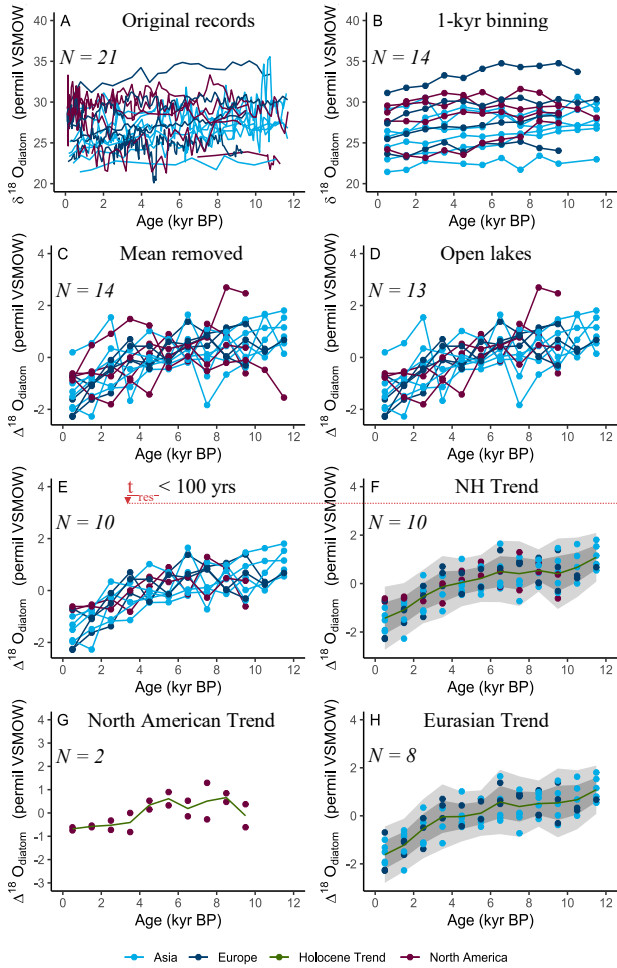
Figure 6. ~~Holocene~~ **Northern hemispheric records (45-90 N) compiled in this study. A) Original records, B) data binned to 1-kyr intervals, only showing records covering at least 7 bins, C) binned records with mean of individual records removed, D) filtered for records from open lakes only, E) filtered for records from lakes with t_{res}<100 yrs, F) NH trend, calculated as mean of all records in each bin. Shadings show 1 and 2 standard deviations, respectively. G) North American and H) Eurasian trend.**

780 Binned records (Fig. 6B, N=14) do not display any common patterns and feature $\delta^{18}O_{BSi}$–values ranging from +20‰ to +35‰ VSMOW, similar to the original records. However, binning of datapoints and exclusion of shorter records results in smoothed amplitudes of less than 5‰ VSMOW. The binned records exhibit Early Holocene $\delta^{18}O_{BSi}$ values (up to 2.5‰) higher than the Holocene mean, whereas late Holocene values are generally up to 2‰ below the Holocene mean. However, some records do not follow this general pattern after mean removal (Fig. 6C). This could be indicative of the different hydrological settings and

785 t_{res} which have a substantial impact on the recorded signal.

Filtering for hydrologically open lakes (Fig. 6D, N=13) and t_{res}<100 yrs (Fig. 6E, N=10) displays a clear decreasing $\delta^{18}O_{BSi}$ trend of 2.5‰ throughout the Holocene. However, differences between individual records do exist, and most notably, the absolute $\delta^{18}O_{BSi}$ maxima of individual records do not occur at the same time. While some records feature maxima at the beginning of the Holocene, other records peak between 5 and 8 kyr BP. This pattern is in line with Holocene T_{air} reconstructions

790 which have found spatial differences of the timing of the Holocene thermal maximum (Kaufman et al., 2004; Renssen et al., 2009).

Based on this subset of hydrologically open lakes with t_{res}<100 yrs, a combined millennial scale NH trend was calculated. This combined Holocene trend (Fig. 6F) shows a decrease throughout the Holocene amounting to ca. 2‰ VSMOW. The absolute maximum is observed for the Early Holocene bin at 11–12 kyr BP. A decrease at the beginning of the Holocene between 12

795 kyr BP and 10 kyr BP is followed by a relatively stable middle Holocene until 6 kyr BP, and subsequent stronger decrease towards the absolute $\delta^{18}O_{BSi}$ minimum in the youngest bin (0–1 kyr BP).

When considered separately, North American (N=2) and Eurasian (N=8) records show different patterns and have been described and interpreted differently in the case studies published to date. While the former are primarily linked to atmospheric circulation changes in Alaska (Bailey et al., 2018; Broadman et al., 2020b; Broadman et al., 2020a), the latter are at least partly

800 interpreted as indicative of T_{air} and insolation changes (Swann et al., 2010; Mackay et al., 2011; Chapligin et al., 2012b; Kostrova et al., 2013a; Kostrova et al., 2019; Kostrova et al., 2021). Eurasian $\delta^{18}O_{BSi}$ records (N=8) display a slight decrease from 12 kyr BP to 10 kyr BP and suggest a second maximum at 7 kyr BP followed by a second relatively stable phase. An accelerated decrease starting at ca. 4 kyr BP constitutes a more abrupt change than in the NH trend. The Holocene trend calculated for the NH (Eurasian) $\delta^{18}O_{BSi}$ stack is -0.19‰/kyr (-0.21‰/kyr) for all 12 bins, with a lower slope of -0.11‰/kyr (-

805 0.10‰/kyr) between 12-7 kyr BP, and a much higher slope of -0.39‰/kyr (-0.36‰/kyr) for bins 1-6 (corresponding to 6-0 kyr BP).

Throughout the Holocene, 10 out of 12 bins are lower than the previous one (i.e., negative sign) for the NH $\delta^{18}O_{BSi}$ reconstruction, except between 9-8 and 7-6 kyr BP (bins 9 and 7) which show an increase in $\delta^{18}O_{BSi}$. For the Eurasian $\delta^{18}O_{BSi}$ stack all bins are lower in $\delta^{18}O_{BSi}$ than the preceding one (except for bin 7, or 7-6 kyr BP, which shows an increase of +0.2‰).

810 The most negative slopes exceeding -0.55‰ per kyr are observed between 2-1 kyrs BP for both, the NH and the Eurasian compilation. For the North American $\delta^{18}O_{BSi}$ reconstruction, a slightly lower trend is observed for the Holocene (-0.13‰/kyr;

820 based on 10 bins), which also shows a steeper slope between 5-0 kyrs BP (bins 5-1) with -0.22‰/kyr. In contrast to the NH and Eurasian $\delta^{18}O_{BSi}$ stack, there is a slight increase of +0.10‰/kyr between 10-6 kyrs BP (bins 10-6), likely driven by bins 6 and 9, which are the only ones showing a positive sign, whereas all 7 other bins show a decrease compared to the preceding one.

Hence, North American records do not show a consistently decreasing trend throughout the Holocene (Fig. 6G), but instead

825 slightly higher $\Delta^{18}O_{BSi}$ values in the first half of the Holocene as compared to the second half. Since there are only two North American records fulfilling our selection criteria, it is difficult to meaningfully go beyond the existing case studies, outlining the necessity for further research in this region. In summary, we observe a mostly continuous decrease in $\delta^{18}O_{BSi}$ throughout the Holocene for NH, Eurasian and North American stacks, which is accelerated in the second half of the Holocene. This phenomenon has been previously described as Neoglacial cooling (e.g. McKay et al., 2018).

830 The regional differences between North America and Eurasia are also manifested in the timing of absolute $\delta^{18}O_{BSi}$ minima and maxima of individual records (Fig. 7). The spatial pattern of the Holocene maxima of binned records shows a different timing of maxima for different regions (Fig. 7). Eastern Eurasian sites feature a pronounced early Holocene maximum (at 12 kyr BP), whereas sites to the west of Eurasia show a tendency towards rather a middle Holocene maximum, around 8-6 kyr BP. This suggests that the double maxima of the Eurasian trend (Fig. 6H) is at least partly caused by the regional differences over

835 Eurasia. There are also individual records, however, which do show two peaks within the Holocene e.g. Lake Bolshoye Shchuchye from the Polar Ural Mountains (#16). Records from Alaska feature later $\delta^{18}O_{BSi}$ maxima (5 kyr BP and 8 kyr BP, respectively).

hat gelöscht: rather

hat gelöscht: the aforementioned

hat gelöscht: ¶

hat gelöscht: more
hat gelöscht: tendentially
hat gelöscht: 6–8

hat gelöscht: 7
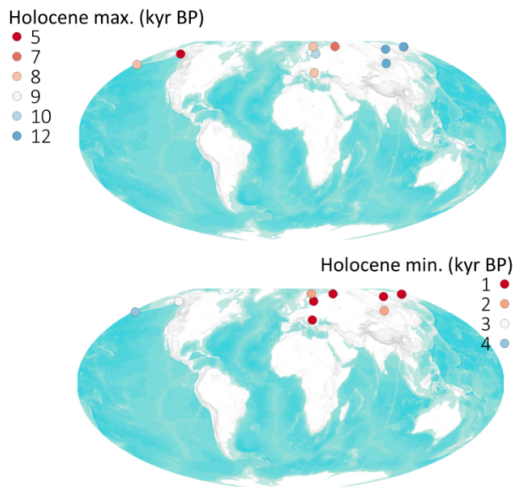
Figure 7. Timing of $\delta^{18}O_{BSi}$ maxima and minima of binned records in the Holocene. Filter criteria are the same as indicated in Fig. 10 and only records covering at least 10 bins have been considered. ©ESRI 2022

850 The timing of Holocene minima is rather consistent across northern Eurasia, where all records reaching their minimum in the last 1 kyr BP or between 2 kyr BP and 1 kyr BP (Fig. 7). While the records generally follow the same decreasing long–term $\delta^{18}O_{BSi}$ trend, they feature either early or late Holocene minima. Since datapoints of 1850 CE and younger have been removed from the dataset prior to analysis to exclude the industrial era, a potential effect of recent climate change is not covered in this subset of data. As with the Holocene maximum, sites in Alaska also differ with regard to the Holocene minimum. They show

855 a tendency towards absolute minima earlier than Eurasian records, between 3 and 4 kyr BP, respectively). Despite the scarcity of the records fulfilling the selection criteria, this suggests a different behaviour of the regions (North America and Eurasia), though we also acknowledge that one of the two North American sites (#35, Heart Lake) is located in the central North Pacific Ocean and has a different climatic history.

The African (N=7) and South American records (N=3) do not fulfill the criteria set for the NH and Eurasian stacks, either due

860 to hydrological or temporal constraints (e.g. too few datapoints). However, all three South American records (see Tab. A2; #18, 28, 32) show an early Holocene maximum around 10 kyr BP. Two out of three South American $\delta^{18}O_{BSi}$ records show a decrease over the Holocene, whereas the third record displays no clear trend.

Due to marked differences in hydrology among sites, an African $\delta^{18}O_{BSi}$ stack has not been calculated either. Instead, individual records (N=5) have been compiled and binned separately for the African continent (Figs. A5A, A5B). We observe the largest $\delta^{18}O_{BSi}$ variability within one individual record ($\delta^{18}O_{BSi}$ range of ca. 20‰, #21) as well as highest absolute $\delta^{18}O_{BSi}$ (with values up to +45‰, #33). This is related to the very different settings both in altitude (Tab. A2) and hydrological characteristics (Fig. A5D). Overall, the first half of the Holocene is characterized by slightly lower $\Delta^{18}O_{BSi}$ values than the second half. As this observation is less obvious for open lakes (Fig. A5D), a bias linked to widely different hydrological settings of the respective lakes (see Tab. A2) has to be assumed, which renders it difficult to disentangle the drivers of $\delta^{18}O_{BSi}$. This further underscores the importance of hydrologically-constrained records to infer a common (climate) signal (see Figs. 5A, 6A).

4.3 Combined Holocene trend in the hemispheric context

The combined trends of $\delta^{18}O_{BSi}$ for NH, Eurasia and North America are shown in comparison to other NH proxy records in Fig. 8. As individual $\delta^{18}O_{BSi}$ records are commonly discussed with respect to insolation, we also include June and December insolation curves for 60°N, calculated using (Laskar et al., 2004, Fig. 8F). As shown in Fig. 8G and 8H, Eurasian and NH combined trends show a similarity with the June insolation as all records feature a decreasing trend throughout the Holocene. However, insolation decreases steadily after an early Holocene maximum whereas combined NH and Eurasian $\delta^{18}O_{BSi}$ trends feature a stable early Holocene and a second peak at 7 kyr BP. This presumably relates to the geographical distribution of the timing of $\delta^{18}O_{BSi}$ maxima and minima as discussed above. Therefore, eastern Eurasian records are most in line with June insolation which has been regarded as a proxy of summer T_{air} (#3, 24). Records stemming from sites further west are less directly correlated with June insolation. A striking difference is the accelerated decrease of $\delta^{18}O_{BSi}$ after 4 kyr BP in the NH and Eurasian timeseries, co-incident with neo-glacial cooling, which is not mirrored in the insolation curve. The relatively stable insolation during this time suggests that the accelerated decrease visible in $\delta^{18}O_{BSi}$ records must be driven by other factors.

Conversely, December insolation (Fig. 8F) shows an anticorrelation with the $\delta^{18}O_{BSi}$ records. However, as both the absolute values and the changes in December insolation are an order of magnitude lower than those of June insolation, a decisive influence of December insolation on $\delta^{18}O_{BSi}$ records can be ruled out. This is in good agreement with previous works, claiming that the $\delta^{18}O_{BSi}$ proxy yields a summer–dominated signal (Shemesh et al., 2001a; Kostrova et al., 2021), supported by the fact that most biogenic production is in late spring-early summer (particularly relevant for NH high-latitude short residence time systems). It has to be noted that the records displayed still stem from different latitudes and the insolation patterns are not identical at all these sites. A decrease of summer insolation, however, is generally the case for high latitude regions throughout the Holocene.

hat gelöscht: ,

hat gelöscht: n

hat gelöscht: provide

hat gelöscht: visible

hat formatiert: Nicht Hochgestellt/ Tiefgestellt

hat gelöscht: ka

hat gelöscht: -
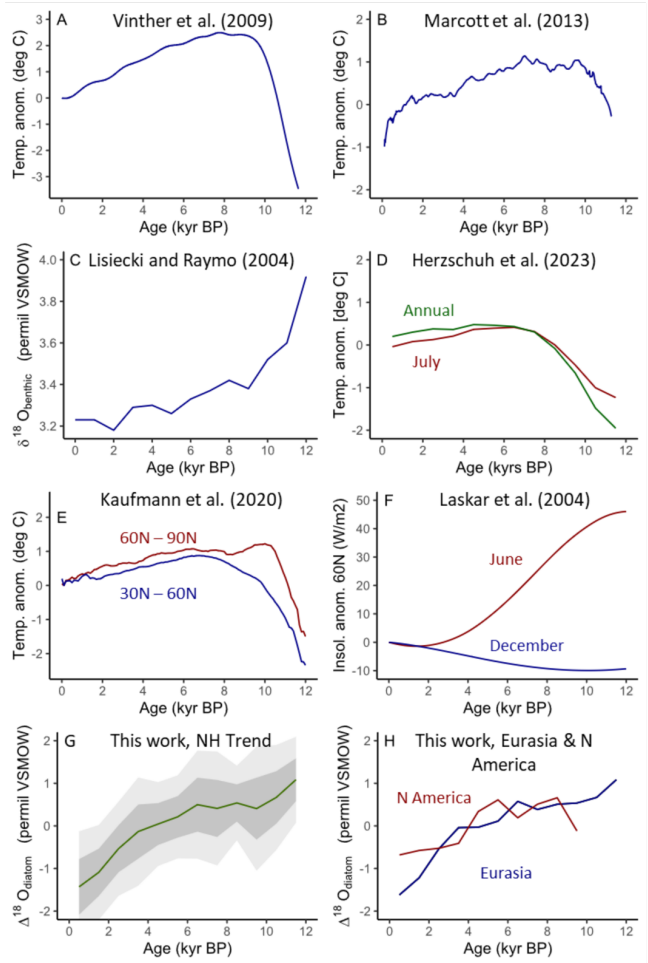
Figure 8. Combined trend of δ¹⁸O$_{BSi}$ compared to other climate reconstructions. A) Greenland ice sheet temperature reconstruction, B) Multi-proxy temperature reconstruction (30-90 N), C) global stack of δ¹⁸O from benthic foraminifera, D) temperature reconstruction (45-90 N) based on pollen data, E) Temperature anomalies of mean surface temperatures (multi-method ensemble).
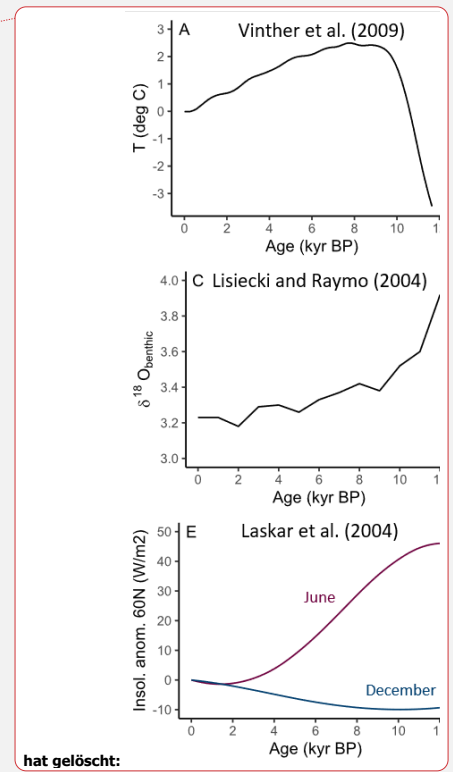
F) Insolation anomaly for June and December, G) Combined NH trend from $\delta^{18}O_{BSi}$ records (this work), H) Combined Eurasian and North American trends from $\delta^{18}O_{BSi}$ records (this work).

Temperature reconstructions by Vinther et al. (2009) using $\delta^{18}O$ data from ice cores at Agassiz ice cap and Greenland (between 65°N and 80°N) show a pronounced T_{air} increase of about 5°C at the beginning of the Holocene until 10 kyr BP, followed by a stable phase until 7 kyr BP (Fig. 8A). While the NH and Eurasian $\delta^{18}O_{BSi}$ trends do not feature this increase during the early Holocene, they do show a relatively stable phase from 10 kyr BP to 7 kyr BP. After 7 kyr BP, both the NH $\delta^{18}O_{BSi}$ trend and the NH T_{air} reconstruction feature a decrease of ca. 2°C and 1.5‰ VSMOW, respectively. As the present–day global average T_{air}–dependent fractionation in precipitation amounts to 0.695‰/°C (Dansgaard, 1964), a 1.5‰ $\delta^{18}O$ decrease would, thus, correspond to a 2°C cooling, the same T_{air}–change as found by Vinther et al. (2009). This good agreement of $\delta^{18}O_{BSi}$ combined trends (NH and Eurasia) and the T_{air}–reconstructions by Vinther et al. (2009) suggests summer T_{air} to have a major impact on $\delta^{18}O_{BSi}$ records on millennial time scales.

Multi–proxy–based temperature reconstructions by Marcott et al. (2013) (regional stack 30°N to 90°N, Fig. 8B) also show a temperature increase until 10 kyr BP, followed by a stable phase until ca. 7 kyr BP and a decrease of ca. 2°C thereafter. This temperature reconstruction includes a much broader geographical focus as well as different land-based and marine proxies (e.g., pollen, chironomids, ice). Thus, the stable phase from 10 kyr BP to 7 kyr BP and a maximum around 7 kyr BP are shared features of the $\delta^{18}O_{BSi}$ trends of this work, the ice core reconstruction from Vinther et al. (2009) and the temperature reconstructions by Marcott et al. (2013). However, the early Holocene maximum of the $\delta^{18}O_{BSi}$ trends is not represented in reconstructions by Vinther et al. (2009) and Marcott et al. (2013). This discrepancy might reflect different regional biases of Marcott et al. (2013) and this work, which is also in line with the different timing of Holocene maxima in the $\delta^{18}O_{BSi}$ data (Fig. 8). Given the discrepancy between temperature reconstructions and $\delta^{18}O_{BSi}$ records in the early Holocene, it is likely that the influence of factors other than T_{air} - such as glacial retreat and ice melt during deglaciation - is especially pronounced in the early Holocene. The LR04 stack of the $\delta^{18}O$ of benthic foraminifera (Lisiecki and Raymo, 2005) features continuously decreasing $\delta^{18}O$ throughout the Holocene, which is in accordance with the combined Eurasian $\delta^{18}O_{BSi}$ trend (Fig. 8C).

Pollen records may help to further investigate this issue as they stem from terrestrial environments, but are also archived in lake sediments. Moreover, they offer a similar temporal and geographical focus compared to our records, extending to high latitudes. For this comparison we have used the Holocene pollen data compilation by Herzschuh (2021, 2022, 2023) extracting data from 864 records from sites north of 45°N. Changes of annual T_{air} and July T_{air} relative to modern values were retrieved from the pollen dataset. Annual and July T_{air} show similar patterns with a pronounced early Holocene increase, followed by middle Holocene maximum and a less pronounced decrease until the present day (Fig. 8D). Both the middle Holocene maximum and the subsequent decrease of T_{air} are in good agreement with the combined Eurasian $\delta^{18}O_{BSi}$ trend (Figs. 8D, 8H). This further supports a substantial influence of T_{air} on the $\delta^{18}O_{BSi}$ signal. However, the early Holocene maximum of $\delta^{18}O_{BSi}$ in our combined NH and Eurasian trends is not reflected by pollen–based reconstructions. Caution has to be applied when using pollen–based climate reconstructions for comparison because vegetation changes may lag millennia behind changes of climatic

970 variables (Herzschuh et al., 2016). In summary, the similarity of our combined $\delta^{18}O_{BSi}$ trends with NH temperature reconstructions and insolation data allows for deducing a clear link to summer T_{air} for the Holocene records. Therefore, our $\delta^{18}O_{BSi}$ record contributes to the understanding of the Holocene climate history.

A significant discrepancy between Holocene cooling deduced from proxy reconstructions (e.g. Marcott et al., 2013; Kaufman et al., 2020; Figs. 8B and 8E) and Holocene warming simulated in climate models has been called the Holocene "temperature
975 conundrum" (Liu et al., 2014), revisited in Wanner et al. (2021), Kaufman et al. (2020) and Kaufman and Broadman (2023). This discrepancy has been attributed to uncertainties in both proxy reconstructions and climate models. One major aspect is the seasonal bias in organic-based proxy records (such as pollen, diatoms etc.) towards summer (Liu et al, 2014). As the Holocene displays opposite trends in summer and winter insolation at 60°N (Fig. 8E, Laskar et al., 2004), high latitudes provide an optimal setting for testing the seasonality aspect in Holocene temperatures. Permafrost ice wedge $\delta^{18}O$, a clear winter-
980 season proxy, shows a continuous warming trend in the last 7 kyr BP (Meyer et al., 2015b) that supports the hypothesis that seasonality in proxy-based records is one key variable to be considered. Pollen-based reconstructions for the Holocene show a clear temperature decrease since an early to mid-Holocene temperature optimum (Fig. 8D; Herzschuh et al. 2021, 2022, 2023), not only valid for the summer season, but, though less pronounced, also for annual reconstructions. Proxy-based reconstructions of Kaufman et al. (2020) also suggest Late Holocene cooling. The $\delta^{18}O_{BSi}$ compilation presented here for
985 lacustrine environments is based on diatoms whose bloom is mostly attributed to the late spring-early summer season. Decreasing summer temperatures throughout the Holocene would manifest in decreasing T_{lake}, which would in turn lead to increasing $\delta^{18}O_{BSi}$ (Fig. 1). The observed decrease of $\delta^{18}O_{BSi}$, however, points towards lower $\delta^{18}O_{lake}$, which would be in line with decreasing $\delta^{18}O_{prec}$ due to decreasing summer T_{air} (Fig. 1). This would imply either a prevalence of summer precipitation or lake basins with sub-annual t_{res}. However, the trend is observed for lake basins with a wide range of t_{res}, suggesting
990 millennial-scale changes in summer T_{air} to be the main driver of the observed $\delta^{18}O_{BSi}$ signal.

It has to be stressed that this influence of T_{air} may act both directly and indirectly, directly by means of the temperature–dependent fractionation during precipitation formation, and indirectly via the impact of temperature within the hydrological cycle and $\delta^{18}O$ of water compartments. This includes factors such as moisture origin, precipitation intermittency and atmospheric circulation patterns which have been described as key drivers in numerous case studies. This underlines the
995 importance of scale when assessing $\delta^{18}O_{BSi}$ records, both temporally and spatially. On a millennial and hemispheric scale, T_{air} can be identified as one main driver of $\delta^{18}O_{BSi}$ records even though the signal formation is generally complex and challenging to interpret with individual records. A T_{air} influence for certain records on the millennial scale is therefore not necessarily a contradiction to the findings of the original publications which may have attributed the record's signal to other factors (e.g., hydrological processes) on shorter timescales.

1000

4.4 Frontiers and Challenges (Records older than the Holocene)

Further back in time than the Holocene, coverage with $\delta^{18}O_{BSi}$ records is generally limited. As MIS 1 (N=37) and MIS 2 (N=18) have the highest numbers of records, they offer the best possibility of comparing glacial and interglacial records. Records beyond MIS 2 are very sparse and do not allow for filtering and generating common trends. Here, the interpretation has to rely on comparison of individual datasets. There are few (N=16) records which cross the MIS 1–MIS 2 boundary and these records cover neither MIS 1 nor MIS 2 entirely. A quantitative comparison of MIS 1 and MIS 2 is therefore difficult. Again, caution has to be applied due to the fact that these records stem from lakes with different hydrological and climatic settings (i.e. maritime Alaskan sites vs. continental Siberian sites).

The most promising approach for investigating MIS 1 and MIS 2 is extending NH MIS 1 datasets to the past (Fig. 9). Five NH $\delta^{18}O_{BSi}$ records (#3,8,15,24,25) extend back from MIS 1 into MIS 2 and offer insight into the hydroclimate history of Siberia during the last glacial and the deglaciation. Four of these records (#3,8,15,24) are continuations of records included in the NH stack (see Fig. 6F), and all stem from Asia. Most records display a maximum near the MIS 1–MIS 2 boundary and a decrease of $\delta^{18}O_{BSi}$ with increasing age in MIS 2, suggesting decreasing T_{air}. This is the case for all records except #3 which displays a relative $\delta^{18}O_{BSi}$ maximum at ca. 16 kyr BP. This maximum may also be caused by dry conditions outperforming the effect of lower T_{air}. Only records #3, #8 and #15 extend beyond 13 kyr BP. Both #3 and #15 reach their absolute minima at 23 kyr BP and 24 kyr BP, respectively. Record #8 does not show such a clear pattern and shows a relative maximum at 25 kyr BP instead. This is likely due to the complex hydrological setting (alternating between open and closed at present) which may have changed over these timescales. Generally, most records suggest a tendentially lower $\delta^{18}O_{BSi}$ in MIS 2 when compared to MIS 1. This is notable as glacial and interglacial periods are characterized by different environments, atmospheric circulation patterns and likely hydrological settings (e.g. formation or closure of outflows from lakes, lake level fluctuations). Potentially, lower $\delta^{18}O_{BSi}$ values would consistent with either lower T_{air} or more humid conditions. In case of MIS2, generally associated with cold and dry conditions, a lower T_{air} is the more plausible scenario. However, it must be stressed that the lack of records covering the complete MIS 2 complicates a robust statistical comparison between MIS 1 and 2. Calculated offsets of MIS 1 and MIS 2 datapoints may show both higher and lower $\delta^{18}O_{BSi}$ values in MIS 2 compared to the Holocene. Again, a MIS 2 climate colder and drier than Holocene (MIS 1) may produce either lower or higher $\delta^{18}O_{BSi}$ values due to opposing effects of T_{air} and evaporation. A geographical pattern of either of these effects prevailing is not obvious, which suggests that rather than the climatic background, the individual hydrological settings of the lakes play a prominent role in determining the $\delta^{18}O_{BSi}$ signal. This supports the approach of using lakes with both similar latitudinal and hydrological characteristics for meaningful inter-site comparison.

Figure 9. Comparison of MIS 1 and MIS 2 data. Continuation of Holocene records from NH Stack (see Fig. 6F) into MIS 2 for color-code records (#3,8,15,24).

Beyond MIS 2, $\delta^{18}O_{BSi}$ records become even scarcer, as do lake sediment records in general. Additionally, lake sediments covering these time periods often lack sufficient diatoms, especially in cold stages, i.e. Lake Baikal during MIS 4 (Mackay et al., 2008; Mackay et al., 2011; Mackay et al., 2013).

Lake El'gygytgyn is a peculiar example of a continuous sedimentation history with $\delta^{18}O_{BSi}$ showing glacial–interglacial cycles at least back to MIS 9 (Chapligin et al., 2012b), which have been attributed by the authors to T_{air} changes. In addition to glacial–interglacial cycles, it is also possible to compare $\delta^{18}O_{BSi}$ of interglacials, i.e. MIS 1, MIS 5, MIS 11, when diatoms during cold stages are absent. In the sedimentary records of Lake El'gygytgyn, Chapligin (2012c) investigated the $\delta^{18}O_{BSi}$ differences between the warm stages MIS 1, MIS 5 and MIS 11 and found MIS 11 as warmest interglacial. This interpretation has been supported by pollen–based T_{air} reconstructions by Melles et al. (2012) and underlines the applicability of the $\delta^{18}O_{BSi}$ proxy on glacial–interglacial timescales. Long-term diagenetic effects have shown to be of little influence on $\delta^{18}O_{BSi}$, at least for the last 250kyr (Chapligin et al., 2012b). Studies on Lake Baikal have also investigated past interglacials and have addressed changes in precipitation intermittency and cooling events during MIS 11 (Mackay et al., 2008). During MIS 5, millennial–scale variability is suggested to have been more stable than during MIS 1 (Mackay et al., 2013).

Older $\delta^{18}O_{BSi}$ records do exist and often rely on paleo–lakes i.e. Ribains Maar, Baringo–Bogoria Basin, Makgadikgadi and Dethlingen (Shemesh et al., 2001b; Koutsodendris et al., 2012; Wilson et al., 2014b; Schmidt et al., 2017). These offer the possibility of extending the picture past extant lakes. However, the absence of modern hydrological observations makes their interpretation and comparison to other, better-constrained records more challenging. Further research using $\delta^{18}O_{BSi}$ is therefore needed in order to complement the picture and provide insight into past climate and environmental conditions in continental

regions, particularly valuable for high latitude and high–altitude areas that are poorly covered by other proxy data. We recommend studies with uniform spatial and temporal coverage, i.e. hydrologically open lakes with a long, continuous sedimentation history, as our synthesis indicates these to be most promising for generating comparable binned time series to extend climate reconstructions further into the past.

5. Conclusions

In this study, we have identified and compiled all existing lacustrine $\delta^{18}O_{BSi}$ records published to date and synthesized them into the first global $\delta^{18}O_{BSi}$ data compilation. We have identified 53 $\delta^{18}O_{BSi}$ records derived from 71 publications. These records stem from across the entire globe with their geographical distribution focusing on high-altitude and high-latitude lacustrine environments. Diatoms bear the advantage of being available in dilute, non–alkaline lakes common in these environments. Regional clusters of records (e.g. northern Eurasia, East Africa) indicative of the research foci of the individual research groups employing the $\delta^{18}O_{BSi}$ proxy allow for generating regional subsets of data. Temporal coverage stretches from sub–recent timescales to the Pliocene which highlights the applicability of $\delta^{18}O_{BSi}$ on different timescales. Best coverage is available in the Holocene (MIS 1) which is linked to the age of lakes, and hence the availability of lake sediments, especially in high latitudes. Moreover, biogenic silica (here entirely diatom–based) is most abundant during warm periods (interstadials and interglacials) compared to colder periods. The interpretability of $\delta^{18}O_{BSi}$ records relies on regional setting, hydrological constraints of individual lakes and catchments, and preferably supported by isotope measurements of modern lake water. Most $\delta^{18}O_{BSi}$ records stem from open lakes (N= 41), suggesting for these lakes a negligible influence of lake evaporation. In contrast, closed lakes (N=12) and paleo–lakes (N=9) have been investigated less. It has to be noted that a lake's ontogeny and hydrology may change throughout time, and thus hydrological changes constitute a valid approach for interpreting these $\delta^{18}O_{BSi}$ records. Spatial resolution of the $\delta^{18}O_{BSi}$ records is determined by the size of the lake and its corresponding catchment with lake water effectively integrating the input signal. While this signal may integrate large areas such as at Lake Baikal, most catchments (N=18) are <100 km^2, suggesting a locally confined signal for these lakes. Regarding temporal resolution, most records feature sampling resolutions which by far exceed t$_{res}$, suggesting sampling resolution to be the decisive factor in determining a record's signal. However, in case of t$_{res}$ >100yrs, lakes may be subject to increased lake evaporation.

Accounting for offsets and different temporal resolution of records and filtering for similar hydrological settings (hydrologically open lakes with t$_{res}$<100 yrs), we find a common pattern throughout the Common Era at the centennial scale, which we attribute to changing hydroclimate conditions. Changes are similar between Eurasia and North America, but they still differ in the timing of $\delta^{18}O_{BSi}$ maxima. Generally, the combined Eurasian $\delta^{18}O_{BSi}$ record seems to include major climate episodes during this period, including Roman Climate Optimum, Migration Period Pessimum, Medieval Climatic Anomaly (MCA) and Little Ice Age. An effect of recent warming is not visible in the Common Era data.

For the entire Holocene in Eurasia and the NH (for hydrologically open lakes with t_{res}<100 yrs), we find a common decreasing $\delta^{18}O_{BSi}$ trend of ca. -0.2‰/kyr on the millennial scale which roughly follows summer insolation. The decreasing $\delta^{18}O_{BSi}$ trend is accelerated in the second half of the Holocene, thus in Neoglacial times. Hence, this summer-based proxy contributes to the understanding of the Holocene climate history and the Holocene conundrum discussion initiated by Liu et al. (2014). The

1145 timing of the absolute $\delta^{18}O_{BSi}$ maxima of individual records in Eurasia differs and shows an east–west gradient with eastern Eurasian records featuring earlier Holocene maxima compared to western Eurasian records. Holocene minima occur within the last 2 kyr for all Eurasian records. North American records diverge from this Holocene pattern with later maxima and earlier minima. This behaviour is likely linked to atmospheric circulation patterns as also described by the authors of the individual records.

1150 Extending the millennial–scale trend of Eurasian records into MIS 2 shows generally lower $\delta^{18}O_{BSi}$ values in MIS 2, suggesting lower T_{air} (and not P/E) in glacial times, also visible in most other records that act on glacial–interglacial timescales. The applicability of the $\delta^{18}O_{BSi}$ proxy beyond MIS 2 is generally constrained by the availability of lake sediments and the abundance of diatoms in the respective sediments. Lake El'gygytgyn, as a prime example of hydrological continuity, displays glacial–interglacial cycles in the $\delta^{18}O_{BSi}$ record, supporting T_{air} being a prominent driver of $\delta^{18}O_{BSi}$ on millennial time scales. In glacial

1155 periods, diatoms abundances are low, and this limitation does sometimes not allow for $\delta^{18}O_{BSi}$ analysis. However, comparison between interglacials where diatoms are generally more abundant, is feasible, i.e. at Lake Baikal and Lake El'gygytgyn. In summary, we demonstrate the applicability and intercomparability of combined $\delta^{18}O_{BSi}$ records into a first lacustrine $\delta^{18}O_{BSi}$ compilation allow for paleoclimate reconstructions, accounting for regional offsets, different temporal resolutions and hydrological backgrounds. $\delta^{18}O_{BSi}$ records compiled in this study are an important tool for reconstructing paleoclimate across

1160 the globe and across a variety of time scales. In NH extratropic regions, their T_{air}–driven quantitative signal makes them especially useful in conjunction with paleoclimate models. Future research would be most valuable in complementing the existing data with longer records (covering MIS 2 and beyond) as well as records from underrepresented regions such as the southern hemisphere.

 Appendices

Appendix A

Figure A1. Geographical distribution of published $\delta^{18}O_{BSi}$ records and year of publication (N=64).
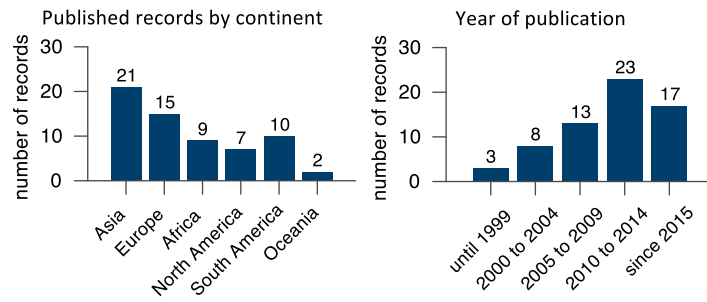
Figure A2. Overview of the dating methods used for age-model creation of published $\delta^{18}O_{BSi}$ time-series (N=64). Note that a single record can rely on multiple methods.
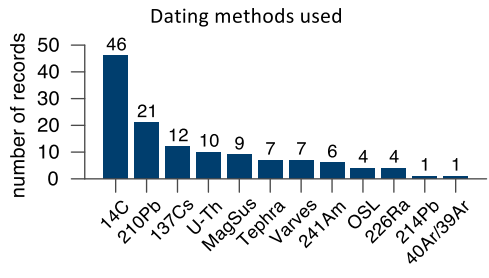
Figure A3. Overview of isotope hydrological background information considered in publications presenting δ¹⁸O$_{BSi}$ records (N=64).
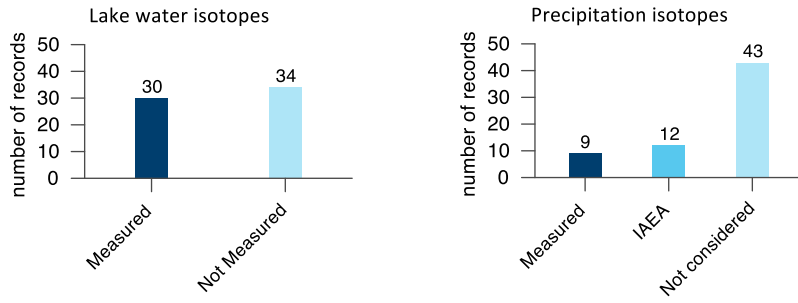
1195 **Figure A4. Hydrological settings of the lakes corresponding to the $\delta^{18}O_{BSi}$ records compiled in this study, as indicated in the original publications (N=64). Owing to a lack of present constraints, paleo lakes are listed as a separate category.**
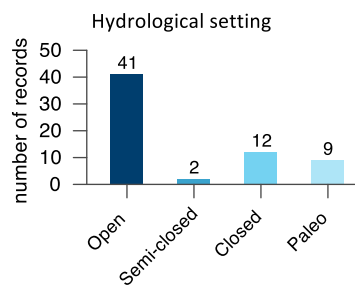
Figure A5. Holocene δ¹⁸O$_{BSi}$ dataset for the African continent. A) Original records, B) data binned to 1-kyr intervals, only showing records covering at least 7 bins, C) binned records with mean of individual records removed, D) with hydrological background information.

200
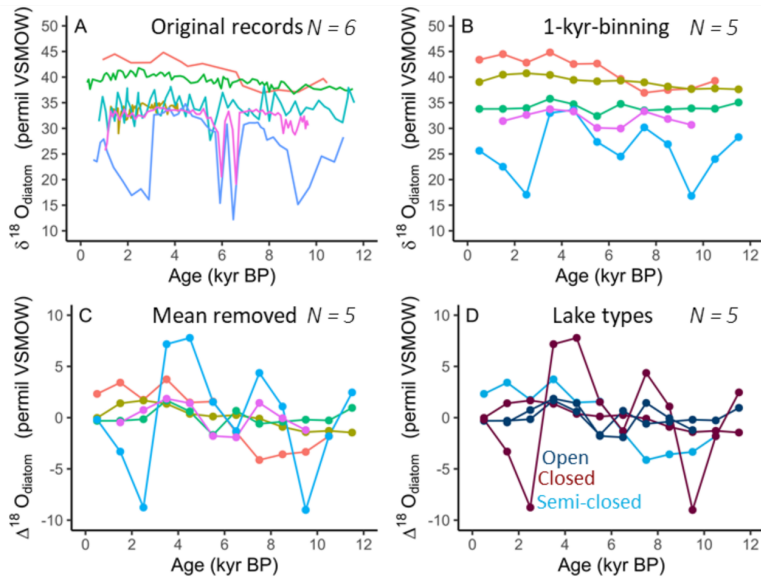
Table A1. Overview of the records and corresponding publications identified by this study (single= single core; composite= several cores; supplemented = information from other publication added (e.g. the age model)

Rec_ID	Archive	Lake	Core Type	original Core ID	Field Campaign (Year)	Short Reference	Used for Record number
EC1	Paleo Lake	Les Echets	single	EC1	2001	Ampel et al. (2009)	#12
HL1	Lake	Heart Lake	composite	10-AS-1D; 09-AS-1A; 09-AS-1B	2009, 2010	Bailey et al. (2018)	#35
LCHA1	Lake	Lake Challa	composite	03-2K; 05-4P	2003	Barker et al. (2011)	#13
M982P	Lake	Lake Malawi	single	M98-2P	1998	Barker et al. (2007)	#14
SHT1	Lake	Small Hall Tarn			1996	Barker et al. (2001)	#21
ST1	Lake	Simba Tarn			1996	Barker et al. (2001)	#34
BALGGU171	Lake	Garba Guracha	composite	BAL-GGU17-1A; BAL-GGU17-1B	2017	Bittner et al. (2021)	#33
SCP162A	Lake	Schrader Pond	single	SCP16-2A	2016	Broadman et al. (2020a)	#39
SILMC	Lake	Sunken Island Lake	composite	SIL-MC	2017	Broadman et al. (2020b)	#26
YL16-2C	Lake	Yellowstone Lake	composite	YL16-2C-1K; YL17-13A-1G	2016	Brown et al. (2021)	#53
PET09P2	Lake	Lac Petit	single	PET09P2	2009	Cartier et al. (2019b)	#44
Ni2B	Lake	Nettilling Lake	supplemented	Ni-2B	2012	Chapligin et al. (2016a)	#41
Lz1024	Lake	El'gygytgyn	single	Lz1024	2003	Chapligin et al. (2012b)	#3
LALB94	Lake	Lake Albano	supplemented	6A, 6B	1994	Chondrogianni et al. (2004)	
NAR0110	Lake	Nar Gölü	single	NAR01/02	2001	Dean et al. (2018)	#23
NAR0110	Lake	Nar Gölü	single	NAR10	2010	Dean et al. (2018)	#23
BNT1418	Lake	Baunt Lake	composite	BNT14	2014	Harding et al. (2020)	#25
LG1	Lake	Lago Chungara	composite	10; 11	2002	Hernandez et al. (2011)	#28
LCHUN02	Lake	Lago Chungara	composite	10; 11	2002	Hernandez et al. (2008)	#28
LG1	Lake	Lago Chungara	composite	10; 11	2002	Hernandez et al. (2013)	#28
LCHUN02	Lake	Lago Chungara	composite	10; 11	2002	Hernandez et al. (2010)	#28
P2	Lake	Lake Pupuke	single	P2	2001	Heyng et al. (2015)	#42
GL1	Lake	Grandfather Lake	single			Hu and Shemesh (2003)	#27
ARL1	Lake	Arolik Lake				Hu et al. (2003)	
LCHUN96	Lake	Lake Chuna	composite		1996	Jones et al. (2004)	#38

Rec_ID	Archive	Lake	Core Type	original Core ID	Field Campaign (Year)	Short Reference	Used for Record number
SS1	Lake	Lake Spaime	single	SS1	2002	Jonsson et al. (2010)	#49
VA	Lake	Vuolep Allakasjaure	supplemented	VAY1	2006	Jonsson et al. (2010)	#43
LB0301	Lake	Lake Baikal	single	03-01		Kalmychkov et al. (2007)	#9
LB0402	Lake	Lake Baikal	single	04-02		Kalmychkov et al. (2007)	#10
Co1412	Lake	Lake Emanda	single	Co 1412	2017	Kostrova et al. (2021)	#24
Co1309	Lake	Lake Ladoga	single	Co 1309	2013	Kostrova et al. (2019)	#31
KTK2	Lake	Kotokel Lake	single	KTK2	2005	Kostrova et al. (2013a)	#8
KTK2	Lake	Kotokel Lake	single	KTK2	2005	Kostrova et al. (2013b)	#8
KTK2	Lake	Kotokel Lake	single	KTK2	2005	Kostrova et al. (2014)	#8
KTK2	Lake	Kotokel Lake	single	KTK2	2005	Kostrova et al. (2016)	#8
D1	Paleo Lake	Dethlingen	single		2004	Koutsodendris et al. (2012)	#52
LT1	Lake	Lake Tilo	composite	T97; T95	1995	Lamb et al. (2005)	#40
PN94C	Lake	Lake Pinarbasi	single	PN94C	1994	Leng et al. (2001)	#7
ZAC3	Lake	Laguna Zacapu	single	ZAC/3	2001	Leng et al. (2005)	#47
ZK2	Lake	Laguna Zacapu	single	ZK2	2001	Leng et al. (2005)	#50
BDP962	Lake	Lake Baikal	single	BDP-96-2	1996	Mackay et al. (2008)	#2
CON016053	Lake	Lake Baikal	supplemented	CON01-605-3	2001	Mackay et al. (2011)	#20
CON016032	Lake	Lake Baikal	single	CON-01-603-2	2001	Mackay et al. (2013)	#4
TDB1	Lake	Lake Brazi	single	TDB-1	2007	Magyari et al. (2013)	#22
Co1321	Lake	Bolshoye Shchuchye	single	Co1321	2016	Meyer et al. (2022)	#16
PG1857	Lake	Two-Yurts Lake	composite	PG1857; PG1857-2	2007	Meyer et al. (2015a)	#45
CON016053	Lake	Lake Baikal	supplemented	CON01-605-3	2001	Morley et al. (2005)	
LVA1	Lake	Laguna Verde Alta	composite			Polissar et al. (2006)	#32
LVB1	Lake	Laguna Verda Baja	supplemented			Polissar et al. (2006)	#18
PTAU1	Paleo Lake	Tauca	supplemented	BT		Quesada et al. (2015)	#17
PTAU1	Paleo Lake	Tauca	supplemented	CB		Quesada et al. (2015)	#17
PTAU1	Paleo Lake	Tauca	supplemented	EWK		Quesada et al. (2015)	#17
PTAU1	Paleo Lake	Tauca	supplemented	PJ		Quesada et al. (2015)	#17

Rec_ID	Archive	Lake	Core Type	original Core ID	Field Campaign (Year)	Short Reference	Used for Record number
HT1	Lake	Hausberg Tarn			1996	Rietti-Shati et al. (1998)	#46
VA	Lake	Vuolep Allakasjaure	supplemented	VA2	2000	Rosqvist et al. (2004)	#43
LS1	Lake	Lake Spaime	supplemented	Core III	2006	Rosqvist et al. (2013)	#49
LSG1	Lake	Lake Stuor Goussasjavri	supplemented	Core III	2007	Rosqvist et al. (2013)	#48
TL1	Lake	Tonsberg Lake	composite		1991	Rosqvist et al. (1999)	#19
G702	Lake	Lake Gosciaz	supplemented	G7/02	2002	Rozanski et al. (2010)	#29
MC2	Lake	Mica Lake	supplemented	MC-2	2006	Schiff et al. (2009)	#36
MBG1	Paleo Lake	Makgadikgadi	outcrop		2011	Schmidt et al. (2017)	#6
RM1	Paleo Lake	Ribains Maar	single		1988	Shemesh et al. (2001b)	#5
LP1	Lake	Linsley Pond	supplemented		1987	Shemesh and Peteet (1998)	#30
L850	Lake	Lake 850	single		1999	Shemesh et al. (2001a)	#37
R1	Lake	Lake Rutundu	single	R-1	1996	Street-Perrott et al. (2008)	#11
BAIK13	Lake	Lake Baikal	single	BAIK13-1	2013	Swann et al. (2018)	#51
BAIK13	Lake	Lake Baikal	single	BAIK13-4	2013	Swann et al. (2018)	#51
BAIK13	Lake	Lake Baikal	single	BAIK13-5	2013	Swann et al. (2018)	#51
BAIK13	Lake	Lake Baikal	single	BAIK13-7	2013	Swann et al. (2018)	#51
Lz1029	Lake	El'gygytgyn	composite	Lz1029	2003	Swann et al. (2010)	#15
BD4	Paleo Lake	Baringo-Bogoria Basin	outcrop	BD 4		Wilson et al. (2014b)	#1

Table A2. Overview of the records compiled and analyzed in this study. Lake basin parameters shown are taken from the HydroLakes database (Messager et al., 2016) for consistency. In case of major discrepancies between the HydroLakes database and the values provided by individual case studies, values of case are given as well and marked with an asterisk.

No.	Archive	Lake	Short Reference	Lat. [dec deg]	Lon. [dec deg]	Water depth [m]	Altitude [m asl]	Lake Area [km²]	Catchment Area [km²]	Residence time [a]	Chron.	Rec_ID
#1	Paleo Lake	Baringo-Bogoria Basin	Wilson et al. (2014b)	0.55	35.94		1178				Y	BD4
#2	Lake	Baikal	Mackay et al. (2008)	53.70	108.35	321	449	31968	569176	375	Y	BDP962
#3	Lake	El'gygytgyn	Chapl3gin et al. (2012b)	67.50	172.08	170	471	119	292	64	Y	Lz1024
#4	Lake	Baikal	Mackay et al. (2013)	53.96	108.91	386	449	31968	569176	375	Y	CON016032
#5	Paleo Lake	Ribains Maar	Shemesh et al. (2001b)	44.84	3.82		1074				N	RM1
#6	Paleo Lake	Makgadikgadi	Schmidt et al. (2017)	-20.29	24.27		934				N	MBG1
#7	Lake	Lake Pinarbasi	Leng et al. (2001)	37.47	33.12		1000	0.002			Y	PN94C
#8	Lake	Kotokel Lake	Kostrova et al. (2013a); Kostrova et al. (2013b); Kostrova et al. (2014); Kostrova et al. (2016)	52.78	108.12	4	453	65.7	170	58	Y	KTK2
#9	Lake	Baikal	Kalmychkov et al. (2007)	53.75	108.41	348	449	31968	569176	375	N	LB0301
#10	Lake	Baikal	Kalmychkov et al. (2007)	53.39	107.53	233	449	31968	569176	375	N	LB0402
#11	Lake	Lake Rutundu	Street-Perrott et al. (2008)	-0.03	37.45	11	3078	0.40			Y	R1
#12	Paleo Lake	Les Echets	Ampel et al. (2009)	45.90	4.93		267				Y	EC1
#13	Lake	Lake Challa	Barker et al. (2011)	-3.32	37.42	94	878	4.12	6.4	86	Y	LCHA1
#14	Lake	Lake Malawi	Barker et al. (2007)	-9.98	34.23	363	476	29544	128727	219	Y	M982P
#15	Lake	El'gygytgyn	Swann et al. (2010)	67.66	172.14	177.0	471	119	292	64	Y	Lz1029
#16	Lake	Bolshoye Shchuchye	Meyer et al. (2022)	67.88	66.32	132.0	186	11.80	227	5	Y	Co1321
#17	Paleo Lake	Tauca	Quesada et al. (2015)	-19.16	-68.20		3685				Y	PTAU1
#18	Lake	Laguna Verda Baja	Polissar et al. (2006)	8.86	-70.87	5	4170				Y	LVB1
#19	Lake	Tonsberg Lake	Rosqvist et al. (1999)	-54.17	-36.69		70	0.01			Y	TL1
#20	Lake	Baikal	Mackay et al. (2011)	51.58	104.85	600.0	449	31968	569176	375	Y	CON016053
#21	Lake	Small Hall Tarn	Barker (2001)	-0.15	37.35		4289				Y	SHT1

No.	Archive	Lake	Short Reference	Lat. [dec deg]	Lon. [dec deg]	Water depth [m]	Altitude [m asl]	Lake Area [km²]	Catchment Area [km²]	Residence time [a]	Chron.	Rec_ID
#22	Lake	Lake Brazi	Magyari et al. (2013)	45.40	22.90	1.1	1740	0.004	0.10	0.5	Y	TDB1
#23	Lake	Nar Gölü	Dean et al. (2018)	38.34	34.46	25.0	1369	0.52	3.5	15	Y	NAR0110
#24	Lake	Lake Emanda	Kostrova et al. (2021)	65.28	135.75	14.6	654	33.10	118	26	Y	Co1412
#25	Lake	Baunt Lake	Harding et al. (2020)	55.19	113.03	33	1052	112	10256	1.1	Y	BNT1418
#26	Lake	Sunken Island Lake	Broadman et al. (2020b)	60.59	-150.89	7	84	0.44	28.3	0.18	Y	SILMC
#27	Lake	Grandfather Lake	Hu and Shemesh (2003)	60.80	-158.52	20	142	0.35			Y	GL1
#28	Lake	Lago Chungara	Hernandez et al. (2008); Hernandez et al. (2010); Hernandez et al. (2011); Hernandez et al. (2013)	-18.25	-69.17	40	4556	21.27	265	289 (15*)	Y	LG1
#29	Lake	Lake Gosciaz	Rozanski et al. (2010)	52.58	19.35	25	63	0.38	20.6	0.51	Y	G702
#30	Lake	Linsley Pond	Shemesh and Peteet (1998)	41.30	-72.75	9	8	0.93			Y	LP1
#31	Lake	Lake Ladoga	Kostrova et al. (2019)	60.98	30.68	111		17444	279581	11	Y	Co1309
#32	Lake	Laguna Verde Alta	Polissar et al. (2006)	8.85	-70.87	3	4215				Y	LVA1
#33	Lake	Garba Guracha	Bittner et al. (2021)	6.88	39.88	5	3950	0.15	0.15		Y	BALGGU171
#34	Lake	Simba Tarn	Barker (2001)	-0.15	37.32		4959	0.00			Y	ST1
#35	Lake	Heart Lake	Bailey et al. (2018)	51.85	-176.69	7.6	60	0.25	8	0.038	Y	HL1
#36	Lake	Mica Lake	Schiff et al. (2009)	60.96	-148.15	58	93	0.63	3.2	0.46	Y	MC2
#37	Lake	Lake 850	Shemesh et al. (2001a)	68.25	19.12	8	850		0.5		Y	L850
#38	Lake	Lake Chuna	Jones et al. (2004)	67.95	32.48		475	0.13	2	0.30	Y	LC1
#39	Lake	Schrader Pond	Broadman et al. (2020a)	69.36	-145.08		869				Y	SCP162A
#40	Lake	Lake Tilo	Lamb et al. (2005)	7.06	38.10	10	1551	0.66	144	0.15	Y	LT1
#41	Lake	Nettilling Lake	Chaplgin et al. (2016b); Narancic et al. (2016)	66.50	-70.50	14	18	4872.70	63400	5.5	N	Ni2B
#42	Lake	Lake Pupuke	Heyng et al. (2015)	-36.78	174.77	58	11	1.01	1	5.8	Y	P210/P260
#43	Lake	Vuolep Allakasjaure	Jonsson et al. (2010)	68.18	18.17	11	991	1.01	1	5.8	Y	VA
#44	Lake	Lac Petit	Cartier et al. (2019a)	44.11	7.19	7	2200	0.018	6		Y	PET09P2
#45	Lake	Two-Yurts Lake	Meyer et al. (2015a)	56.82	160.11	28	264	0.02	6		Y	PG1857
#46	Lake	Hausberg Tarn	Rietti-Shati et al. (1998)	-0.15	37.30		4369	11.39	206	1.9	Y	

No	Archive	Lake	Short Reference	Lat. [dec deg]	Lon. [dec deg]	Water depth [m]	Altitude [m asl]	Lake Area [km²]	Catchment Area [km²]	Residence time [a]	Chron.	Rec_ID
#47	Lake	Laguna Zacapu	Leng et al. (2005)	19.83	-101.79	2.0	1987	0.23	66	0.037	N	ZAC3
#48	Lake	Lake Stuor Goussasjavri	Rosqvist et al. (2013)	67.85	19.68	6	559	0.28	0.5	5.6	Y	LSG1
#49	Lake	Lake Spaime	Rosqvist et al. (2013)	63.12	12.32	4	887	0.03	3.5	0.04	Y	LS1
#50	Lake	Laguna Zacapu	Leng et al. (2005)	19.82	-101.79	8	1987	0.23	66	0.037	N	ZK2
#51	Lake	Baikal	Swann et al. (2018)	51.77	104.42	1360	449	31968	569176	375	Y	BAIK13
#52	Paleo Lake	Dethlingen	Koutsodendris et al. (2012)	52.96	10.14		65				N	D110
#53	Lake	Yellowstone Lake	Brown et al., (2021)	44.54	-110.39	61	2360	340	2579	21 (14*)	Y	YL16-2C

Data availability

The dataset is being submitted to PANGAEA and will be available here after publication: https://doi.pangaea.de/10.1594/PANGAEA.957160.

Author contributions

PM, HM, BD and BB designed the research project and structure of the manuscript. PM compiled the data base, carried out statistical analyses and produced all figures and tables and wrote the main part of the manuscript. ML, GR, AH, GS, AM, HM, HB and PB contributed data publicly not available. All co-authors brought in their expertise have made substantial contributions to the manuscript. All authors have written parts of the manuscript, commented on drafts and have approved its final submitted version.

Competing Interests

The authors declare that they have no conflict of interest.

Disclaimer

Maps throughout this article were created using ArcGIS® software by Esri. ArcGIS® and ArcMap™ are the intellectual property of Esri and are used herein under license. Copyright © Esri. All rights reserved. For more information about Esri® software, please visit www.esri.com.'

Acknowledgements

PM is funded by German Ministry of Education and Research via the Palmod2 project (01LP1923B). HB is funded by the Academy of Finland (grant 348536). AH is funded by the Spanish Ministry of Science and Innovation through the Ramón y Cajal Scheme (RYC2020-029253-I). We thank Heinz Wanner, Witold Bagniewski, and one anonymous reviewer, whose comments helped substantially improving the manuscript. We also thank all scientists and technicians developing and advancing the research field of oxygen isotopes in diatom silica.

References

Akse, S. P., Polerecky, L., Kienhuis, M. V. M. and Middelburg, J. J.: The influence of sediment diagenesis and aluminium on oxygen isotope exchange of diatom frustules, Geochimica et Cosmochimica Acta 333, 362-372, 10.1016/j.gca.2022.07.015, 2022.

Ampel, L., Wohlfarth, B., Risberg, J., Veres, D., Leng, M. J., and Tillman, P. K.: Diatom assemblage dynamics during abrupt climate change: the response of lacustrine diatoms to Dansgaard–Oeschger cycles during the last glacial period, J Paleolimnol, 44, 397-404, 10.1007/s10933-009-9350-7, 2009.

Andersen, K. K., Azuma, N., Barnola, J. M., Bigler, M., Biscaye, P., Caillon, N., Chappellaz, J., Clausen, H. B., Dahl-Jensen, D., Fischer, H., Flückiger, J., Fritzsche, D., Fujii, Y., Goto-Azuma, K., Grønvold, K., Gundestrup, N. S., Hansson, M., Huber, C., Hvidberg, C. S., Johnsen, S. J., Jonsell, U., Jouzel, J., Kipfstuhl, S., Landais, A., Leuenberger, M., Lorrain, R., Masson-Delmotte, V., Miller, H., Motoyama, H., Narita, H., Popp, T., Rasmussen, S. O., Raynaud, D., Rothlisberger, R., Ruth, U., Samyn, D., Schwander, J., Shoji, H., Siggard-Andersen, M. L., Steffensen, J. P., Stocker, T., Sveinbjörnsdóttir, A. E., Svensson, A., Takata, M., Tison, J. L., Thorsteinsson, T., Watanabe, O., Wilhelms, F., White, J. W. C., and North Greenland Ice Core Project, m.: High-resolution record of Northern Hemisphere climate extending into the last interglacial period, Nature, 431, 147-151, 10.1038/nature02805, 2004.

Bailey, H.L., Kaufman, D.S., Henderson, A.C. and Leng, M.J.: Synoptic scale controls on the δ^{18}O in precipitation across Beringia, Geophys. Res. Lett, 42(11), 4608-4616, 10.1002/2015GL063983, 2015.

Bailey, H. L., Kaufman, D. S., Sloane, H. J., Hubbard, A. L., Henderson, A. C. G., Leng, M. J., Meyer, H., and Welker, J. M.: Holocene atmospheric circulation in the central North Pacific: A new terrestrial diatom and δ18O dataset from the Aleutian Islands, Quaternary Sci Rev, 194, 27-38, 10.1016/j.quascirev.2018.06.027, 2018.

Barker, P. A.: A 14,000-Year Oxygen Isotope Record from Diatom Silica in Two Alpine Lakes on Mt. Kenya, Science, 292, 2307-2310, 10.1126/science.1059612, 2001.

Barker, P. A., Leng, M. J., Gasse, F., and Huang, Y.: Century-to-millennial scale climatic variability in Lake Malawi revealed by isotope records, Earth Planet Sc Lett, 261, 93-103, 10.1016/j.epsl.2007.06.010, 2007.

Barker, P. A., Hurrell, E. R., Leng, M. J., Wolff, C., Cocquyt, C., Sloane, H. J., and Verschuren, D.: Seasonality in equatorial climate over the past 25 k.y. revealed by oxygen isotope records from Mount Kilimanjaro, Geology, 39, 1111-1114, 10.1130/g32419.1, 2011.

Barker, P. A., Street-Perrott, F. A., Leng, M. J., Greenwood, P. B., Swain, D. L., Perrott, R. A., Telford, R. J., and Ficken, K. J.: A 14,000-year oxygen isotope record from diatom silica in two alpine lakes on Mt. Kenya, Science, 292, 2307-2310, DOI 10.1126/science.1059612, 2001.

Biskaborn, B. K., Subetto, D. A., Savelieva, L. A., Vakhrameeva, P. S., Hansche, A., Herzschuh, U., Klemm, J., Heinecke, L., Pestryakova, L. A., Meyer, H., Kuhn, G., and Diekmann, B.: Late Quaternary vegetation and lake system dynamics in north-eastern Siberia: Implications for seasonal climate variability, Quaternary Sci Rev, 147, 406-421, https://doi.org/10.1016/j.quascirev.2015.08.014, 2016.

Bittner, L., Gil-Romera, G., Grady, D., Lamb, H. F., Lorenz, E., Weiner, M., Meyer, H., Bromm, T., Glaser, B., and Zech, M.: The Holocene lake-evaporation history of the afro-alpine Lake Garba Guracha in the Bale Mountains, Ethiopia, based on δ18O records of sugar biomarker and diatoms, Quaternary Res, 1-14, 10.1017/qua.2021.26, 2021.

The Online Isotopes in Precipitation Calculator version OIPC3.1: http://www.waterisotopes.org, last access: 8/2022.

Bradley, R. S., Hughes, M. K., and Diaz, H. F.: Climate in Medieval Time, Science, 302, 404-405, doi:10.1126/science.1090372, 2003.

Brewer, T. S., Leng, M. J., Mackay, A. W., Lamb, A. L., Tyler, J. J., and Marsh, N. G.: Unravelling contamination signals in biogenic silica oxygen isotope composition: the role of major and trace element geochemistry, J Quaternary Sci, 23, 321-330, https://doi.org/10.1002/jqs.1171, 2008.

Broadman, E., Kaufman, D. S., Henderson, A. C. G., Malmierca-Vallet, I., Leng, M. J., and Lacey, J. H.: Coupled impacts of sea ice variability and North Pacific atmospheric circulation on Holocene hydroclimate in Arctic Alaska, Proceedings of the National Academy of Sciences, 117, 33034-33042, 10.1073/pnas.2016544117, 2020a.

Broadman, E., Kaufman, D. S., Henderson, A. C. G., Berg, E. E., Anderson, R. S., Leng, M. J., Stahnke, S. A., and Muñoz, S. E.: Multi-proxy evidence for millennial-scale changes in North Pacific Holocene hydroclimate from the Kenai Peninsula lowlands, south-central Alaska, Quaternary Sci Rev, 241, 10.1016/j.quascirev.2020.106420, 2020b.

Brown, S. R., Cartier, R., Schiller, C. M., Zahajská, P., Fritz, S. C., Morgan, L. A., Whitlock, C., Conley, D. J., Lacey, J. H., Leng, M. J., and Shanks, W. C. P.: Multi-proxy record of Holocene paleoenvironmental conditions from Yellowstone Lake, Wyoming, USA, Quaternary Sci Rev, 274, 107275, https://doi.org/10.1016/j.quascirev.2021.107275, 2021.

Büntgen, U., Myglan, V. S., Ljungqvist, F. C., McCormick, M., Di Cosmo, N., Sigl, M., Jungclaus, J., Wagner, S., Krusic, P. J., Esper, J., Kaplan, J. O., de Vaan, M. A. C., Luterbacher, J., Wacker, L., Tegel, W., and Kirdyanov, A. V.: Cooling and societal change during the Late Antique Little Ice Age from 536 to around 660 AD, Nature Geoscience, 9, 231-236, 10.1038/ngeo2652, 2016.

Cartier, R., Sylvestre, F., Paillès, C., Sonzogni, C., Couapel, M., Alexandre, A., Mazur, J.-C., Brisset, E., Miramont, C., and Guiter, F.: Diatom-oxygen isotope record from high-altitude Lake Petit (2200 m a.s.l.) in the Mediterranean Alps: shedding light on a climatic pulse at 4.2 ka, Clim Past, 15, 253-263, 10.5194/cp-15-253-2019, 2019a.

Cartier, R., Sylvestre, F., Pailles, C., Sonzogni, C., Couapel, M., Alexandre, A., Mazur, J. C., Brisset, E., Miramont, C., and Guiter, F.: Diatom-oxygen isotope record from high-altitude Lake Petit (2200 m a.s.l.) in the Mediterranean Alps: shedding light on a climatic pulse at 4.2 ka, Clim Past, 15, 253-263, 10.5194/cp-15-253-2019, 2019b.

Chapligin, B., Narancic, B., Meyer, H., and Pienitz, R.: Paleo-environmental gateways in the eastern Canadian arctic – Recent isotope hydrology and diatom oxygen isotopes from Nettilling Lake, Baffin Island, Canada, Quaternary Sci Rev, 147, 379-390, 10.1016/j.quascirev.2016.03.028, 2016a.

Chapligin, B., Narancic, B., Meyer, H., and Pienitz, R.: Paleo-environmental gateways in the eastern Canadian arctic - Recent isotope hydrology and diatom oxygen isotopes from Nettilling Lake, Baffin Island, Canada, Quaternary Sci Rev, 147, 379-390, 10.1016/j.quascirev.2016.03.028, 2016b.

Chapligin, B., Meyer, H., Bryan, A., Snyder, J., and Kemnitz, H.: Assessment of purification and contamination correction methods for analysing the oxygen isotope composition from biogenic silica, Chem Geol, 300, 185-199, 10.1016/j.chemgeo.2012.01.004, 2012a.

Chapligin, B., Meyer, H., Swann, G. E. A., Meyer-Jacob, C., and Hubberten, H. W.: A 250 ka oxygen isotope record from diatoms at Lake El'gygytgyn, far east Russian Arctic, Clim Past, 8, 1621-1636, 10.5194/cp-8-1621-2012, 2012b.

Chapligin, B., Leng, M. J., Webb, E., Alexandre, A., Dodd, J. P., Ijiri, A., Lücke, A., Shemesh, A., Abelmann, A., Herzschuh, U., Longstaffe, F. J., Meyer, H., Moschen, R., Okazaki, Y., Rees, N. H., Sharp, Z. D., Sloane, H. J., Sonzogni, C., Swann, G. E. A., Sylvestre, F., Tyler, J. J., and Yam, R.: Inter-laboratory comparison of oxygen isotope compositions from biogenic silica, Geochim Cosmochim Ac, 75, 7242-7256, https://doi.org/10.1016/j.gca.2011.08.011, 2011.

Chapligin, B., Meyer, H., Langer, M. and Hubberten, H. W.: A 250 ka oxygen isotope record from diatoms and investigation of "super-interglacial" conditions during MIS 11 at Lake El'gygytgyn, Far East Russian Arctic. AGU Fall Meeting 2012, San Francisco, USA, 3 December 2012 - 7 December 2012, 2012.

Chondrogianni, C., Ariztegui, D., Rolph, T., Juggins, S., Shemesh, A., Rietti-Shati, M., Niessen, F., Guilizzoni, P., Lami, A., McKenzie, J. A., and Oldfield, F.: Millennial to interannual climate variability in the Mediterranean during the Last Glacial Maximum, Quatern Int, 122, 31-41, 10.1016/j.quaint.2004.01.029, 2004.

Danek, C., Gierz, P., Kostrova, S. S., Meister, P., Meyer, H., and Werner, M.: Eurasian Holocene climate trends in transient coupled climate simulations and stable oxygen isotope records, J Quaternary Sci, n/a, https://doi.org/10.1002/jqs.3396, 2021.

Dansgaard, W.: Stable isotopes in precipitation, Tellus, 16, 436-468, https://doi.org/10.1111/j.2153-3490.1964.tb00181.x, 1964.

Dean, J. R., Jones, M. D., Leng, M. J., Metcalfe, S. E., Sloane, H. J., Eastwood, W. J., and Roberts, C. N.: Seasonality of Holocene hydroclimate in the Eastern Mediterranean reconstructed using the oxygen isotope composition of carbonates and diatoms from Lake Nar, central Turkey, Holocene, 28, 267-276, 10.1177/0959683617721326, 2018.

Dodd, J. P. and Sharp, Z. D.: A laser fluorination method for oxygen isotope analysis of biogenic silica and a new oxygen isotope calibration of modern diatoms in freshwater environments, Geochim Cosmochim Ac, 74, 1381-1390, 10.1016/j.gca.2009.11.023, 2010.

Harding, P., Bezrukova, E. V., Kostrova, S. S., Lacey, J. H., Leng, M. J., Meyer, H., Pavlova, L. A., Shchetnikov, A., Shtenberg, M. V., Tarasov, P. E., and Mackay, A. W.: Hydrological (in)stability in Southern Siberia during the Younger Dryas and early Holocene, Global Planet Change, 195, 10.1016/j.gloplacha.2020.103333, 2020.

Downing, J.A., Duarte, C.M. Abundance and size distribution of lakes, ponds and impoundments, in: Likens, G.E. (Ed.), Encyclopedia of Inland Waters. Elsevier, Oxford, UK, pp. 469-478, 2009.

Helama, S., Jones, P. D., and Briffa, K. R.: Dark Ages Cold Period: A literature review and directions for future research, The Holocene, 27, 1600-1606, 10.1177/0959683617693898, 2017.

Hernandez, A., Giralt, S., Bao, R., Saez, A., Leng, M. J., and Barker, P. A.: ENSO and solar activity signals from oxygen isotopes in diatom silica during late glacial-Holocene transition in Central Andes (18A degrees S), J Paleolimnol, 44, 413-429, 10.1007/s10933-010-9412-x, 2010.

Hernandez, A., Bao, R., Giralt, S., Barker, P. A., Leng, M. J., Sloane, H. J., and Saez, A.: Biogeochemical processes controlling oxygen and carbon isotopes of diatom silica in Late Glacial to Holocene lacustrine rhythmites, Palaeogeogr Palaeocl, 299, 413-425, 10.1016/j.palaeo.2010.11.020, 2011.

Hernandez, A., Bao, R., Giralt, S., Saez, A., Leng, M. J., Barker, P. A., Kendrick, C. P., and Sloane, H. J.: Climate, catchment runoff and limnological drivers of carbon and oxygen isotope composition of diatom frustules from the central Andean Altiplano during the Lateglacial and Early Holocene, Quaternary Sci Rev, 66, 64-73, 10.1016/j.quascirev.2012.10.013, 2013.

Hernandez, A., Bao, R., Giralt, S., Leng, M. J., Barker, P. A., Saez, A., Pueyo, J. J., Moreno, A., Valero-Garces, B. L., and Sloane, H. J.: The palaeohydrological evolution of Lago Chungara (Andean Altiplano, northern Chile) during the Lateglacial and early Holocene using oxygen isotopes in diatom silica, J Quaternary Sci, 23, 351-363, 10.1002/jqs.1173, 2008.

Herzschuh, U., Birks, H. J. B., Laepple, T., Andreev, A., Melles, M., and Brigham-Grette, J.: Glacial legacies on interglacial vegetation at the Pliocene-Pleistocene transition in NE Asia, Nature Communications, 7, 11967, 10.1038/ncomms11967, 2016.

Herzschuh, U. B., Thomas; Li, Chenzhi; Cao, Xianyong: Northern Hemisphere temperature and precipitation reconstruction from taxonomically harmonized pollen data set with revised chronologies using WA-PLS and MAT (LegacyClimate 1.0). PANGAEA [dataset], https://doi.pangaea.de/10.1594/PANGAEA.930512, 2021.

Herzschuh, U., Böhmer, T., Li, C., Chevalier, M., Dallmeyer, A., Cao, X.,. LegacyClimate 1.0: A dataset of pollen-based climate reconstructions from 2594 Northern Hemisphere sites covering the late quaternary. Earth System Science Data, 1–29. https://doi.org/10.5194/essd-2022-38, 2022.

405 Herzschuh, U., Böhmer, T., Li, C., Chevalier, M., Hébert, R., Dallmeyer, A., Cao, X. Bigelow, N. H., Nazarova, L., Novenko, E. Y., Park, J., Peyron, O., Rudaya, N. A., Schlütz, F., Shumilovskikh, L. S., Tarasov, P. E., Wang, Y., Wen, R., Xu, Q., and Zheng, Z.: LegacyClimate 1.0: a dataset of pollen-based climate reconstructions from 2594 Northern Hemisphere sites covering the last 30 kyr and beyond, Earth Syst. Sci. Data, 15, 2235–2258, https://doi.org/10.5194/essd-15-2235-2023, 2023a

Herzschuh, U., Böhmer, T., Chevalier, M., Hébert, R., Dallmeyer, A., Li, C., Cao, X., Peyron, O., Nazarova, L., Novenko, E. Y., Park, J., Rudaya, N. A., Schlütz, F., Shumilovskikh, L. S., Tarasov, P. E., Wang, Y., Wen, R., Xu, Q., and Zheng, Z.: Regional pollen-based Holocene

410 temperature and precipitation patterns depart from the Northern Hemisphere mean trends, Clim. Past, 19, 1481–1506, https://doi.org/10.5194/cp-19-1481-2023, 2023b.

Heyng, A. M., Mayr, C., Lücke, A., Moschen, R., Wissel, H., Striewski, B., and Bauersachs, T.: Middle and Late Holocene paleotemperatures reconstructed from oxygen isotopes and GDGTs of sediments from Lake Pupuke, New Zealand, Quatern Int, 374, 3-14, 10.1016/j.quaint.2014.12.040, 2015.

415 Hu, F. S. and Shemesh, A.: A biogenic-silica δ18O record of climatic change during the last glacial–interglacial transition in southwestern Alaska, Quaternary Res, 59, 379-385, 10.1016/s0033-5894(03)00056-5, 2003.

Hu, F. S., Kaufman, D., Yoneji, S., Nelson, D., Shemesh, A., Huang, Y., Tian, J., Bond, G., Clegg, B., and Brown, T.: Cyclic Variation and Solar Forcing of Holocene Climate in the Alaskan Subarctic, Science, 301, 1890-1893, doi:10.1126/science.1088568, 2003.

IAEA/WMO: Global Network of Isotopes in Precipitation. The GNIP Database. [dataset], 2022.

420 Jones, V. J., Leng, M. J., Solovieva, N., Sloane, H. J., and Tarasov, P.: Holocene climate of the Kola Peninsula; evidence from the oxygen isotope record of diatom silica, Quaternary Sci Rev, 23, 833-839, 10.1016/j.quascirev.2003.06.014, 2004.

Jonsson, C. E., Rosqvist, G. C., Leng, M. J., Bigler, C., Bergman, J., Tillman, P. K., and Sloane, H. J.: High-resolution diatom δ18O records, from the last 150 years, reflecting changes in amount of winter precipitation in two sub-Arctic high-altitude lakes in the Swedish Scandes, J Quaternary Sci, 25, 918-930, https://doi.org/10.1002/jqs.1372, 2010.

425 Kalmychkov, G., Kuz'min, M., Pokrovskii or Pokrovsky, B., and Kostrova, S.: Oxygen isotopic composition in diatom algae frustules from Lake Baikal sediments: Annual mean temperature variations during the last 40 Ka, Dokl Earth Sci, 413, 206-209, 10.1134/S1028334X07020158, 2007.

Kaufman, D., McKay, N., Routson, C., Erb, M., Dätwyler, C., Sommer, P. S., Heiri, O., and Davis, B.: Holocene global mean surface temperature, a multi-method reconstruction approach, Scientific Data, 7, 201, 10.1038/s41597-020-0530-7, 2020.

430 Kaufman, D.S., Broadman, E. Revisiting the Holocene global temperature conundrum. Nature 614, 425-435. doi: 10.1038/s41586-022-05536-w, 2023.

Kaufman, D. S., Ager, T. A., Anderson, N. J., Anderson, P. M., Andrews, J. T., Bartlein, P. J., Brubaker, L. B., Coats, L. L., Cwynar, L. C., Duvall, M. L., Dyke, A. S., Edwards, M. E., Eisner, W. R., Gajewski, K., Geirsdóttir, A., Hu, F. S., Jennings, A. E., Kaplan, M. R., Kerwin, M. W., Lozhkin, A. V., MacDonald, G. M., Miller, G. H., Mock, C. J., Oswald, W. W., Otto-Bliesner, B. L., Porinchu, D. F., Rühland, K.,

435 Smol, J. P., Steig, E. J., and Wolfe, B. B.: Holocene thermal maximum in the western Arctic (0–180°W), Quaternary Sci Rev, 23, 529-560, https://doi.org/10.1016/j.quascirev.2003.09.007, 2004.

Konecky, B. L., McKay, N. P., Churakova, O. V., Comas-Bru, L., Dassié, E. P., DeLong, K. L., Falster, G. M., Fischer, M. J., Jones, M. D., Jonkers, L., Kaufman, D. S., Leduc, G., Managave, S. R., Martrat, B., Opel, T., Orsi, A. J., Partin, J. W., Sayani, H. R., Thomas, E. K., Thompson, D. M., Tyler, J. J., Abram, N. J., Atwood, A. R., Cartapanis, O., Conroy, J. L., Curran, M. A., Dee, S. G., Deininger, M., Divine,

440 D. V., Kern, Z., Porter, T. J., Stevenson, S. L., von Gunten, L., and Iso2k Project, M.: The Iso2k database: a global compilation of paleo-δ18O and δ2H records to aid understanding of Common Era climate, Earth Syst. Sci. Data, 12, 2261-2288, 10.5194/essd-12-2261-2020, 2020.

Kostrova, S. S., Meyer, H., Chaplgin, B., Tarasov, P. E., and Bezrukova, E. V.: The last glacial maximum and late glacial environmental and climate dynamics in the Baikal region inferred from an oxygen isotope record of lacustrine diatom silica, Quatern Int, 348, 25-36,

445 10.1016/j.quaint.2014.07.034, 2014.

Kostrova, S. S., Biskaborn, B. K., Pestryakova, L. A., Fernandoy, F., Lenz, M. M., and Meyer, H.: Climate and environmental changes of the Lateglacial transition and Holocene in northeastern Siberia: Evidence from diatom oxygen isotopes and assemblage composition at Lake Emanda, Quaternary Sci Rev, 259, 106905, https://doi.org/10.1016/j.quascirev.2021.106905, 2021.

Kostrova, S. S., Meyer, H., Chaplgin, B., Bezrukova, E. V., Tarasov, P. E., and Kuz'min, M. I.: Reconstruction of the Holocene climate of

450 Transbaikalia: Evidence from the oxygen isotope analysis of fossil diatoms from Kotokel Lake, Dokl Earth Sci, 451, 732-736, 10.1134/S1028334x13070039, 2013a.

Kostrova, S. S., Meyer, H., Chaplgin, B., Kossler, A., Bezrukova, E. V., and Tarasov, P. E.: Holocene oxygen isotope record of diatoms from Lake Kotokel (southern Siberia, Russia) and its palaeoclimatic implications, Quatern Int, 290, 21-34, 10.1016/j.quaint.2012.05.011, 2013b.

455 Kostrova, S. S., Meyer, H., Tarasov, P. E., Bezrukova, E. V., Chaplgin, B., Kossler, A., Pavlova, L. A., and Kuzmin, M. I.: Oxygen isotope composition of diatoms from sediments of Lake Kotokel (Buryatia), Russ Geol Geophys+, 57, 1239-1247, 10.1016/j.rgg.2016.08.009, 2016.

Kostrova, S. S., Meyer, H., Bailey, H. L., Ludikova, A. V., Gromig, R., Kuhn, G., Shibaev, Y. A., Kozachek, A. V., Ekaykin, A. A., and Chapligin, B.: Holocene hydrological variability of Lake Ladoga, northwest Russia, as inferred from diatom oxygen isotopes, Boreas, 48, 361-376, 10.1111/bor.12385, 2019.

Koutsodendris, A., Pross, J., Müller, U. C., Brauer, A., Fletcher, W. J., Kühl, N., Kirilova, E., Verhagen, F. T. M., Lücke, A., and Lotter, A. F.: A short-term climate oscillation during the Holsteinian interglacial (MIS 11c): An analogy to the 8.2ka climatic event?, Global Planet Change, 92-93, 224-235, 10.1016/j.gloplacha.2012.05.011, 2012.

Kwiecien, O., Stockhecke, M., Pickarski, N., Heumann, G., Litt, T., Sturm, M., Anselmetti, F., Kipfer, R., and Haug, G. H.: Dynamics of the last four glacial terminations recorded in Lake Van, Turkey, Quaternary Sci Rev, 104, 42-52, https://doi.org/10.1016/j.quascirev.2014.07.001, 2014.

Lamb, A. L., Leng, M. J., Sloane, H. J., and Telford, R. J.: A comparison of the palaeoclimate signals from diatom oxygen isotope ratios and carbonate oxygen isotope ratios from a low latitude crater lake, Palaeogeogr Palaeocl, 223, 290-302, 10.1016/j.palaeo.2005.04.011, 2005.

Lasher, G., Axford, Y., McFarlin, J., Kelly, M., Osterberg, E., and Berkelhammer, M.: Holocene temperatures and isotopes of precipitation in Northwest Greenland recorded in lacustrine organic materials, Quaternary Sci Rev, 170, 45-55, 10.1016/j.quascirev.2017.06.016, 2017.

Laskar, J., Robutel, P., Joutel, F., Gastineau, M., Correia, A. C. M., and Levrard, B.: A long-term numerical solution for the insolation quantities of the Earth, A&A, 428, 261-285, 2004.

Leclerc, A. J. and Labeyrie, L.: Temperature dependence of the oxygen isotopic fractionation between diatom silica and water, Earth Planet Sc Lett, 84, 69-74, https://doi.org/10.1016/0012-821X(87)90177-4, 1987.

Leng, M., Barker, P., Greenwood, P., Roberts, N., and Reed, J.: Oxygen isotope analysis of diatom silica and authigenic calcite from Lake Pinarbasi, Turkey, J Paleolimnol, 25, 343-349, Doi 10.1023/A:1011169832093, 2001.

Leng, M. J.: Isotopes in palaeoenvironmental research, Developments in paleoenvironmental research :, 10, Springer, Dordrecht, xviii, 307 p. pp.2006.

Leng, M. J. and Barker, P. A.: A review of the oxygen isotope composition of lacustrine diatom silica for palaeoclimate reconstruction, Earth-Sci Rev, 75, 5-27, 10.1016/j.earscirev.2005.10.001, 2006.

Leng, M. J. and Marshall, J. D.: Palaeoclimate interpretation of stable isotope data from lake sediment archives, Quaternary Sci Rev, 23, 811-831, https://doi.org/10.1016/j.quascirev.2003.06.012, 2004.

Leng, M. J., Metcalfe, S. E., and Davies, S. J.: Investigating late holocene climate variability in central mexico using carbon isotope ratios in organic materials and oxygen isotope ratios from diatom silica within lacustrine sediments, J Paleolimnol, 34, 413-431, 10.1007/s10933-005-6748-8, 2005.

Lisiecki, L. E. and Raymo, M. E.: A Pliocene-Pleistocene stack of 57 globally distributed benthic δ18O records, Paleoceanography, 20, n/a-n/a, 10.1029/2004pa001071, 2005.

Liu, Z. , Zhu, J. , Rosenthal, Y. , Zhang, X. , Otto-Bliesner, B. L. , Timmermann, A. , Smith, R. S. , Lohmann, G. , Zheng, W. and Timm, O. E. The Holocene temperature conundrum, Proceedings of the National Academy of Sciences of the U.S 111 (34), E3501-E3505. doi: 10.1073/pnas.1407229111, 2014.

Ljungqvist, F. C.: A new reconstruction of temperature variability in the extra-tropical northern hemisphere during the last two millennia, Geografiska Annaler: Series A, Physical Geography, 92, 339-351, 10.1111/j.1468-0459.2010.00399.x, 2010.

Mackay, A. W., Karabanov, E., Leng, M. J., Sloane, H. J., Morley, D. W., Panizzo, V. N., Khursevich, G., and Williams, D.: Reconstructing hydrological variability in Lake Baikal during MIS 11: an application of oxygen isotope analysis of diatom silica, J Quaternary Sci, 23, 365-374, 10.1002/jqs.1174, 2008.

Mackay, A. W., Swann, G. E. A., Brewer, T. S., Leng, M. J., Morley, D. W., Piotrowska, N., Rioual, P., and White, D.: A reassessment of late glacial - Holocene diatom oxygen isotope record from Lake Baikal using a geochemical mass-balance approach, J Quaternary Sci, 26, 627-634, 10.1002/jqs.1484, 2011.

Mackay, A. W., Swann, G. E. A., Fagel, N., Fietz, S., Leng, M. J., Morley, D., Rioual, P., and Tarasov, P.: Hydrological instability during the Last Interglacial in central Asia: a new diatom oxygen isotope record from Lake Baikal, Quaternary Sci Rev, 66, 45-54, 10.1016/j.quascirev.2012.09.025, 2013.

Magyari, E. K., Demeny, A., Buczko, K., Kern, Z., Vennemann, T., Forizs, I., Vincze, I., Braun, M., Kovacs, J. I., Udvardi, B., and Veres, D.: A 13,600-year diatom oxygen isotope record from the South Carpathians (Romania): Reflection of winter conditions and possible links with North Atlantic circulation changes, Quatern Int, 293, 136-149, 10.1016/j.quaint.2012.05.042, 2013.

Mann, M. E., Zhang, Z., Rutherford, S., Bradley, R. S., Hughes, M. K., Shindell, D., Ammann, C., Faluvegi, G., and Ni, F.: Global Signatures and Dynamical Origins of the Little Ice Age and Medieval Climate Anomaly, Science, 326, 1256-1260, doi:10.1126/science.1177303, 2009.

Marcott, S., Shakun, J., Clark, P., and Mix, A.: A Reconstruction of Regional and Global Temperature for the Past 11,300 Years, Science (New York, N.Y.), 339, 1198-1201, 10.1126/science.1228026, 2013.

Matheney, R. K. and Knauth, L. P.: Oxygen-isotope fractionation between marine biogenic silica and seawater, Geochim Cosmochim Ac, 53, 3207-3214, 10.1016/0016-7037(89)90101-4, 1989.

Matthews, J. A. and Briffa, K. R.: The 'Little Ice Age': Re-Evaluation of an Evolving Concept, Geografiska Annaler. Series A, Physical Geography, 87, 17-36, 2005.

McKay, N. P., Kaufman, D. S., Routson, C. C., Erb, M. P., and Zander, P. D.: The onset and rate of Holocene Neoglacial cooling in the Arctic, Geophysical Research Letters, 45, 12,487–12,496, 10.1029/2018GL079773, 2018.

Meister, P., Alexandre, A., Bailey, H., Barker, P., Biskaborn, B. K, Broadman, E., Cartier, R., Chapligin, B., Couapel, M.J. J, Dean, J. R., Diekmann, B., Harding, P., Henderson, A., Hernandez, A., Herzschuh, U., Kostrova, S. S., Lacey, J. H., Leng, M. J., Lücke, A., Mackay, A. W., Magyari, E. K., Narancic, B., Porchier, C., Rosqvist, G. C., Shemesh, A., Sonzogni, C., Swann, G. E. A., Sylvestre, F., Meyer, H.: A global compilation of diatom silica oxygen isotope records from lake sediment. PANGAEA, https://doi.pangaea.de/10.1594/PANGAEA.957160, 2023.

Melles, M., Brigham-Grette, J., Minyuk, P. S., Nowaczyk, N. R., Wennrich, V., DeConto, R. M., Anderson, P. M., Andreev, A. A., Coletti, A., Cook, T. L., Haltia-Hovi, E., Kukkonen, M., Lozhkin, A. V., Rosén, P., Tarasov, P., Vogel, H., and Wagner, B.: 2.8 Million Years of Arctic Climate Change from Lake El'gygytgyn, NE Russia, Science, 337, 315-320, doi:10.1126/science.1222135, 2012.

Messager, M. L., Lehner, B., Grill, G., Nedeva, I., and Schmitt, O.: Estimating the volume and age of water stored in global lakes using a geo-statistical approach, Nature Communications, 7, 13603, 10.1038/ncomms13603, 2016.

Meyer, H., Chapligin, B., Hoff, U., Nazarova, L., and Diekmann, B.: Oxygen isotope composition of diatoms as Late Holocene climate proxy at Two-Yurts Lake, Central Kamchatka, Russia, Global Planet Change, 134, 118-128, 10.1016/j.gloplacha.2014.04.008, 2015a.

Meyer, H., Opel, T., Laepple, T., Dereviagin, A. Y., Hoffmann, K., and Werner, M.: Long-term winter warming trend in the Siberian Arctic during the mid- to late Holocene, Nature Geoscience, 8, 122-125, 10.1038/ngeo2349, 2015b.

Meyer, H., Kostrova, S. S., Meister, P., Lenz, M. M., Kuhn, G., Nazarova, L., Syrykh, L. S., and Dvornikov, Y.: Lacustrine diatom oxygen isotopes as palaeo precipitation proxy - Holocene environmental and snowmelt variations recorded at Lake Bolshoye Shchuchye, Polar Urals, Russia, Quaternary Sci Rev, 290, 107620, https://doi.org/10.1016/j.quascirev.2022.107620, 2022.

Morley, D. W., Leng, M. J., Mackay, A. W., and Sloane, H. J.: Late glacial and Holocene environmental change in the Lake Baikal region documented by oxygen isotopes from diatom silica, Global Planet Change, 46, 221-233, 10.1016/j.gloplacha.2004.09.018, 2005.

Morley, D. W., Leng, M. J., Mackay, A. W., Sloane, H. J., Rioual, P., and Battarbee, R. W.: Cleaning of lake sediment samples for diatom oxygen isotope analysis, J Paleolimnol, 31, 391-401, DOI 10.1023/B:JOPL.0000021854.70714.6b, 2004.

Moschen, R., Lücke, A., and Schleser, G. H.: Sensitivity of biogenic silica oxygen isotopes to changes in surface water temperature and palaeoclimatology, Geophys Res Lett, 32, https://doi.org/10.1029/2004GL022167, 2005.

Narancic, B., Pienitz, R., Chapligin, B., Meyer, H., Francus, P., and Guilbault, J.-P.: Postglacial environmental succession of Nettilling Lake (Baffin Island, Canadian Arctic) inferred from biogeochemical and microfossil proxies, Quaternary Sci Rev, 147, 391-405, 10.1016/j.quascirev.2015.12.022, 2016.

Neukom, R., Steiger, N., Gómez-Navarro, J. J., Wang, J., and Werner, J. P.: No evidence for globally coherent warm and cold periods over the preindustrial Common Era, Nature, 571, 550-554, 10.1038/s41586-019-1401-2, 2019.

Opel, T., Wetterich, S., Meyer, H., Dereviagin, A. Y., Fuchs, M. C., and Schirrmeister, L.: Ground-ice stable isotopes and cryostratigraphy reflect late Quaternary palaeoclimate in the Northeast Siberian Arctic (Oyogos Yar coast, Dmitry Laptev Strait), Clim. Past, 13, 587-611, 10.5194/cp-13-587-2017, 2017.

Patton, H., Hubbard, A., Andreassen, K., Winsborrow, M. and Stroeven, A.P.: The build-up, configuration, and dynamical sensitivity of the Eurasian ice-sheet complex to Late Weichselian climatic and oceanic forcing. Quaternary Sci Rev, 153, 97-121, 10.1016/j.quascirev.2016.10.009, 2016.

Pfalz, G., Diekmann, B., Freytag, J.-C., and Biskaborn, B. K.: Harmonizing heterogeneous multi-proxy data from lake systems, Computers & Geosciences, 153, 104791, https://doi.org/10.1016/j.cageo.2021.104791, 2021.

Polissar, P., Abbott, M., Shemesh, A., Wolfe, A., and Bradley, R.: Holocene hydrologic balance of tropical South America from oxygen isotopes of lake sediment opal, Venezuelan Andes, Earth Planet Sc Lett, 242, 375-389, 10.1016/j.epsl.2005.12.024, 2006.

Quesada, B., Sylvestre, F., Vimeux, F., Black, J., Paillès, C., Sonzogni, C., Alexandre, A., Blard, P.-H., Tonetto, A., Mazur, J.-C., and Bruneton, H.: Impact of Bolivian paleolake evaporation on the δ18O of the Andean glaciers during the last deglaciation (18.5–11.7 ka): diatom-inferred δ18O values and hydro-isotopic modeling, Quaternary Sci Rev, 120, 93-106, 10.1016/j.quascirev.2015.04.022, 2015.

Renssen, H., Seppä, H., Heiri, O., Roche, D. M., Goosse, H., and Fichefet, T.: The spatial and temporal complexity of the Holocene thermal maximum, Nature Geoscience, 2, 411-414, 10.1038/ngeo513, 2009.

Richter, F.M., Turekian, K.K.: Simple models for the geochemical response of the ocean to climatic and tectonic forcing. Earth and Planetary Science Letters 119, 121-131, doi:10.1016/0012-821X(93)90010-7, 1993.

Rietti-Shati, M., Shemesh, A., and Karlen, W.: A 3000-Year Climatic Record from Biogenic Silica Oxygen Isotopes in an Equatorial High-Altitude Lake, Science, 281, 980-982, 10.1126/science.281.5379.980, 1998.

Rosqvist, G., Rietti-Shati, M., and Shemesh, A.: Late Glacial to middle Holocene climatic record of lacustrine biogenic silica oxygen isotopes from a Southern Ocean Island, Geology, 27, 10.1130/0091-7613(1999)027<0967:LGTMHC>2.3.CO;2, 1999.

Rosqvist, G., Jonsson, C., Yam, R., Karlen, W., and Shemesh, A.: Diatom oxygen isotopes in pro-glacial lake sediments from northern Sweden: a 5000 year record of atmospheric circulation, Quaternary Sci Rev, 23, 851-859, 10.1016/j.quascirev.2003.06.009, 2004.

Rosqvist, G. C., Leng, M. J., Goslar, T., Sloane, H. J., Bigler, C., Cunningham, L., Dadal, A., Bergman, J., Berntsson, A., Jonsson, C., and Wastegård, S.: Shifts in precipitation during the last millennium in northern Scandinavia from lacustrine isotope records, Quaternary Sci Rev, 66, 22-34, 10.1016/j.quascirev.2012.10.030, 2013.

Rozanski, K., Klisch, M. A., Wachniew, P., Gorczyca, Z., Goslar, T., Edwards, T. W. D., and Shemesh, A.: Oxygen-isotope geothermometers in lacustrine sediments: New insights through combined δ18O analyses of aquatic cellulose, authigenic calcite and biogenic silica in Lake Gościąż, central Poland, Geochim Cosmochim Ac, 74, 2957-2969, 10.1016/j.gca.2010.02.026, 2010.

Ryves, D. B., Leng, M. J., Barker, P. A., Snelling, A. M., Sloane, H. J., Arrowsmith, C., Tyler, J. J., Scott, D. R., Radbourne, A. D., and Anderson, N. J.: Understanding the transfer of contemporary temperature signals into lake sediments via paired oxygen isotope ratios in carbonates and diatom silica: Problems and potential, Chem Geol, 552, ARTN 119705

10.1016/j.chemgeo.2020.119705, 2020.

Schiff, C., Kaufman, D., Wolfe, A., Dodd, J., and Sharp, Z.: Late Holocene storm-trajectory changes inferred from the oxygen isotope composition of lake diatoms, south Alaska, J Paleolimnol, 41, 189-208, 10.1007/s10933-008-9261-z, 2009.

Schmidt, M., Fuchs, M., Henderson, A. C. G., Kossler, A., Leng, M. J., Mackay, A. W., Shemang, E., and Riedel, F.: Paleolimnological features of a mega-lake phase in the Makgadikgadi Basin (Kalahari, Botswana) during Marine Isotope Stage 5 inferred from diatoms, J Paleolimnol, 58, 373-390, 10.1007/s10933-017-9984-9, 2017.

Shemesh, A. and Peteet, D.: Oxygen isotopes in fresh water biogenic opal - Northeastern US Alleröd-Younger Dryas temperature shift, Geophys Res Lett, 25, 1935-1938, 10.1029/98gl01443, 1998.

Shemesh, A., Rosqvist, G., Rietti-Shati, M., Rubensdotter, L., Bigler, C., Yam, R., and Karlén, W.: Holocene climatic change in Swedish Lapland inferred from an oxygen-isotope record of lacustrine biogenic silica, The Holocene, 11, 447-454, 10.1191/095968301678302887, 2001a.

Shemesh, A., Rietti-Shati, M., Rioual, P., Battarbee, R., de Beaulieu, J.-L., Reille, M., Andrieu-Ponel, V., and Svitavská-Svobodová, H.: An oxygen isotope record of lacustrine opal from a European Maar indicates climatic stability during the Last Interglacial, Geophys Res Lett, 28, 2305-2308, 10.1029/2000GL012720, 2001b.

Smith, A. C., Leng, M. J., Swann, G. E. A., Barker, P. A., Mackay, A. W., Ryves, D. B., Sloane, H. J., Chenery, S. R. N., and Hems, M.: An experiment to assess the effects of diatom dissolution on oxygen isotope ratios, Rapid Commun Mass Sp, 30, 293-300, 10.1002/rcm.7446, 2016.

Spielhagen, R. F. and Mackensen, A.: Upper ocean variability off NE Greenland (79°N) since the last glacial maximum reconstructed from stable isotopes in planktic foraminifer morphotypes, Quaternary Sci Rev, 265, 107070, https://doi.org/10.1016/j.quascirev.2021.107070, 2021.

Street-Perrott, F. A., Barker, P. A., Leng, M. J., Sloane, H. J., Wooller, M. J., Ficken, K. J., and Swain, D. L.: Towards an understanding of late Quaternary variations in the continental biogeochemical cycle of silicon: multi-isotope and sediment-flux data for Lake Rutundu, Mt Kenya, East Africa, since 38 ka BP, J Quaternary Sci, 23, 375-387, 10.1002/jqs.1187, 2008.

Subetto, D. A., Nazarova, L. B., Pestryakova, L. A., Syrykh, L. S., Andronikov, A. V., Biskaborn, B., Diekmann, B., Kuznetsov, D. D., Sapelko, T. V., and Grekov, I. M.: Paleolimnological studies in Russian northern Eurasia: A review, Contemporary Problems of Ecology, 10, 327-335, 10.1134/S1995425517040102, 2017.

Swann, G. E. A., Leng, M. J., Juschus, O., Melles, M., Brigham-Grette, J., and Sloane, H. J.: A combined oxygen and silicon diatom isotope record of Late Quaternary change in Lake El'gygytgyn, North East Siberia, Quaternary Sci Rev, 29, 774-786, 10.1016/j.quascirev.2009.11.024, 2010.

Swann, G. E. A., Mackay, A. W., Vologina, E., Jones, M. D., Panizzo, V. N., Leng, M. J., Sloane, H. J., Snelling, A. M., and Sturm, M.: Lake Baikal isotope records of Holocene Central Asian precipitation, Quaternary Sci Rev, 189, 210-222, 10.1016/j.quascirev.2018.04.013, 2018.

Tyler, J. J., Sloane, H. J., Rickaby, R. E. M., Cox, E. J., and Leng, M. J.: Post-mortem oxygen isotope exchange within cultured diatom silica, Rapid Commun Mass Sp, 31, 1749-1760, 10.1002/rcm.7954, 2017.

Vinther, B. M., Buchardt, S. L., Clausen, H. B., Dahl-Jensen, D., Johnsen, S. J., Fisher, D. A., Koerner, R. M., Raynaud, D., Lipenkov, V., Andersen, K. K., Blunier, T., Rasmussen, S. O., Steffensen, J. P., and Svensson, A. M.: Holocene thinning of the Greenland ice sheet, Nature, 461, 385-388, 10.1038/nature08355, 2009.

Vyse, S. A., Herzschuh, U., Andreev, A. A., Pestryakova, L. A., Diekmann, B., Armitage, S. J., and Biskaborn, B. K.: Geochemical and sedimentological responses of arctic glacial Lake Ilirney, chukotka (far east Russia) to palaeoenvironmental change since ~51.8 ka BP, Quaternary Sci Rev, 247, 106607, https://doi.org/10.1016/j.quascirev.2020.106607, 2020.

Wanner, H. Late-Holocene: cooler or warmer? The Holocene, 31(9), 1501-1506, https://doi.org/10.1177/09596836211019106, 2021.

Wanner, H., Pfister, C. and Neukom, R.: The variable European Little Ice Age. Quaternary Science Reviews 287, 107531. https://doi.org/10.1016/j.quascirev.2022.107531, 2022.

Wilson, K. E., Leng M. J., and Mackay, A. W.: The use of multivariate statistics to resolve multiple contamination signals in the oxygen isotope analysis of biogenic silica, J Quaternary Sci, 29, 641-649, https://doi.org/10.1002/jqs.2729, 2014a.

Wilson, K. E., Maslin, M. A., Leng, M. J., Kingston, J. D., Deino, A. L., Edgar, R. K., and Mackay, A. W.: East African lake evidence for Pliocene millennial-scale climate variability, Geology, 42, 955-958, 10.1130/g35915.1, 2014b.

Wolfe, B. B., Falcone, M. D., Clogg-Wright, K. P., Mongeon, C. L., Yi, Y., Brock, B. E., Amour, N. A. S., Mark, W. A., and Edwards, T. W. D.: Progress in isotope paleohydrology using lake sediment cellulose, J Paleolimnol, 37, 221-231, 10.1007/s10933-006-9015-8, 2007.

Seite 19: [1] hat gelöscht Hanno Meyer   05.10.23 08:11:00

Seite 38: [2] hat gelöscht Hanno Meyer   29.09.23 16:32:00

Seite 38: [3] Formatiert   Hanno Meyer   29.09.23 14:13:00

Links

Seite 38: [4] Formatierte Tabelle   Hanno Meyer

Formatierte Tabelle

Seite 38: [5] hat formatiert   Hanno Meyer   29.09.23 14:13:00

Schriftart: (Standard) Times New Roman

Seite 38: [6] Formatiert   Hanno Meyer   29.09.23 14:12:00

Links

Seite 38: [7] hat formatiert   Hanno Meyer   29.09.23 14:13:00

Schriftart: (Standard) Times New Roman

Seite 38: [7] hat formatiert   Hanno Meyer   29.09.23 14:13:00

Schriftart: (Standard) Times New Roman

Seite 38: [8] hat formatiert   Hanno Meyer   29.09.23 14:46:00

Schriftart: 9 Pt.

Seite 38: [8] hat formatiert   Hanno Meyer   29.09.23 14:46:00

Schriftart: 9 Pt.

Seite 38: [9] hat formatiert   Hanno Meyer   29.09.23 14:13:00

Schriftart: (Standard) Times New Roman

Seite 38: [10] Formatiert   Hanno Meyer   29.09.23 14:12:00

Links

Seite 38: [11] hat formatiert   Hanno Meyer   29.09.23 14:13:00

Schriftart: (Standard) Times New Roman

Seite 38: [11] hat formatiert   Hanno Meyer   29.09.23 14:13:00

Schriftart: (Standard) Times New Roman

Seite 38: [12] hat formatiert   Hanno Meyer   29.09.23 14:46:00

Schriftart: (Standard) Times New Roman, 9 Pt.

Seite 38: [13] hat formatiert   Hanno Meyer   29.09.23 14:13:00

Schriftart: (Standard) Times New Roman

Seite 38: [14] Formatiert   Hanno Meyer   29.09.23 14:12:00

Links

Seite 38: [15] hat formatiert   **Hanno Meyer**   **29.09.23 14:13:00**

Schriftart: (Standard) Times New Roman

Seite 38: [15] hat formatiert   **Hanno Meyer**   **29.09.23 14:13:00**

Schriftart: (Standard) Times New Roman

Seite 38: [16] hat formatiert   **Hanno Meyer**   **29.09.23 14:46:00**

Schriftart: (Standard) Times New Roman, 9 Pt.

Seite 38: [17] hat formatiert   **Hanno Meyer**   **29.09.23 14:13:00**

Schriftart: (Standard) Times New Roman

Seite 38: [18] Formatiert   **Hanno Meyer**   **29.09.23 14:12:00**

Links

Seite 38: [19] hat formatiert   **Hanno Meyer**   **29.09.23 14:13:00**

Schriftart: (Standard) Times New Roman

Seite 38: [19] hat formatiert   **Hanno Meyer**   **29.09.23 14:13:00**

Schriftart: (Standard) Times New Roman

Seite 38: [20] hat formatiert   **Hanno Meyer**   **29.09.23 14:46:00**

Schriftart: (Standard) Times New Roman, 9 Pt.

Seite 38: [21] hat formatiert   **Hanno Meyer**   **29.09.23 14:13:00**

Schriftart: (Standard) Times New Roman

Seite 38: [22] Formatiert   **Hanno Meyer**   **29.09.23 14:12:00**

Links

Seite 38: [23] hat formatiert   **Hanno Meyer**   **29.09.23 14:13:00**

Schriftart: (Standard) Times New Roman

Seite 38: [23] hat formatiert   **Hanno Meyer**   **29.09.23 14:13:00**

Schriftart: (Standard) Times New Roman

Seite 38: [24] hat formatiert   **Hanno Meyer**   **29.09.23 14:46:00**

Schriftart: (Standard) Times New Roman, 9 Pt.

Seite 38: [25] hat formatiert   **Hanno Meyer**   **29.09.23 14:13:00**

Schriftart: (Standard) Times New Roman

Seite 38: [26] Formatiert   **Hanno Meyer**   **29.09.23 14:12:00**

Links

Seite 38: [27] hat formatiert   **Hanno Meyer**   **29.09.23 14:13:00**

Schriftart: (Standard) Times New Roman

Seite 38: [27] hat formatiert   Hanno Meyer   29.09.23 14:13:00

Schriftart: (Standard) Times New Roman

Seite 38: [28] hat formatiert   Hanno Meyer   29.09.23 14:46:00

Schriftart: (Standard) Times New Roman, 9 Pt.

Seite 38: [29] hat formatiert   Hanno Meyer   29.09.23 14:13:00

Schriftart: (Standard) Times New Roman

Seite 38: [30] Formatiert   Hanno Meyer   29.09.23 14:12:00

Links

Seite 38: [31] hat formatiert   Hanno Meyer   29.09.23 14:13:00

Schriftart: (Standard) Times New Roman

Seite 38: [31] hat formatiert   Hanno Meyer   29.09.23 14:13:00

Schriftart: (Standard) Times New Roman

Seite 38: [32] hat formatiert   Hanno Meyer   29.09.23 14:46:00

Schriftart: (Standard) Times New Roman, 9 Pt.

Seite 38: [33] hat formatiert   Hanno Meyer   29.09.23 14:13:00

Schriftart: (Standard) Times New Roman

Seite 38: [34] Formatiert   Hanno Meyer   29.09.23 14:12:00

Links

Seite 38: [35] hat formatiert   Hanno Meyer   29.09.23 14:13:00

Schriftart: (Standard) Times New Roman

Seite 38: [35] hat formatiert   Hanno Meyer   29.09.23 14:13:00

Schriftart: (Standard) Times New Roman

Seite 38: [36] hat formatiert   Hanno Meyer   29.09.23 14:46:00

Schriftart: (Standard) Times New Roman, 9 Pt.

Seite 38: [37] hat formatiert   Hanno Meyer   29.09.23 14:13:00

Schriftart: (Standard) Times New Roman

Seite 38: [38] Formatiert   Hanno Meyer   29.09.23 14:12:00

Links

Seite 38: [39] hat formatiert   Hanno Meyer   29.09.23 14:13:00

Schriftart: (Standard) Times New Roman

Seite 38: [39] hat formatiert   Hanno Meyer   29.09.23 14:13:00

Schriftart: (Standard) Times New Roman

Seite 38: [40] hat formatiert   Hanno Meyer   29.09.23 14:46:00

Schriftart: (Standard) Times New Roman, 9 Pt.

Seite 38: [41] hat formatiert **Hanno Meyer** **29.09.23 14:13:00**

Schriftart: (Standard) Times New Roman

Seite 38: [42] Formatiert Hanno Meyer **29.09.23 14:12:00**

Links

Seite 38: [43] hat formatiert **Hanno Meyer** **29.09.23 14:46:00**

Schriftart: (Standard) Times New Roman

Seite 38: [44] hat formatiert **Hanno Meyer** **29.09.23 14:13:00**

Schriftart: (Standard) Times New Roman

Seite 38: [45] Formatiert Hanno Meyer **29.09.23 14:12:00**

Links

Seite 38: [46] hat formatiert **Hanno Meyer** **29.09.23 14:13:00**

Schriftart: (Standard) Times New Roman

Seite 38: [46] hat formatiert **Hanno Meyer** **29.09.23 14:13:00**

Schriftart: (Standard) Times New Roman

Seite 38: [47] hat formatiert **Hanno Meyer** **29.09.23 14:46:00**

Schriftart: (Standard) Times New Roman, 9 Pt.

Seite 38: [48] hat formatiert **Hanno Meyer** **29.09.23 14:13:00**

Schriftart: (Standard) Times New Roman

Seite 38: [49] Formatiert Hanno Meyer **29.09.23 14:12:00**

Links

Seite 38: [50] hat formatiert **Hanno Meyer** **29.09.23 14:13:00**

Schriftart: (Standard) Times New Roman

Seite 38: [50] hat formatiert **Hanno Meyer** **29.09.23 14:13:00**

Schriftart: (Standard) Times New Roman

Seite 38: [51] hat formatiert **Hanno Meyer** **29.09.23 14:46:00**

Schriftart: (Standard) Times New Roman, 9 Pt.

Seite 38: [52] hat formatiert **Hanno Meyer** **29.09.23 14:13:00**

Schriftart: (Standard) Times New Roman

Seite 38: [53] Formatiert Hanno Meyer **29.09.23 14:12:00**

Links

Seite 38: [54] hat formatiert **Hanno Meyer** **29.09.23 14:13:00**

Schriftart: (Standard) Times New Roman

Seite 38: [54] hat formatiert   **Hanno Meyer**   **29.09.23 14:13:00**

Schriftart: (Standard) Times New Roman

Seite 38: [55] hat formatiert   **Hanno Meyer**   **29.09.23 14:46:00**

Schriftart: (Standard) Times New Roman, 9 Pt.

Seite 38: [56] hat formatiert   **Hanno Meyer**   **29.09.23 14:13:00**

Schriftart: (Standard) Times New Roman

Seite 38: [57] Formatiert   **Hanno Meyer**   **29.09.23 14:12:00**

Links

Seite 38: [58] hat formatiert   **Hanno Meyer**   **29.09.23 14:13:00**

Schriftart: (Standard) Times New Roman

Seite 38: [58] hat formatiert   **Hanno Meyer**   **29.09.23 14:13:00**

Schriftart: (Standard) Times New Roman

Seite 38: [59] hat formatiert   **Hanno Meyer**   **29.09.23 14:46:00**

Schriftart: (Standard) Times New Roman, 9 Pt.

Seite 38: [60] hat formatiert   **Hanno Meyer**   **29.09.23 14:13:00**

Schriftart: (Standard) Times New Roman

Seite 38: [61] Formatiert   **Hanno Meyer**   **29.09.23 14:12:00**

Links

Seite 38: [62] hat formatiert   **Hanno Meyer**   **29.09.23 14:13:00**

Schriftart: (Standard) Times New Roman

Seite 38: [62] hat formatiert   **Hanno Meyer**   **29.09.23 14:13:00**

Schriftart: (Standard) Times New Roman

Seite 38: [63] hat formatiert   **Hanno Meyer**   **29.09.23 14:46:00**

Schriftart: (Standard) Times New Roman, 9 Pt.

Seite 38: [64] hat formatiert   **Hanno Meyer**   **29.09.23 14:13:00**

Schriftart: (Standard) Times New Roman

Seite 38: [65] Formatiert   **Hanno Meyer**   **29.09.23 14:12:00**

Links

Seite 38: [66] hat formatiert   **Hanno Meyer**   **29.09.23 14:13:00**

Schriftart: (Standard) Times New Roman

Seite 38: [66] hat formatiert   **Hanno Meyer**   **29.09.23 14:13:00**

Schriftart: (Standard) Times New Roman

Seite 38: [67] hat formatiert   **Hanno Meyer**   **29.09.23 14:46:00**

Schriftart: (Standard) Times New Roman, 9 Pt.

Seite 38: [68] hat formatiert   **Hanno Meyer**   **29.09.23 14:13:00**

Schriftart: (Standard) Times New Roman

Seite 38: [69] Formatiert   **Hanno Meyer**   **29.09.23 14:12:00**

Links

Seite 38: [70] hat formatiert   **Hanno Meyer**   **29.09.23 14:13:00**

Schriftart: (Standard) Times New Roman

Seite 38: [70] hat formatiert   **Hanno Meyer**   **29.09.23 14:13:00**

Schriftart: (Standard) Times New Roman

Seite 38: [71] hat formatiert   **Hanno Meyer**   **29.09.23 14:46:00**

Schriftart: (Standard) Times New Roman, 9 Pt.

Seite 38: [72] hat formatiert   **Hanno Meyer**   **29.09.23 14:13:00**

Schriftart: (Standard) Times New Roman

Seite 38: [73] Formatiert   **Hanno Meyer**   **29.09.23 14:12:00**

Links

Seite 38: [74] hat formatiert   **Hanno Meyer**   **29.09.23 14:13:00**

Schriftart: (Standard) Times New Roman

Seite 38: [74] hat formatiert   **Hanno Meyer**   **29.09.23 14:13:00**

Schriftart: (Standard) Times New Roman

Seite 38: [75] hat formatiert   **Hanno Meyer**   **29.09.23 14:46:00**

Schriftart: (Standard) Times New Roman, 9 Pt.

Seite 38: [76] hat formatiert   **Hanno Meyer**   **29.09.23 14:13:00**

Schriftart: (Standard) Times New Roman

Seite 38: [77] Formatiert   **Hanno Meyer**   **29.09.23 14:12:00**

Links

Seite 38: [78] hat formatiert   **Hanno Meyer**   **29.09.23 14:13:00**

Schriftart: (Standard) Times New Roman

Seite 38: [78] hat formatiert   **Hanno Meyer**   **29.09.23 14:13:00**

Schriftart: (Standard) Times New Roman

Seite 38: [79] hat formatiert   **Hanno Meyer**   **29.09.23 14:46:00**

Schriftart: (Standard) Times New Roman, 9 Pt.

Seite 38: [80] hat formatiert   **Hanno Meyer**   **29.09.23 14:13:00**

Schriftart: (Standard) Times New Roman

Seite 38: [81] Formatiert   Hanno Meyer   29.09.23 14:12:00

Links

Seite 38: [82] hat formatiert   Hanno Meyer   29.09.23 14:13:00

Schriftart: (Standard) Times New Roman

Seite 38: [82] hat formatiert   Hanno Meyer   29.09.23 14:13:00

Schriftart: (Standard) Times New Roman

Seite 38: [83] hat formatiert   Hanno Meyer   29.09.23 14:46:00

Schriftart: (Standard) Times New Roman, 9 Pt.

Seite 38: [84] hat formatiert   Hanno Meyer   29.09.23 14:13:00

Schriftart: (Standard) Times New Roman

Seite 38: [85] Formatiert   Hanno Meyer   29.09.23 14:12:00

Links

Seite 38: [86] hat formatiert   Hanno Meyer   29.09.23 14:13:00

Schriftart: (Standard) Times New Roman

Seite 38: [86] hat formatiert   Hanno Meyer   29.09.23 14:13:00

Schriftart: (Standard) Times New Roman

Seite 38: [87] hat formatiert   Hanno Meyer   29.09.23 14:46:00

Schriftart: (Standard) Times New Roman, 9 Pt.

Seite 38: [88] hat formatiert   Hanno Meyer   29.09.23 14:13:00

Schriftart: (Standard) Times New Roman

Seite 38: [89] Formatiert   Hanno Meyer   29.09.23 14:12:00

Links

Seite 38: [90] hat formatiert   Hanno Meyer   29.09.23 14:13:00

Schriftart: (Standard) Times New Roman

Seite 38: [90] hat formatiert   Hanno Meyer   29.09.23 14:13:00

Schriftart: (Standard) Times New Roman

Seite 38: [91] hat formatiert   Hanno Meyer   29.09.23 14:46:00

Schriftart: (Standard) Times New Roman, 9 Pt.

Seite 38: [92] hat formatiert   Hanno Meyer   29.09.23 14:13:00

Schriftart: (Standard) Times New Roman

Seite 38: [93] Formatiert   Hanno Meyer   29.09.23 14:12:00

Links

Seite 38: [94] hat formatiert   **Hanno Meyer**   **29.09.23 14:13:00**

Schriftart: (Standard) Times New Roman

Seite 38: [94] hat formatiert   **Hanno Meyer**   **29.09.23 14:13:00**

Schriftart: (Standard) Times New Roman

Seite 38: [95] hat formatiert   **Hanno Meyer**   **29.09.23 14:46:00**

Schriftart: (Standard) Times New Roman, 9 Pt.

Seite 38: [96] hat formatiert   **Hanno Meyer**   **29.09.23 14:13:00**

Schriftart: (Standard) Times New Roman

Seite 38: [97] Formatiert   **Hanno Meyer**   **29.09.23 14:12:00**

Links

Seite 38: [98] hat formatiert   **Hanno Meyer**   **29.09.23 14:13:00**

Schriftart: (Standard) Times New Roman

Seite 38: [98] hat formatiert   **Hanno Meyer**   **29.09.23 14:13:00**

Schriftart: (Standard) Times New Roman

Seite 38: [99] hat formatiert   **Hanno Meyer**   **10.10.23 12:09:00**

Nicht Hervorheben

Seite 38: [99] hat formatiert   **Hanno Meyer**   **10.10.23 12:09:00**

Nicht Hervorheben

Seite 38: [100] hat formatiert   **Hanno Meyer**   **29.09.23 14:13:00**

Schriftart: (Standard) Times New Roman

Seite 38: [101] Formatiert   **Hanno Meyer**   **29.09.23 14:12:00**

Links

Seite 38: [102] hat formatiert   **Hanno Meyer**   **29.09.23 14:13:00**

Schriftart: (Standard) Times New Roman

Seite 38: [102] hat formatiert   **Hanno Meyer**   **29.09.23 14:13:00**

Schriftart: (Standard) Times New Roman

Seite 38: [103] hat formatiert   **Hanno Meyer**   **29.09.23 14:46:00**

Schriftart: (Standard) Times New Roman, 9 Pt.

Seite 39: [104] hat formatiert   **Hanno Meyer**   **29.09.23 14:13:00**

Schriftart: (Standard) Times New Roman

Seite 39: [105] Formatiert   **Hanno Meyer**   **29.09.23 14:12:00**

Links

Seite 39: [106] Formatierte Tabelle   Hanno Meyer

Formatierte Tabelle

Seite 39: [107] hat formatiert   Hanno Meyer   29.09.23 14:13:00

Schriftart: (Standard) Times New Roman

Seite 39: [107] hat formatiert   Hanno Meyer   29.09.23 14:13:00

Schriftart: (Standard) Times New Roman

Seite 39: [108] Formatiert   Hanno Meyer   05.10.23 13:36:00

Zentriert

Seite 39: [109] hat formatiert   Hanno Meyer   29.09.23 14:46:00

Schriftart: (Standard) Times New Roman, 9 Pt.

Seite 39: [110] hat formatiert   Hanno Meyer   29.09.23 14:13:00

Schriftart: (Standard) Times New Roman

Seite 39: [111] Formatiert   Hanno Meyer   29.09.23 14:12:00

Links

Seite 39: [112] hat formatiert   Hanno Meyer   29.09.23 14:13:00

Schriftart: (Standard) Times New Roman

Seite 39: [112] hat formatiert   Hanno Meyer   29.09.23 14:13:00

Schriftart: (Standard) Times New Roman

Seite 39: [113] hat formatiert   Hanno Meyer   05.10.23 13:37:00

Schriftart: 9 Pt.

Seite 39: [114] Formatiert   Hanno Meyer   29.09.23 14:58:00

Zentriert

Seite 39: [115] hat formatiert   Hanno Meyer   29.09.23 14:58:00

Schriftart: (Standard) Times New Roman, 9 Pt.

Seite 39: [116] hat formatiert   Hanno Meyer   29.09.23 14:13:00

Schriftart: (Standard) Times New Roman

Seite 39: [117] Formatiert   Hanno Meyer   29.09.23 14:12:00

Links

Seite 39: [118] hat formatiert   Hanno Meyer   29.09.23 14:13:00

Schriftart: (Standard) Times New Roman

Seite 39: [118] hat formatiert   Hanno Meyer   29.09.23 14:13:00

Schriftart: (Standard) Times New Roman

Seite 39: [119] Formatiert   Hanno Meyer   29.09.23 14:58:00

Zentriert

| Seite 39: [120] hat formatiert | Hanno Meyer | 29.09.23 14:58:00 |

Schriftart: (Standard) Times New Roman, 9 Pt.

| Seite 39: [121] hat formatiert | Hanno Meyer | 29.09.23 14:13:00 |

Schriftart: (Standard) Times New Roman

| Seite 39: [122] Formatiert | Hanno Meyer | 29.09.23 14:12:00 |

Links

| Seite 39: [123] hat formatiert | Hanno Meyer | 29.09.23 14:13:00 |

Schriftart: (Standard) Times New Roman

| Seite 39: [123] hat formatiert | Hanno Meyer | 29.09.23 14:13:00 |

Schriftart: (Standard) Times New Roman

| Seite 39: [124] Formatiert | Hanno Meyer | 29.09.23 14:58:00 |

Zentriert

| Seite 39: [125] hat formatiert | Hanno Meyer | 29.09.23 14:58:00 |

Schriftart: (Standard) Times New Roman, 9 Pt.

| Seite 39: [126] hat formatiert | Hanno Meyer | 29.09.23 14:13:00 |

Schriftart: (Standard) Times New Roman

| Seite 39: [127] Formatiert | Hanno Meyer | 29.09.23 14:12:00 |

Links

| Seite 39: [128] hat formatiert | Hanno Meyer | 29.09.23 14:13:00 |

Schriftart: (Standard) Times New Roman

| Seite 39: [128] hat formatiert | Hanno Meyer | 29.09.23 14:13:00 |

Schriftart: (Standard) Times New Roman

| Seite 39: [129] hat formatiert | Hanno Meyer | 29.09.23 14:58:00 |

Schriftart: 9 Pt.

| Seite 39: [130] Formatiert | Hanno Meyer | 29.09.23 14:58:00 |

Zentriert

| Seite 39: [131] hat formatiert | Hanno Meyer | 29.09.23 14:58:00 |

Schriftart: (Standard) Times New Roman, 9 Pt.

| Seite 39: [132] hat formatiert | Hanno Meyer | 29.09.23 14:13:00 |

Schriftart: (Standard) Times New Roman

| Seite 39: [133] Formatiert | Hanno Meyer | 29.09.23 14:12:00 |

Links

Seite 39: [134] hat formatiert	Hanno Meyer	29.09.23 14:13:00

Schriftart: (Standard) Times New Roman

Seite 39: [134] hat formatiert	Hanno Meyer	29.09.23 14:13:00

Schriftart: (Standard) Times New Roman

Seite 39: [135] hat formatiert	Hanno Meyer	29.09.23 14:58:00

Schriftart: 9 Pt.

Seite 39: [136] Formatiert	Hanno Meyer	29.09.23 14:58:00

Zentriert

Seite 39: [137] hat formatiert	Hanno Meyer	29.09.23 14:58:00

Schriftart: (Standard) Times New Roman, 9 Pt.

Seite 39: [138] hat formatiert	Hanno Meyer	29.09.23 14:13:00

Schriftart: (Standard) Times New Roman

Seite 39: [139] Formatiert	Hanno Meyer	29.09.23 14:12:00

Links

Seite 39: [140] hat formatiert	Hanno Meyer	29.09.23 14:13:00

Schriftart: (Standard) Times New Roman

Seite 39: [140] hat formatiert	Hanno Meyer	29.09.23 14:13:00

Schriftart: (Standard) Times New Roman

Seite 39: [141] hat formatiert	Hanno Meyer	29.09.23 14:58:00

Schriftart: 9 Pt.

Seite 39: [142] Formatiert	Hanno Meyer	29.09.23 14:58:00

Zentriert

Seite 39: [143] hat formatiert	Hanno Meyer	29.09.23 14:58:00

Schriftart: (Standard) Times New Roman, 9 Pt.

Seite 39: [144] hat formatiert	Hanno Meyer	29.09.23 14:13:00

Schriftart: (Standard) Times New Roman

Seite 39: [145] Formatiert	Hanno Meyer	29.09.23 14:12:00

Links

Seite 39: [146] hat formatiert	Hanno Meyer	29.09.23 14:13:00

Schriftart: (Standard) Times New Roman

Seite 39: [146] hat formatiert	Hanno Meyer	29.09.23 14:13:00

Schriftart: (Standard) Times New Roman

Seite 39: [147] hat formatiert	Hanno Meyer	29.09.23 14:58:00

Schriftart: 9 Pt.

Seite 39: [148] Formatiert	Hanno Meyer	29.09.23 14:58:00

Zentriert

Seite 39: [149] hat formatiert	Hanno Meyer	29.09.23 14:58:00

Schriftart: (Standard) Times New Roman, 9 Pt.

Seite 39: [150] hat formatiert	Hanno Meyer	29.09.23 14:13:00

Schriftart: (Standard) Times New Roman

Seite 39: [151] Formatiert	Hanno Meyer	29.09.23 14:12:00

Links

Seite 39: [152] hat formatiert	Hanno Meyer	29.09.23 14:13:00

Schriftart: (Standard) Times New Roman

Seite 39: [152] hat formatiert	Hanno Meyer	29.09.23 14:13:00

Schriftart: (Standard) Times New Roman

Seite 39: [153] hat formatiert	Hanno Meyer	29.09.23 14:58:00

Schriftart: 9 Pt.

Seite 39: [154] Formatiert	Hanno Meyer	29.09.23 14:58:00

Zentriert

Seite 39: [155] hat formatiert	Hanno Meyer	29.09.23 14:58:00

Schriftart: (Standard) Times New Roman, 9 Pt.

Seite 39: [156] hat formatiert	Hanno Meyer	29.09.23 14:13:00

Schriftart: (Standard) Times New Roman

Seite 39: [157] Formatiert	Hanno Meyer	29.09.23 14:12:00

Links

Seite 39: [158] hat formatiert	Hanno Meyer	29.09.23 14:13:00

Schriftart: (Standard) Times New Roman

Seite 39: [158] hat formatiert	Hanno Meyer	29.09.23 14:13:00

Schriftart: (Standard) Times New Roman

Seite 39: [159] hat formatiert	Hanno Meyer	29.09.23 14:58:00

Schriftart: 9 Pt.

Seite 39: [160] Formatiert	Hanno Meyer	29.09.23 14:58:00

Zentriert

Seite 39: [161] hat formatiert	Hanno Meyer	29.09.23 14:58:00

Schriftart: (Standard) Times New Roman, 9 Pt.

Seite 39: [162] hat formatiert	Hanno Meyer	29.09.23 14:15:00

Schriftart: (Standard) Times New Roman

Seite 39: [163] Formatiert	Hanno Meyer	29.09.23 14:12:00

Links

Seite 39: [164] hat formatiert	Hanno Meyer	29.09.23 14:15:00

Schriftart: (Standard) Times New Roman

Seite 39: [164] hat formatiert	Hanno Meyer	29.09.23 14:15:00

Schriftart: (Standard) Times New Roman

Seite 39: [165] hat formatiert	Hanno Meyer	29.09.23 14:58:00

Schriftart: (Standard) Times New Roman, 9 Pt.

Seite 39: [166] Formatiert	Hanno Meyer	29.09.23 14:58:00

Zentriert

Seite 39: [167] hat formatiert	Hanno Meyer	29.09.23 14:15:00

Schriftart: (Standard) Times New Roman

Seite 39: [168] Formatiert	Hanno Meyer	29.09.23 14:12:00

Links

Seite 39: [169] hat formatiert	Hanno Meyer	29.09.23 14:15:00

Schriftart: (Standard) Times New Roman

Seite 39: [169] hat formatiert	Hanno Meyer	29.09.23 14:15:00

Schriftart: (Standard) Times New Roman

Seite 39: [170] hat formatiert	Hanno Meyer	29.09.23 14:58:00

Schriftart: (Standard) Times New Roman, 9 Pt.

Seite 39: [171] Formatiert	Hanno Meyer	29.09.23 14:58:00

Zentriert

Seite 39: [172] hat formatiert	Hanno Meyer	29.09.23 14:15:00

Schriftart: (Standard) Times New Roman

Seite 39: [173] Formatiert	Hanno Meyer	29.09.23 14:12:00

Links

Seite 39: [174] hat formatiert	Hanno Meyer	29.09.23 14:15:00

Schriftart: (Standard) Times New Roman

Seite 39: [174] hat formatiert	Hanno Meyer	29.09.23 14:15:00

Schriftart: (Standard) Times New Roman

Seite 39: [175] hat formatiert	Hanno Meyer	29.09.23 14:58:00

Schriftart: (Standard) Times New Roman, 9 Pt.

Seite 39: [176] Formatiert	Hanno Meyer	29.09.23 14:58:00

Zentriert

Seite 39: [177] hat formatiert	Hanno Meyer	29.09.23 14:15:00

Schriftart: (Standard) Times New Roman

Seite 39: [178] Formatiert	Hanno Meyer	29.09.23 14:12:00

Links

Seite 39: [179] hat formatiert	Hanno Meyer	29.09.23 14:15:00

Schriftart: (Standard) Times New Roman

Seite 39: [179] hat formatiert	Hanno Meyer	29.09.23 14:15:00

Schriftart: (Standard) Times New Roman

Seite 39: [180] hat formatiert	Hanno Meyer	29.09.23 14:58:00

Schriftart: (Standard) Times New Roman, 9 Pt.

Seite 39: [181] Formatiert	Hanno Meyer	29.09.23 14:58:00

Zentriert

Seite 39: [182] hat formatiert	Hanno Meyer	29.09.23 14:15:00

Schriftart: (Standard) Times New Roman

Seite 39: [183] Formatiert	Hanno Meyer	29.09.23 14:12:00

Links

Seite 39: [184] hat formatiert	Hanno Meyer	29.09.23 14:15:00

Schriftart: (Standard) Times New Roman

Seite 39: [184] hat formatiert	Hanno Meyer	29.09.23 14:15:00

Schriftart: (Standard) Times New Roman

Seite 39: [185] hat formatiert	Hanno Meyer	29.09.23 14:58:00

Schriftart: (Standard) Times New Roman, 9 Pt.

Seite 39: [186] Formatiert	Hanno Meyer	29.09.23 14:58:00

Zentriert

Seite 39: [187] hat formatiert	Hanno Meyer	29.09.23 14:15:00

Schriftart: (Standard) Times New Roman

Seite 39: [188] Formatiert	Hanno Meyer	29.09.23 14:12:00

Links

| Seite 39: [189] hat formatiert | Hanno Meyer | 29.09.23 14:15:00 |

Schriftart: (Standard) Times New Roman

| Seite 39: [189] hat formatiert | Hanno Meyer | 29.09.23 14:15:00 |

Schriftart: (Standard) Times New Roman

| Seite 39: [190] hat formatiert | Hanno Meyer | 29.09.23 14:58:00 |

Schriftart: (Standard) Times New Roman, 9 Pt.

| Seite 39: [191] Formatiert | Hanno Meyer | 29.09.23 14:58:00 |

Zentriert

| Seite 39: [192] hat formatiert | Hanno Meyer | 29.09.23 14:15:00 |

Schriftart: (Standard) Times New Roman

| Seite 39: [193] Formatiert | Hanno Meyer | 29.09.23 14:12:00 |

Links

| Seite 39: [194] hat formatiert | Hanno Meyer | 29.09.23 14:15:00 |

Schriftart: (Standard) Times New Roman

| Seite 39: [194] hat formatiert | Hanno Meyer | 29.09.23 14:15:00 |

Schriftart: (Standard) Times New Roman

| Seite 39: [195] hat formatiert | Hanno Meyer | 29.09.23 14:58:00 |

Schriftart: (Standard) Times New Roman, 9 Pt.

| Seite 39: [196] Formatiert | Hanno Meyer | 29.09.23 14:58:00 |

Zentriert

| Seite 39: [197] hat formatiert | Hanno Meyer | 29.09.23 14:15:00 |

Schriftart: (Standard) Times New Roman

| Seite 39: [198] Formatiert | Hanno Meyer | 29.09.23 14:12:00 |

Links

| Seite 39: [199] hat formatiert | Hanno Meyer | 29.09.23 14:15:00 |

Schriftart: (Standard) Times New Roman

| Seite 39: [199] hat formatiert | Hanno Meyer | 29.09.23 14:15:00 |

Schriftart: (Standard) Times New Roman

| Seite 39: [200] hat formatiert | Hanno Meyer | 29.09.23 14:58:00 |

Schriftart: (Standard) Times New Roman, 9 Pt.

| Seite 39: [201] Formatiert | Hanno Meyer | 29.09.23 14:58:00 |

Zentriert

| Seite 39: [202] hat formatiert | Hanno Meyer | 29.09.23 14:15:00 |

Schriftart: (Standard) Times New Roman

Seite 39: [203] Formatiert	Hanno Meyer	29.09.23 14:12:00

Links

Seite 39: [204] hat formatiert	Hanno Meyer	29.09.23 14:15:00

Schriftart: (Standard) Times New Roman

Seite 39: [204] hat formatiert	Hanno Meyer	29.09.23 14:15:00

Schriftart: (Standard) Times New Roman

Seite 39: [205] hat formatiert	Hanno Meyer	29.09.23 14:58:00

Schriftart: (Standard) Times New Roman, 9 Pt.

Seite 39: [206] Formatiert	Hanno Meyer	29.09.23 14:58:00

Zentriert

Seite 39: [207] hat formatiert	Hanno Meyer	29.09.23 14:15:00

Schriftart: (Standard) Times New Roman

Seite 39: [208] Formatiert	Hanno Meyer	29.09.23 14:12:00

Links

Seite 39: [209] hat formatiert	Hanno Meyer	29.09.23 14:15:00

Schriftart: (Standard) Times New Roman

Seite 39: [209] hat formatiert	Hanno Meyer	29.09.23 14:15:00

Schriftart: (Standard) Times New Roman

Seite 39: [210] Formatiert	Hanno Meyer	29.09.23 14:58:00

Zentriert

Seite 39: [211] hat formatiert	Hanno Meyer	29.09.23 14:15:00

Schriftart: (Standard) Times New Roman

Seite 39: [212] Formatiert	Hanno Meyer	29.09.23 14:12:00

Links

Seite 39: [213] hat formatiert	Hanno Meyer	29.09.23 14:15:00

Schriftart: (Standard) Times New Roman

Seite 39: [213] hat formatiert	Hanno Meyer	29.09.23 14:15:00

Schriftart: (Standard) Times New Roman

Seite 39: [214] hat formatiert	Hanno Meyer	29.09.23 14:58:00

Schriftart: (Standard) Times New Roman, 9 Pt.

Seite 39: [215] Formatiert	Hanno Meyer	29.09.23 14:58:00

Zentriert

Seite 39: [216] hat formatiert	Hanno Meyer	29.09.23 14:15:00

Schriftart: (Standard) Times New Roman

Seite 39: [217] Formatiert	Hanno Meyer	29.09.23 14:12:00

Links

Seite 39: [218] hat formatiert	Hanno Meyer	29.09.23 14:15:00

Schriftart: (Standard) Times New Roman

Seite 39: [218] hat formatiert	Hanno Meyer	29.09.23 14:15:00

Schriftart: (Standard) Times New Roman

Seite 39: [219] Formatiert	Hanno Meyer	29.09.23 14:58:00

Zentriert

Seite 39: [220] hat formatiert	Hanno Meyer	29.09.23 14:58:00

Schriftart: (Standard) Times New Roman, 9 Pt.

Seite 39: [221] hat formatiert	Hanno Meyer	29.09.23 14:15:00

Schriftart: (Standard) Times New Roman

Seite 39: [222] Formatiert	Hanno Meyer	29.09.23 14:12:00

Links

Seite 39: [223] hat formatiert	Hanno Meyer	29.09.23 14:15:00

Schriftart: (Standard) Times New Roman

Seite 39: [223] hat formatiert	Hanno Meyer	29.09.23 14:15:00

Schriftart: (Standard) Times New Roman

Seite 39: [224] hat formatiert	Hanno Meyer	29.09.23 14:58:00

Schriftart: (Standard) Times New Roman, 9 Pt.

Seite 39: [225] Formatiert	Hanno Meyer	29.09.23 14:58:00

Zentriert

Seite 39: [226] hat formatiert	Hanno Meyer	29.09.23 14:15:00

Schriftart: (Standard) Times New Roman

Seite 39: [227] Formatiert	Hanno Meyer	29.09.23 14:12:00

Links

Seite 39: [228] hat formatiert	Hanno Meyer	29.09.23 14:15:00

Schriftart: (Standard) Times New Roman

Seite 39: [228] hat formatiert	Hanno Meyer	29.09.23 14:15:00

Schriftart: (Standard) Times New Roman

Seite 39: [229] hat formatiert	Hanno Meyer	29.09.23 14:58:00

Schriftart: (Standard) Times New Roman, 9 Pt.

Seite 39: [230] Formatiert	Hanno Meyer	29.09.23 14:58:00

Zentriert

Seite 39: [231] hat formatiert	Hanno Meyer	29.09.23 14:15:00

Schriftart: (Standard) Times New Roman

Seite 39: [232] Formatiert	Hanno Meyer	29.09.23 14:12:00

Links

Seite 39: [233] hat formatiert	Hanno Meyer	29.09.23 14:15:00

Schriftart: (Standard) Times New Roman

Seite 39: [233] hat formatiert	Hanno Meyer	29.09.23 14:15:00

Schriftart: (Standard) Times New Roman

Seite 39: [234] hat formatiert	Hanno Meyer	29.09.23 14:58:00

Schriftart: (Standard) Times New Roman, 9 Pt.

Seite 39: [235] Formatiert	Hanno Meyer	29.09.23 14:58:00

Zentriert

Seite 39: [236] hat formatiert	Hanno Meyer	29.09.23 14:15:00

Schriftart: (Standard) Times New Roman

Seite 39: [237] Formatiert	Hanno Meyer	29.09.23 14:12:00

Links

Seite 39: [238] hat formatiert	Hanno Meyer	29.09.23 14:15:00

Schriftart: (Standard) Times New Roman

Seite 39: [238] hat formatiert	Hanno Meyer	29.09.23 14:15:00

Schriftart: (Standard) Times New Roman

Seite 39: [239] hat formatiert	Hanno Meyer	29.09.23 14:58:00

Schriftart: (Standard) Times New Roman, 9 Pt.

Seite 39: [240] Formatiert	Hanno Meyer	29.09.23 14:58:00

Zentriert

Seite 39: [241] hat formatiert	Hanno Meyer	29.09.23 14:15:00

Schriftart: (Standard) Times New Roman

Seite 39: [242] Formatiert	Hanno Meyer	29.09.23 14:12:00

Links

Seite 39: [243] hat formatiert	Hanno Meyer	29.09.23 14:15:00

Schriftart: (Standard) Times New Roman

Seite 39: [243] hat formatiert	Hanno Meyer	29.09.23 14:15:00

Schriftart: (Standard) Times New Roman

Seite 39: [244] hat formatiert	Hanno Meyer	29.09.23 14:58:00

Schriftart: (Standard) Times New Roman, 9 Pt.

Seite 39: [245] Formatiert	Hanno Meyer	29.09.23 14:58:00

Zentriert

Seite 39: [246] hat formatiert	Hanno Meyer	29.09.23 14:15:00

Schriftart: (Standard) Times New Roman

Seite 39: [247] Formatiert	Hanno Meyer	29.09.23 14:12:00

Links

Seite 39: [248] hat formatiert	Hanno Meyer	29.09.23 14:15:00

Schriftart: (Standard) Times New Roman

Seite 39: [248] hat formatiert	Hanno Meyer	29.09.23 14:15:00

Schriftart: (Standard) Times New Roman

Seite 39: [249] hat formatiert	Hanno Meyer	29.09.23 14:58:00

Schriftart: (Standard) Times New Roman, 9 Pt.

Seite 39: [250] Formatiert	Hanno Meyer	29.09.23 14:58:00

Zentriert

Seite 40: [251] Formatiert	Hanno Meyer	29.09.23 16:41:00

Zentriert

Seite 40: [252] hat formatiert	Hanno Meyer	29.09.23 14:15:00

Schriftart: (Standard) Times New Roman

Seite 40: [253] Formatiert	Hanno Meyer	29.09.23 14:12:00

Links

Seite 40: [254] Formatierte Tabelle	Hanno Meyer	

Formatierte Tabelle

Seite 40: [255] hat formatiert	Hanno Meyer	29.09.23 14:15:00

Schriftart: (Standard) Times New Roman

Seite 40: [255] hat formatiert	Hanno Meyer	29.09.23 14:15:00

Schriftart: (Standard) Times New Roman

Seite 40: [256] hat formatiert	Hanno Meyer	29.09.23 14:58:00

Schriftart: (Standard) Times New Roman, 9 Pt.

Seite 40: [257] Formatiert	**Hanno Meyer**	**29.09.23 16:41:00**

Zentriert

Seite 40: [258] hat formatiert	**Hanno Meyer**	**29.09.23 14:16:00**

Schriftart: (Standard) Times New Roman

Seite 40: [259] Formatiert	**Hanno Meyer**	**29.09.23 14:12:00**

Links

Seite 40: [260] hat formatiert	**Hanno Meyer**	**29.09.23 15:15:00**

Schriftart: (Standard) Times New Roman, 9 Pt.

Seite 40: [260] hat formatiert	**Hanno Meyer**	**29.09.23 15:15:00**

Schriftart: (Standard) Times New Roman, 9 Pt.

Seite 40: [261] hat formatiert	**Hanno Meyer**	**29.09.23 15:15:00**

Schriftart: 9 Pt.

Seite 40: [262] Formatiert	**Hanno Meyer**	**29.09.23 16:41:00**

Zentriert

Seite 40: [263] hat formatiert	**Hanno Meyer**	**29.09.23 14:16:00**

Schriftart: (Standard) Times New Roman

Seite 40: [264] Formatiert	**Hanno Meyer**	**29.09.23 14:12:00**

Links

Seite 40: [265] hat formatiert	**Hanno Meyer**	**29.09.23 14:16:00**

Schriftart: (Standard) Times New Roman

Seite 40: [266] hat formatiert	**Hanno Meyer**	**29.09.23 15:15:00**

Schriftart: (Standard) Times New Roman, 9 Pt.

Seite 40: [266] hat formatiert	**Hanno Meyer**	**29.09.23 15:15:00**

Schriftart: (Standard) Times New Roman, 9 Pt.

Seite 40: [267] hat formatiert	**Hanno Meyer**	**29.09.23 15:15:00**

Schriftart: 9 Pt.

Seite 40: [268] Formatiert	**Hanno Meyer**	**29.09.23 16:41:00**

Zentriert

Seite 40: [269] hat formatiert	**Hanno Meyer**	**29.09.23 14:16:00**

Schriftart: (Standard) Times New Roman

Seite 40: [270] Formatiert	**Hanno Meyer**	**29.09.23 14:12:00**

Links

Seite 40: [271] hat formatiert	Hanno Meyer	29.09.23 15:15:00

Schriftart: (Standard) Times New Roman, 9 Pt.

Seite 40: [271] hat formatiert	Hanno Meyer	29.09.23 15:15:00

Schriftart: (Standard) Times New Roman, 9 Pt.

Seite 40: [272] hat formatiert	Hanno Meyer	29.09.23 15:15:00

Schriftart: 9 Pt.

Seite 40: [273] Formatiert	Hanno Meyer	29.09.23 16:41:00

Zentriert

Seite 40: [274] hat formatiert	Hanno Meyer	29.09.23 14:16:00

Schriftart: (Standard) Times New Roman

Seite 40: [275] Formatiert	Hanno Meyer	29.09.23 14:12:00

Links

Seite 40: [276] hat formatiert	Hanno Meyer	29.09.23 15:15:00

Schriftart: (Standard) Times New Roman, 9 Pt.

Seite 40: [276] hat formatiert	Hanno Meyer	29.09.23 15:15:00

Schriftart: (Standard) Times New Roman, 9 Pt.

Seite 40: [277] hat formatiert	Hanno Meyer	29.09.23 15:15:00

Schriftart: 9 Pt.

Seite 40: [278] Formatiert	Hanno Meyer	29.09.23 16:41:00

Zentriert

Seite 40: [279] hat formatiert	Hanno Meyer	29.09.23 14:16:00

Schriftart: (Standard) Times New Roman

Seite 40: [280] Formatiert	Hanno Meyer	29.09.23 14:12:00

Links

Seite 40: [281] hat formatiert	Hanno Meyer	29.09.23 15:15:00

Schriftart: (Standard) Times New Roman, 9 Pt.

Seite 40: [281] hat formatiert	Hanno Meyer	29.09.23 15:15:00

Schriftart: (Standard) Times New Roman, 9 Pt.

Seite 40: [282] hat formatiert	Hanno Meyer	29.09.23 15:15:00

Schriftart: 9 Pt.

Seite 40: [283] Formatiert	Hanno Meyer	29.09.23 16:41:00

Zentriert

Seite 40: [284] hat formatiert	Hanno Meyer	29.09.23 14:16:00

Schriftart: (Standard) Times New Roman

Seite 40: [285] Formatiert	Hanno Meyer	29.09.23 14:12:00

Links

Seite 40: [286] hat formatiert	Hanno Meyer	29.09.23 15:15:00

Schriftart: (Standard) Times New Roman, 9 Pt.

Seite 40: [286] hat formatiert	Hanno Meyer	29.09.23 15:15:00

Schriftart: (Standard) Times New Roman, 9 Pt.

Seite 40: [287] hat formatiert	Hanno Meyer	29.09.23 15:15:00

Schriftart: 9 Pt.

Seite 40: [288] Formatiert	Hanno Meyer	29.09.23 16:41:00

Zentriert

Seite 40: [289] hat formatiert	Hanno Meyer	29.09.23 14:16:00

Schriftart: (Standard) Times New Roman

Seite 40: [290] Formatiert	Hanno Meyer	29.09.23 14:12:00

Links

Seite 40: [291] hat formatiert	Hanno Meyer	29.09.23 15:15:00

Schriftart: (Standard) Times New Roman, 9 Pt.

Seite 40: [291] hat formatiert	Hanno Meyer	29.09.23 15:15:00

Schriftart: (Standard) Times New Roman, 9 Pt.

Seite 40: [292] hat formatiert	Hanno Meyer	29.09.23 15:15:00

Schriftart: 9 Pt.

Seite 40: [293] Formatiert	Hanno Meyer	29.09.23 16:41:00

Zentriert

Seite 40: [294] hat formatiert	Hanno Meyer	29.09.23 14:16:00

Schriftart: (Standard) Times New Roman

Seite 40: [295] Formatiert	Hanno Meyer	29.09.23 14:12:00

Links

Seite 40: [296] hat formatiert	Hanno Meyer	29.09.23 15:15:00

Schriftart: (Standard) Times New Roman, 9 Pt.

Seite 40: [296] hat formatiert	Hanno Meyer	29.09.23 15:15:00

Schriftart: (Standard) Times New Roman, 9 Pt.

Seite 40: [297] hat formatiert	Hanno Meyer	29.09.23 15:15:00

Schriftart: 9 Pt.

Seite 40: [298] Formatiert	Hanno Meyer	29.09.23 16:41:00

Zentriert

Seite 40: [299] hat formatiert	Hanno Meyer	29.09.23 14:16:00

Schriftart: (Standard) Times New Roman

Seite 40: [300] Formatiert	Hanno Meyer	29.09.23 14:12:00

Links

Seite 40: [301] hat formatiert	Hanno Meyer	29.09.23 15:15:00

Schriftart: (Standard) Times New Roman, 9 Pt.

Seite 40: [301] hat formatiert	Hanno Meyer	29.09.23 15:15:00

Schriftart: (Standard) Times New Roman, 9 Pt.

Seite 40: [302] hat formatiert	Hanno Meyer	29.09.23 15:15:00

Schriftart: 9 Pt.

Seite 40: [303] Formatiert	Hanno Meyer	29.09.23 16:41:00

Zentriert

Seite 40: [304] hat formatiert	Hanno Meyer	29.09.23 14:16:00

Schriftart: (Standard) Times New Roman

Seite 40: [305] Formatiert	Hanno Meyer	29.09.23 14:12:00

Links

Seite 40: [306] hat formatiert	Hanno Meyer	29.09.23 15:15:00

Schriftart: (Standard) Times New Roman, 9 Pt.

Seite 40: [306] hat formatiert	Hanno Meyer	29.09.23 15:15:00

Schriftart: (Standard) Times New Roman, 9 Pt.

Seite 40: [307] hat formatiert	Hanno Meyer	29.09.23 15:15:00

Schriftart: 9 Pt.

Seite 40: [308] Formatiert	Hanno Meyer	29.09.23 16:41:00

Zentriert

Seite 40: [309] hat formatiert	Hanno Meyer	29.09.23 14:16:00

Schriftart: (Standard) Times New Roman

Seite 40: [310] Formatiert	Hanno Meyer	29.09.23 14:12:00

Links

Seite 40: [311] hat formatiert	Hanno Meyer	29.09.23 15:15:00

Schriftart: (Standard) Times New Roman, 9 Pt.

Seite 40: [311] hat formatiert	**Hanno Meyer**	**29.09.23 15:15:00**

Schriftart: (Standard) Times New Roman, 9 Pt.

Seite 40: [312] Formatiert	**Hanno Meyer**	**29.09.23 16:41:00**

Zentriert

Seite 40: [313] hat formatiert	**Hanno Meyer**	**29.09.23 15:15:00**

Schriftart: 9 Pt.

Seite 40: [314] hat formatiert	**Hanno Meyer**	**29.09.23 14:16:00**

Schriftart: (Standard) Times New Roman

Seite 40: [315] Formatiert	**Hanno Meyer**	**29.09.23 14:12:00**

Links

Seite 40: [316] hat formatiert	**Hanno Meyer**	**29.09.23 15:15:00**

Schriftart: (Standard) Times New Roman, 9 Pt.

Seite 40: [316] hat formatiert	**Hanno Meyer**	**29.09.23 15:15:00**

Schriftart: (Standard) Times New Roman, 9 Pt.

Seite 40: [317] hat formatiert	**Hanno Meyer**	**29.09.23 15:15:00**

Schriftart: 9 Pt.

Seite 40: [318] Formatiert	**Hanno Meyer**	**29.09.23 16:41:00**

Zentriert

Seite 40: [319] hat formatiert	**Hanno Meyer**	**29.09.23 14:16:00**

Schriftart: (Standard) Times New Roman

Seite 40: [320] Formatiert	**Hanno Meyer**	**29.09.23 14:12:00**

Links

Seite 40: [321] hat formatiert	**Hanno Meyer**	**29.09.23 15:15:00**

Schriftart: (Standard) Times New Roman, 9 Pt.

Seite 40: [321] hat formatiert	**Hanno Meyer**	**29.09.23 15:15:00**

Schriftart: (Standard) Times New Roman, 9 Pt.

Seite 40: [322] hat formatiert	**Hanno Meyer**	**29.09.23 15:15:00**

Schriftart: 9 Pt.

Seite 40: [323] Formatiert	**Hanno Meyer**	**29.09.23 16:41:00**

Zentriert

Seite 40: [324] hat formatiert	**Hanno Meyer**	**29.09.23 14:16:00**

Schriftart: (Standard) Times New Roman

Seite 40: [325] Formatiert	**Hanno Meyer**	**29.09.23 14:12:00**

Links

Seite 40: [326] hat formatiert   Hanno Meyer   29.09.23 15:15:00

Schriftart: (Standard) Times New Roman, 9 Pt.

Seite 40: [326] hat formatiert   Hanno Meyer   29.09.23 15:15:00

Schriftart: (Standard) Times New Roman, 9 Pt.

Seite 40: [327] hat formatiert   Hanno Meyer   29.09.23 15:15:00

Schriftart: 9 Pt.

Seite 40: [328] Formatiert   Hanno Meyer   29.09.23 16:41:00

Zentriert

Seite 40: [329] Formatiert   Hanno Meyer   29.09.23 14:12:00

Links

Seite 40: [330] Formatierte Tabelle   Hanno Meyer

Formatierte Tabelle

Seite 40: [331] hat formatiert   Hanno Meyer   29.09.23 14:16:00

Schriftart: (Standard) Times New Roman

Seite 40: [332] hat formatiert   Hanno Meyer   29.09.23 14:16:00

Schriftart: (Standard) Times New Roman

Seite 40: [333] hat formatiert   Hanno Meyer   29.09.23 14:16:00

Schriftart: (Standard) Times New Roman

Seite 40: [334] hat formatiert   Hanno Meyer   12.10.23 15:05:00

Schriftart: (Standard) Times New Roman

Seite 40: [335] hat formatiert   Hanno Meyer   12.10.23 15:05:00

Schriftart: (Standard) Times New Roman

Seite 40: [336] hat formatiert   Hanno Meyer   05.10.23 13:49:00

Schriftart: (Standard) Times New Roman, Hervorheben

Seite 40: [337] hat formatiert   Hanno Meyer   29.09.23 15:15:00

Schriftart: (Standard) Times New Roman

Seite 40: [338] Formatiert   Hanno Meyer   29.09.23 16:41:00

Zentriert

Seite 40: [339] hat formatiert   Hanno Meyer   29.09.23 15:15:00

Schriftart: 9 Pt.

Seite 44: [340] hat gelöscht   Hanno Meyer   29.09.23 14:12:00